ISSN 1410-6175

BULLETIN OF THE MARINE GEOLOGY

VOLUME 36. NUMBER 1 . JUNE 2021

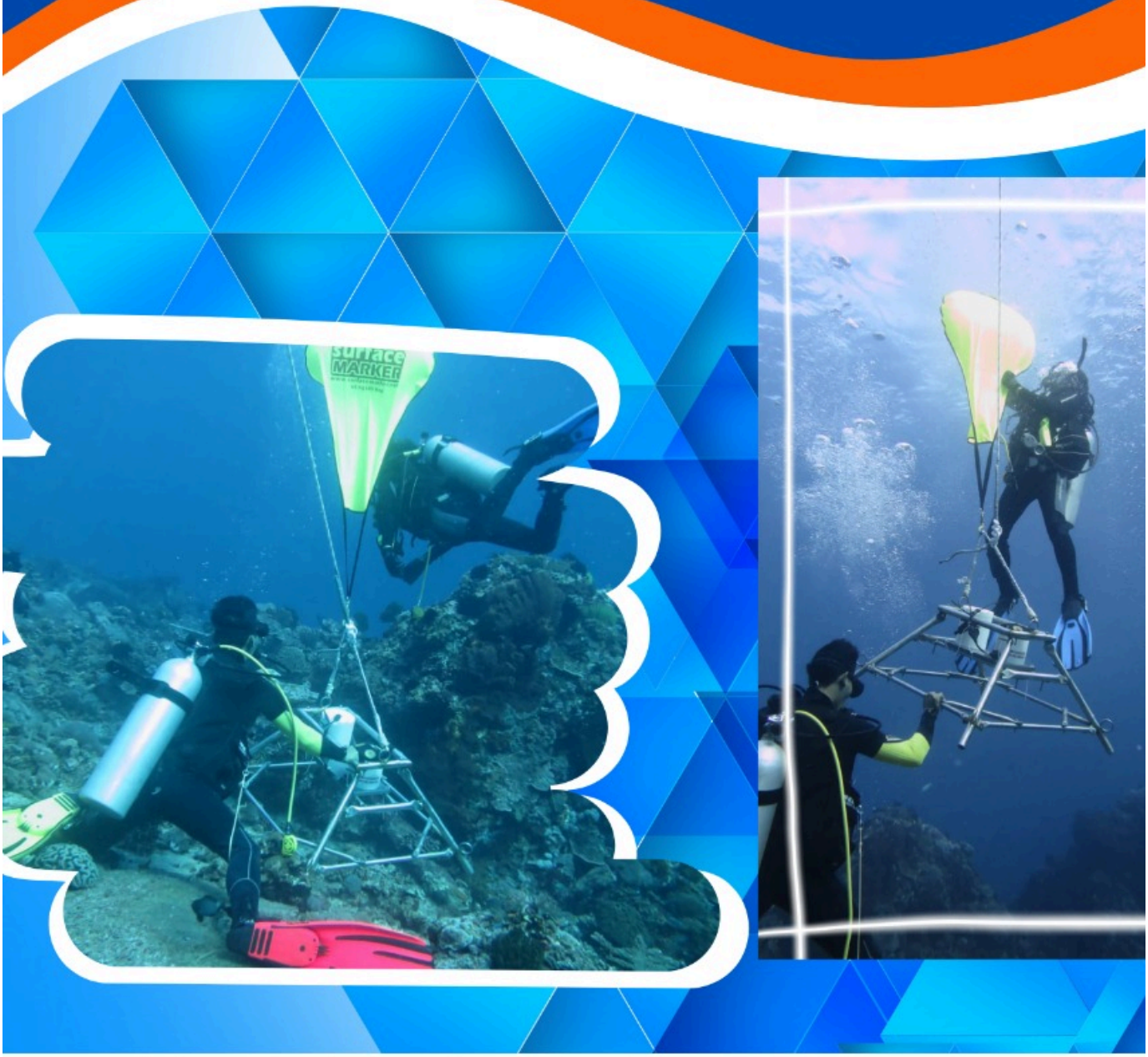

BULL MGI / VOL. 36 / NO.1 / PAGE 1-56 / BANDUNG, JUNE 2021 / ISSN 1410-6175

Accredited :RISTEKDIKTI No. 21/E/KPT/2018

MARINE GEOLOGICAL INSTITUTE
RESEARCH AND DEVELOPMENT AGENCIES FOR ENERGY AND MINERAL RESOURCES
MINISTRY OF ENERGY AND MINERAL RESOURCES

PUSAT PENELITIAN DAN PENGEMBANGAN GEOLOGI KELAUTAN
BADAN PENELITIAN DAN PENGEMBANGAN ENERGI DAN SUMBER DAYA MINERAL
KEMENTERIAN ENERGI DAN SUMBER DAYA MINERAL

BULLETIN OF THE MARINE GEOLOGY

Vol. 36, No. 1, June 2021

INSURED EDITOR
Director of Marine Geological Institute

CHIEF OF EDITORIAL BOARD
Prof. Dr. Ir. Hananto Kurnio, M. Sc.

VICE CHIEF OF EDITORIAL BOARD
Dr. Luli Gustiantini, S.T., M.T.

EDITORIAL BOARDS
Dr. Ir. Susilohadi *(Marine Geological Institute of Indonesia)*
Dr. Ir. Noor Cahyo Dwi Aryanto, M.T. *(Marine Geological Institute of Indonesia)*
Imam Setiadi, S.Si., M.T. *(Marine Geological Institute of Indonesia)*
Ir. Immaculata Christiana, MT. *(Marine Geological Institute of Indonesia)*
Ir. Mustafa Hanafi, M.Si. *(Marine Geological Institute of Indonesia)*
Ir. Joni Widodo, M.Si. *(Marine Geological Institute of Indonesia)*
Tumpal Bernhard Nainggolan, S.T., M.T. *(Marine Geological Institute of Indonesia)*
Dra. Ai Yuningsih *(Marine Geological Institute of Indonesia)*
Nazar Nurdin, S.T., M.T. *(Marine Geological Institute of Indonesia)*
Yulinar Firdaus, S.Si., M.T. *(Marine Geological Institute of Indonesia)*
Siti Marina, S.T., M.Phil. *(Marine Geological Institute of Indonesia)*
Drs. Judy Muliawan Eddy *(Marine Geological Institute of Indonesia)*

SCIENTIFIC REVIEWERS
Dr. Eng. Totok Suprijo, *(Institute of Technology Bandung)*
Dr. Eddy Hartantyo, M.Si. *(Gadjah Mada University)*
Dr. Hermes Panggabean, M.Sc. *(Geological Agency)*
Dr. Muhammad Ma'ruf Mukti *(Research Center for Geotechnology)*
Dr. Ir. Baskoro Rohadi, M.T. *(Diponegoro University)*

PUBLISHER BOARDS
Adithya Kandiawan S.P., M.M.
Slamet
Swasty Aninda Piranti, ST.
Dwinanda Pratya Annisa M., S.pd.
Dery Rochiman, A.Md.

GRAPHIC DESIGN
Arif Suprayitno, S.Kom., M.Kom.

For communication of this publications, please contact :
MARINE GEOLOGICAL INSTITUTE
Dr. Junjunan 236, Bandung-40174, Indonesia
Telephone : +62-22-6032020, 6032201, Fax : +62-22- 6017887
E-mail : ejournal.p3gl@gmail.com

PREFACE

The possibility of generating electrical power from ocean currents in Indonesia has been recognized. Ocean current power demonstrates as possible significant energy resources for developing renewable energy. One of the advantages of ocean current energy utilization, i.e., the production of electricity, is more predictable and more environmentally friendly. Highlighting the importance of its research and contribution to the country, our Marine Geological Institute (MGI) has selected several straits in the Lesser Sunda Islands for sea current research, and in this issue results of such studies are presented.

The first edition of Bulletin of Marine Geology (BoMG) in the year 2021 proudly presents five inspiring papers as great stimuli in marine science. The first paper is Quartz-Feldspar-Lithics (QFL) and Lithofacies: Predicting Reservoir Quality of the Middle Miocene Deep-water Facies in Kutei and North Makassar Basins, contributed by the Faculty of Geological Engineering, Universitas Padjadjaran. The second, Distribution of Subsurface Quaternary Sediment in South Bintan Island Waters as a Potential Heavy Mineral Placer or Rare Earth Element Deposit Based on Seismic Interpretation, contributed by MGI in collaboration with the Faculty of Geological Engineering, Universitas Padjadjaran. The third, Assessment of Potential Marine Current Energy in the Straits of the Lesser Sunda Islands, contributed by MGI. The fourth, The Seawater and Freshwater Influence on Expansivity Behaviors of Clay Minerals, contributed by the Faculty of Fisheries and Marine Science, Diponegoro University. Just as importantly the fifth, Petrophysical Analysis And Seismic Stratigraphy Interpretation To Determine Hydrocarbon Reservoir In Tarakan Basin, Bunyu Island Waters contributed by the Geophysics Department, Faculty of Mathematics and Natural Sciences, Universitas Padjadjaran and MGI. The editors appreciate the valuable contribution of the authors for this edition.

Chief Editor

ISSN 1410-6175

BULLETIN OF THE MARINE GEOLOGY

Vol. 36, No. 1, June 2021

CONTENTS

QFL AND LITHO FACIES: PREDICTING RESERVOIR QUALITY OF THE MIDDLE MIOCENE DEEP-WATER FACIES AT KUTEI AND NORTH MAKASSAR BASINS

QFL DAN FASIES BATUAN: PREDIKSI KUALITAS RESERVOIR FASIES LAUT DALAM BERUMUR MIOSEN TENGAH DI CEKUNGAN KUTEI DAN MAKASSAR UTARA

Kuntadi Nugrahanto[1,2], Ildrem Syafri[1], and Budi Muljana[1]

[1] Postgraduate Program, Faculty of Geological Engineering, the University of Padjadjaran

[2] Upstream Subholding Pertamina Hulu Energi (PHE)

Corresponding author: kuntadi19001@mail.unpad.ac.id; kuntadi.nugrahanto@pertamina.com

(Received 21 June 2021; in revised form 16 June 2021; accepted 08 July 2021)

ABSTRACT: As it is widely known the oil and gas wellbores offshore Kutei and North Makassar have not optimally penetrated the objective strata, which is the Middle Miocene's deep-water reservoirs. Therefore, evaluating the quality of these reservoirs with onshore dataset then comparing them with the proven Late Miocene's deep-water producing reservoirs had been very fundamental. The study focuses on the assessment of QFL (Quartz, Feldspar and Lithic fragments) and sandstones litho-facies based on the rock samples from conventional-core and side-wall core, and well-logs data from forty wells onshore and offshore. These rock samples are bounded by the key biostratigraphy intervals of M40M33, M45M40, M50M45 (Middle Miocene), and M65M50, M66M65, M70M66, M80M70 (Late Miocene). Subdivisions of the reservoirs considered the sandstone litho facies, NTG ratio, sorting, and grain size, to come up with five groups in the Middle Miocene deltaic facies: FLU_SX, DC_SX, DC_SM, DC_SM, and DF_SC; and four groups in the Late Miocene deep-water facies: SSWS, MSWS, SSPS, and MSPS. Core-based porosity and permeability further explain the relationship between the reservoir quality with the sandstones' composition and litho facies, and concluded that high-energy depositional system is mainly associated with the FLU_SX, DC_SX, SSWS and MSWS being the reservoir with best quality. Oppositely, the DF_SC, SSPS, and MSPS are classified the reservoir with worst to none quality. A cross plot between core-based porosity and maximum burial depth is able to postulate the relational trend of decreasing reservoir quality with deeper depth.

Keywords: Middle Miocene, deep water, QFL, litho facies, Kutei, North Makassar

ABSTRAK: *Telah umum diketahui bahwa sumur bor minyak dan gas di lepas pantai Kutei dan Makassar Utara belum secara optimal menembus reservoir fasies laut dalam berumur Miosen Tengah, yang merupakan obyektif utama dalam penelitian ini. Oleh karenanya penulis melakukan studi banding antara reservoir obyektif yang umumnya berlokasi di daratan dengan reservoir berumur Miosen Atas yang telah terbukti memproduksi hasil migas di lepas pantai laut dalam. Fokus studi ini adalah melakukan pengkajian komposisi QFL (fragmen Kuarsa, Felsfar dan Litik) dan fasies batuan batupasir berdasarkan sampel batuan yang diambil dari data inti batuan (core) dan data dinding bor (side-wall core), serta data log elektrik yang berasal dari sekitar empat puluh buah sumur. Sampel batuan ini dibatasi oleh marker biostratigrafi: M40M33, M45M40, M50M45 (Miosen Tengah), dan M65M50, M66M65, M70M66, M80M70 (Miosen Akhir). Fasies reservoir dapat dikenali berdasarkan fasies batuan batupasir, rasio NTG, sortasi, dan ukuran butir terutama pada fasies delta berumur Miosen Tengah: FLU_SX, DC_SX, DC_SM, DC_SM, dan DF_SC, dan untuk fasies laut dalam Miosen Akhir: SSWS, MSWS, SSPS, dan MSPS. Selanjutnya porositas dan permeabilitas yang diukur pada batuan inti bor tersebut dapat digunakan untuk menerangkan hubungan antara kualitas reservoir dengan komposisi batupasir maupun fasies batuan. Sistem pengendapan berenergi tinggi terutama yang berhubungan dengan fasies batuan FLU_SX, DC_SX, SSWS dan MSWS merupakan reservoir dengan kualitas terbaik; dan fasies batuan DF_SC, SSPS, dan MSPS kebalikannya. Hubungan antara porositas berbasis data inti batuan dengan kedalaman (depth of burial) secara umum dapat menggambarkan pola penurunan kualitas reservoir seiring bertambahnya kedalaman.*

Kata Kunci: *Miosen Tengah, laut dalam, QFL, fasies batuan, Kutai, Makassar Utara*

INTRODUCTION

Kutei basin is one of the major hydrocarbon basins in Indonesia with multi-billions barrel reserves of oil equivalent (bboe) have been discovered to date. More than 8.0-km thick sediment has been deposited in the basin where the thickest is reached around the modern-day Mahakam delta (after Hall & Nichols, 2002; in Witts et al., 2015). The study area includes the onshore and offshore parts of the Kutei and north Makassar basins (Figure 1). After the last big discoveries of the "classical" middle-to-late Miocene deltaic play; Sisi and NW Peciko (Duval, 1992), the sequence-stratigraphic concept was applied to delineate more hydrocarbon reserves in the late Miocene-to-Pliocene deep-water play.

To prove the concept, Unocal Indonesia initiated the SX deep-water drilling technology and pioneered a back-to-back drilling campaign along the modern-day deep-water slope during the 1996-to-2005 (Unocal Indonesia Exploration and Drilling Team, 2016; in Nugrahanto et al., 2021). Several deep-water wells, including the discovery ones had confirmed the deltaic progradation easterly from Miocene to Recent intervals, however most of the middle Miocene deep-water play remains unpenetrated. The integration of seismic stratigraphy, core-log facies description, and petrology data had been integrated to correlate and describe the relationship between sedimentary rate and facies, with the mineral composition at different ages. The aim of the study is to classify the clusters of quartz, feldspar, and lithic fragments (QFL) composition with respect to the reservoir age, and qualitative reservoir quality of the middle Miocene as the focus of the study, to the late Miocene reservoirs to be compared with.

The study area is tectonically situated on the continental crust that accreted to the Sundaland during the Cretaceous to Cenozoic, and is side-by-side with several continental blocks derived from the Gondwanaland such as Mangkalihat, West Sulawesi, Paternoster, and southwest Borneo in the late Triassic to late Jurassic (Metcalf, 2011 and 2013; Hall and Sevastjanova, 2012). Several key major tectono-stratigraphic events in the study area are:

1) The results of Zircon U-Pb dating conducted in the Oligocene and early Miocene rock samples at Barito Basin (Witts *et al*., 2014), and the same dating from the insitu diorite porphiry at Lamandau (Shuang Li *et al*., 2015), both suggested the latest plate-tectonic related volcanisms in the Borneo was recorded at the Late Cretaceous of 82-70 Ma.

2) The South China Sea rifting opened in the Eocene-Oligocene and triggered movement of the Luconia Continent to the southeast direction. It led part of the South China Sea Plate subducted beneath the Sundaland. Due to the opening of South China Sea Plate, the Luconia

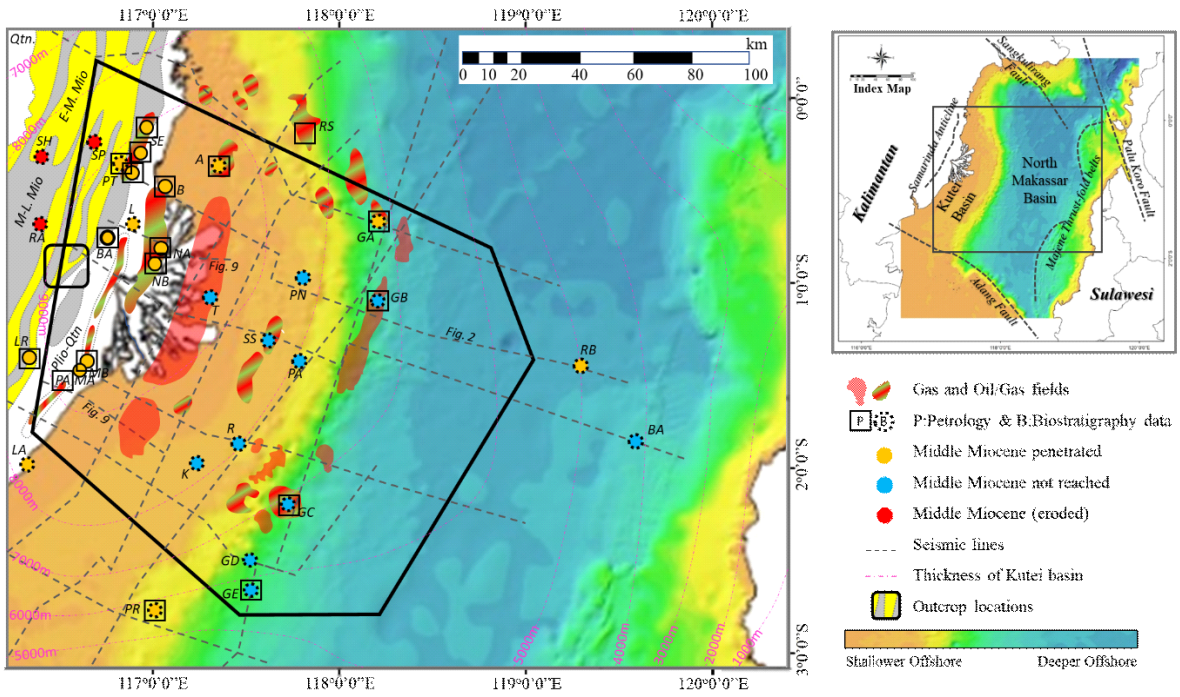

Figure 1. It shows simplified surface geological map (modified *from* Supriatna *et al*., 1995), hydrocarbon fields, well symbols, 2D seismic lines, Kutei sedimentary isopach, and water depth. Black rectangle is the study area. Index map shows the major bounding faults (*from* Nugrahanto *et al*., 2021)

continental crust had collided and docked onto the northern tip of of the Sundaland during the Middle Oligocene (Daines, 1985 and Hutchison, 1996; both *in* Soeria-Atmadja *et al*., 1999). The curvature suture of this collision is associated with the the Lupar Line where the imbricated ophiolites are found. The Late Eocene to Oligocene sag-related deep-to-shallow marine fine-grained materials deposited in a large embayment paleogeography (Morley and Morley, 2013; *in* Hall, 2013). This sub-regional sag was potentially associated with the ~35^{o} counter-clock wised (CCW) Borneo rotation (Advokaat *et al*., 2018).

3) As the subsidence gradually ceased by Late Oligocene, back-stepping reefal carbonates developed over the syn-depositional highs along the southern and northern edges of the Kutei Basin (van de Weerd *et al*., 1987; *in* Saller and Vijaya, 2002).

4) Early Miocene uplift and erosion along with the initiation of huge clastics progradation (Chambers and Daley, 1995; *in* Werdaya *et al*., 2017) had resulted in the proto Mahakam deltaic succession until the Late Miocene towards the present day, easterly (Moss and Chambers, 1999; *in* Werdaya *et al*., 2017). This contractional event is interpreted due to another ~10^{o} counter-clockwise Borneo rotation (Advokaat *et al*., 2018).

5) The prograded deltaic systems reached its highest sedimentation rate in Middle Miocene, known Middle Miocene Unconformity (MMU) that corresponds to the VIM 58-59, and up to the earliest late Miocene that fits with the VIM 62-64 (Morley *et al*., 2016).

6) Pliocene compressional event had emerged the West Sulawesi highlands to expose and erode the Mamasa granitoid then transported it into the deep-water Kutei Basin until the Recent. At the same time, N-S trend Samarinda Anticlinorium had been formed (Moss *et al*., 1997).

METHODS AND MATERIALS

Seismic-sequence stratigraphy

Basic concept of sequence stratigraphy is applied as it discusses rocks relationships in a chronostratigraphic framework of repetitive, genetically-related strata bounded by either erosional surfaces, hiatus, or correlative conformable stratas (Wagoner *et al*., 1988; *in* Nugrahanto *et al*., 2021). Lowstand, transgressive, and highstand system tracts (LST, TST, HST) are described based on the parasequence-sets. The most important system tract to notice is the type-1 sequence boundary (LST) that seismically may indicate forced-regressive shelf breaks (Posamentier, 2004; *in* Nugrahanto *et al*., 2021). At the same time, it can generate incised-valley erosional shape to deliver clastics deposits further into the slope break and basin floor during significant fall of relative sea-level.

The other alternative would be a gravity-driven mechanism at the down-slope along the sub-marine shelf margin was introduced by Shanmugam (2013, 2015, 2017) as the reasonable process in transporting the gravel to coarse-grained clastics into the slope and basin floor settings. The process includes debris flow, slump, and slide.

Integrating the outcrops, wells, and 2D seismic data are essential to generate the chronostratigraphic chart, isopach maps, and gross depositional environment (GDE) maps (Nugrahanto *et al*., 2021). These are able to define the depositional trends onshore and offshore.

Sedimentary-rock petrology

The tectonic setting of the provenance may contribute to the clastic-rocks composition (Dickinson and Suczek, 1979; *in* Tanean, 1994) and the sedimentary evolution that corresponds to the morphology gradient, depositional environments, distance between the hinterland to basin, subsidence rate, and weathering potential (Heins *et al*., 2007). The long process of transportation and sedimentation through the Proto Mahakam's fluvio-deltaic drainage systems toward the deep-water setting of north Makassar Basin become important aspect to indicate. The massive sediment transport through the incised valleys (IV) during periodic relative sea-level drops is thought to be inline with high-sedimentation rates. During the transportation process, the rocks went through the grain sorting, changed in the grain size and shape, until the post-sedimentation processes of burial compaction and at the same time depressed and exposed to the high temperatures (Tanean *et al*., 1996).

To extend the author's previous publication on the Early Miocene's rock samples *in* Werdaya *et al*. (2017), this study focuses to the Middle Miocene's petrography dataset taken from point-count analysis at the conventional core and side-wall core data. In addition to the previous well data, this study has added the other data points onshore-transition areas from Tanean (1994) and Tanean *et al*. (1996), as well as ten additional wellbores located offshore Kutei and deep-water North Makassar (Corelab, 2003). It is important to notice that various petrographers and service contractors, who had looked at the onshore and offshore dataset may apply different level of detail in their mineralogical descriptions.

This study will qualitatively predict the reservoir quality at the Middle Miocene's deep-water interval using

quartz, feldspar, and lithics (QFL) ternary diagram introduced by Folk (1988; *in* Aryati *et al*., 2019). The QFL generally demonstrates the sedimentary-source provenance, as well as the dominant composition of quartz minerals relative to the lithics and feldspars that have mainly related to the depositional facies. The rigid minerals comprise the lithics and feldspar components, while the ductile minerals consist of chert and clay minerals. Both minerals correspond to non-reservoir components as they have been very sensitive to the depth of burial (Werdaya *et al*., 2017). For the purpose of exhibiting the reservoir quality, the authors only utilize the porosity and permeability data from conventional core data.

RESULTS

Sub-regional Structure Geology and Depositional System

A schematic cross section was generated using the west-northwest to east-southeast (WNW-ESE) 2D seismic composite lines at the northern portion of the study area. The seismic-biostratigraphy correlation of the "M" markers had been carefully correlated to the sedimentation rates (Morley *et al*., 2016; *in* Nugrahanto *et al*., 2021). This section shows an overal prograding package with potential incised-valley (IV) features easterly. The western tip of the cross section structurally suggests a general trend of south-southwest to north-northeast (SSW-NNE) high-relief and tight inverted-fold belts that shifted into lower-relief and wider folds toward the present-day deep-water slope. It finally changes into much lower-to-no relief structure into the deep-water setting at the eastern tip of the study area (Figure 2).

The isopach maps within the "M markers" are utilized in generating several GDE maps (Figure 3) despite of the limitation of middle Miocene data points and seismic quality offshore deep water (Nugrahanto *et al*., 2021). Proto Mahakam River; red color in Figure 4 has been believed the paleo-drainage system in the Upper and Lower Kutei Basins covering the onshore areas such as Nyaan, Muyup, Kelian, Muara Wahau, Busang, and continues to the offshore depositional settings into the study area. Thicker isopach in Figure 3 shows the potential paleo-drainage systems that may represent incised-valley (IV) fill as well as sedimentary pods in the deltaic into the shallow marine environments. It established the potential clastic-reservoir filled into the slope and basin floor settings of the deep-water environment. Thinner isopach more easterly relates to the distal and / or condensed sections throughout the deep-water region.

QFL Composition

Previous analyses at mainly onshore petrographic samples throughout the delta to marine facies of the early-to-late Miocene's sediments provided four apparent petrologic subdivisions (Tanean, 1994 and Tanean *et al*., 1996): 1) the early Miocene's sediment (23-17 Ma), which was older than the M33 marker had moderate quartz and lithic components but high in volcanic-lithic components, 2) the latest early Miocene to the earliest Middle Miocene's sandstones (17-14.5 Ma) that nearly correlated to the M40-M33 zone were dominantly volcanogenic, 3) Middle to Late Miocene's sandstones, the equivalent to the M40-M65 zone, were highly composed by quartz with non-associated volcanic minerals, and finally 4) the Pliocene to Recent sandstones were similar to the type-2 (volcanogenic). All rock samples were the recycled orogen dominated by the lithic components that gradually changed to quartz dominant towards the younger-age formations.

Samples in this study come from twenty-nine onshore wells at the SE, PT, B, NA, NB, BA, MA, MB, and PA fields, and offshore wells at the A, RS, GA, GB, GC, GE, and PR fields (Figure 1) represent the deltaic to

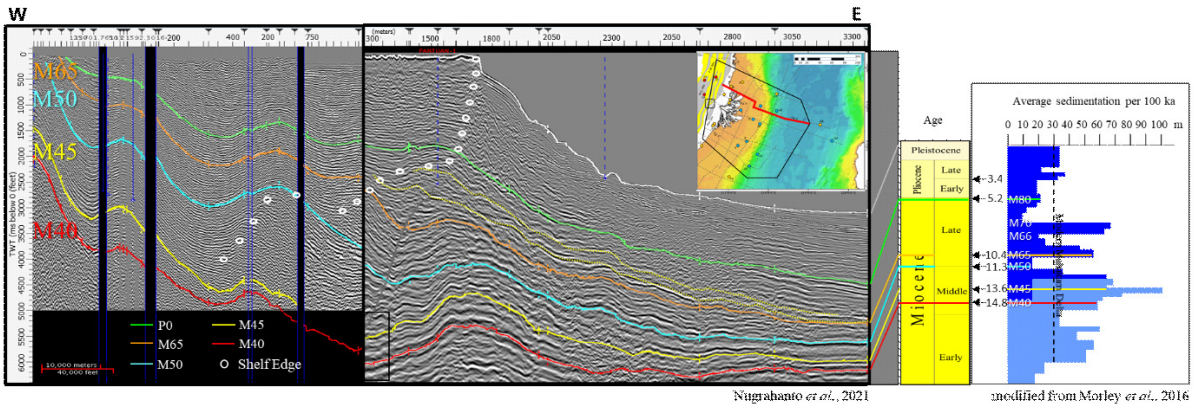

Figure 2. A 2D-seismic composite line showing "M" markers in prograding succession with Miocene's stratigraphic column and average sedimentation rates (modified from Nugrahanto *et al.,* 2021).

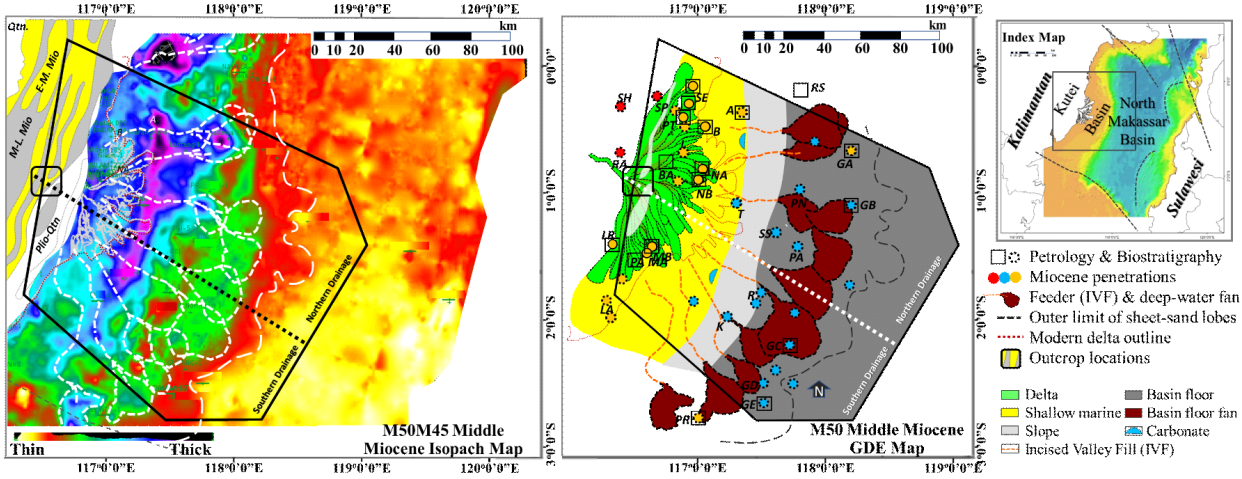

Figure 3. M45-M50 isopach maps (left) showing the paleo-drainage patterns, and a GDE map (Nugrahanto *et al*., 2021) of its uppermost part of the M45-M50 (right) illustrating the northern and southern drainage systems.

deep-marine depositional settings of the Kutei and North Makassar Basins (Figures 1 and 4). The QFL plot of the Middle to Late Miocene clastics shows that the samples mainly lie along the litharenitic trend on the right side of the ternary diagram. The remaining samples are located along the arkosic trends as shown on the left-hand side of the ternary diagram (Figure 4).

The Cretaceous-age rocks exposed along the Sibu-Rajang Accretionary Prism is interpreted to be the sedimentary provenance for the Early Miocene's (N4-N7 or older than the younger section that equivalent to the M40M33 (N8A-early N10), volcanogenic sandstones were defined since the volcanic-lithic fragments in it increased from the average of <10% to >20% of the framework grains (Tanean *et al*., 1996). The overall Middle Miocene sections (M40-M50 or N10-N14) was categorized high-quartzose sandstones as they have an average of >80% of the framework grains (Tanean *et al*., 1996; and Figure 5 in this study, 2021). The Middle Miocene's (M50M45 and M45M40) and the lower part of Late Miocene's sam-

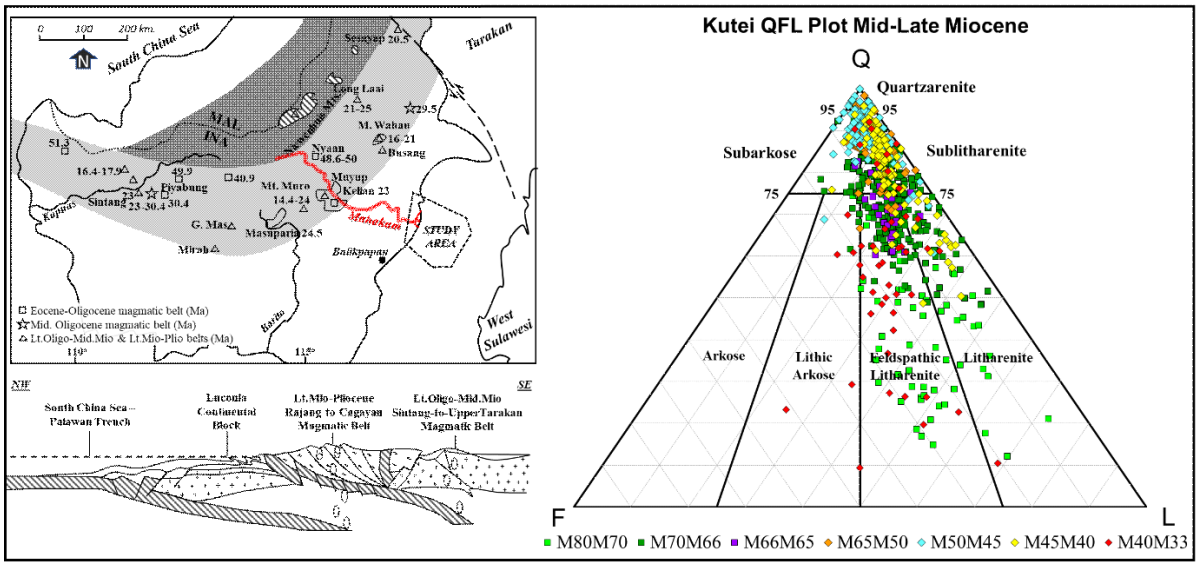

Figure 4. A NW-SE section and basemap showing the dark-grey and light-grey polygons, which are the magmatic belt of Late Oligocene to Middle Miocene (Eocene subduction) and Middle Miocene to Pliocene (Palawan subduction), respectively (modified from Soeria-Atmadja *et al*., 1999). The ternary diagram is the QFL grouping of the Middle-to-Late Miocene mineralogy in the study area.

M33 marker) moderately quartzose sandstones (Tanean *et al*., 1996; Soeria-Atmadja *et al*., 1999), where most of the lithic content is from the sedimentary and metamorphic-rock particles (Werdaya *et al*., 2017). Going up to ples (M65M50) have the highest quartz (the average of >80%) but oppositely have the lowest feldspar and lithic compositions (Figure 5). In summary, the rock samples in this study exhibit a turtle-shaped trend that goes from

the lowermost part of Middle Miocene (M40M33) with the low-quartz content but high in rigid materials (feldspar and lithics). It gradually changes into the majority of the Middle to Late Miocene rock samples that show higher-quartz content but low in rigid materials. And interestingly, the uppermost part of Late Miocene had inspired this study's hypothesis that there must have been long but sufficient processes of sediment transport and its sedimentation through the drainage systems of the proto-Mahakam's deltaic (Kutei Basin) towards the deep-water settings at the North Makassar Basins (Figures 3 and 4).

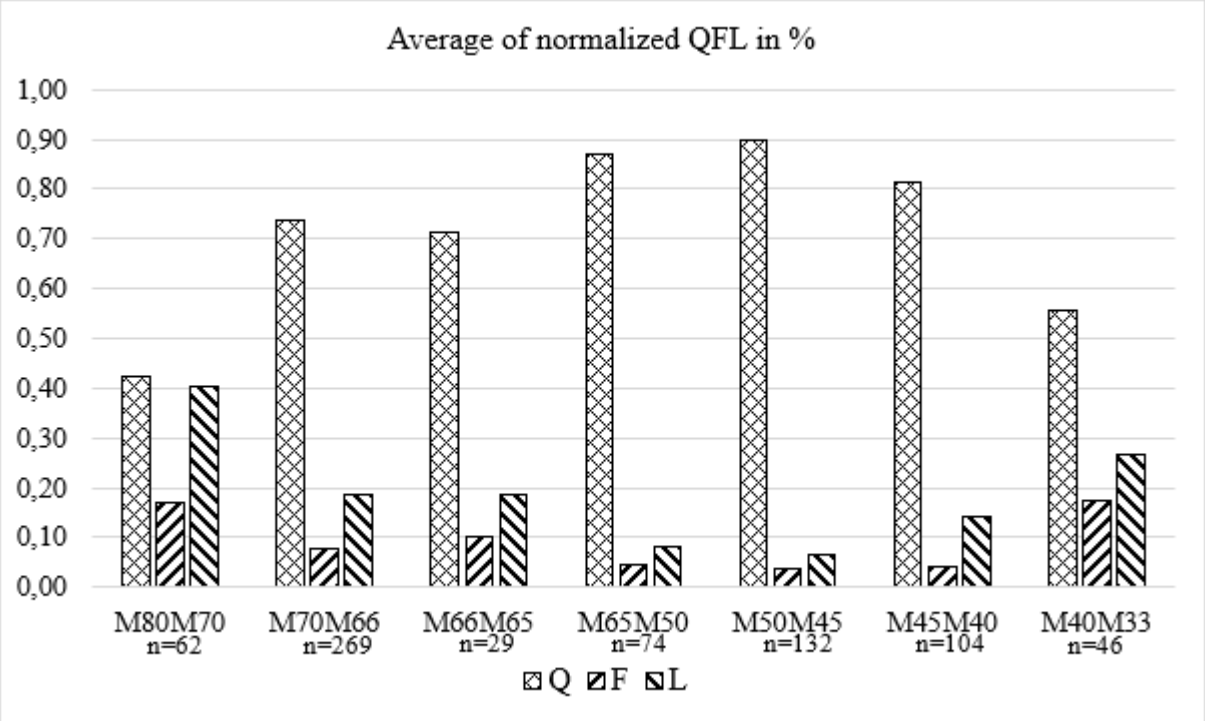

Figure 5. A bar graph showing the average composition of normalized QFL grains from the earliest Middle Miocene (M40M33) to the upper part of Late Miocene (M80M70).

(M80M70) is nearly similar to the composition of the M40M33's rock samples (Figure 5).

DISCUSSIONS

This study observes the QFL classification of the onshore and offshore samples, but mainly focuses in predicting the unpenetrated Middle Miocene's deep-water sandstones. To be compared with the existing deep-water's producing sandstones, this study includes the Late Miocene's rock samples. The highest sedimentation rate of the Kutei and outboard Sabah Basins was indicated in the middle to late Miocene as the result of Sabah uplift and erosion (Hutchinson, 2005; *in* Morley *et al*., 2016), and is potentially able to deliver huge clastics materials into the paleo deep-water slope of the north Makassar Basin through the incised valleys (IV) and slump scars trending parallely to the anticline of Tunu Field (Yoga *et al*. 2009 *in* Nugrahanto *et al*., 2021). This huge sedimentary mass initiated the gravitational flow to form the toe-thrust fold belt in the distal part of the system (McClay, 2000). These references This study pays more attention to lowstand and highstand system tracts (LST and HST) that enable periodic sub-regional incisions and / or collapses along the marine-shelf edge. Forced regressions that responded to the relative sea-level fall were observed by well and seismic data onshore and offshore (Nugrahanto *et al*., 2021). These events were indicated by the increase in sedimentation rates with significant shelf-break progradation at the northern and southern parts of the Kutei Basin during the deposition of M40M45 intervals. Decreasing of the sedimentation rates took place at the lower part of the M45M50, and had reached the lowest rate at the top most of the M50 before the rate was back to increase towards the top of M65 marker. These dynamic process of Middle Miocene deposition had subdivided drainage clusters of the Kutei Basin into north and south (Figure 3).

Middle Miocene's Mineralogy, Litho Facies, and Reservoir Quality

The Middle Miocene's rock samples are taken from around thirty wellbores located onshore. The deposi-

tional environment of the sandstone reservoirs is divided into fluvial-deltaic plain channels and delta-front bars. The sandstone's litho facies is further subdivided into four classifications: 1) cross-bedded fluvial sandstones (FLU_SX and DC_SX), 2) massive distributary channels (DC_SM), 3) bioturbated distributary channels (DC_SB), 4) bioturbated with mud/clay drapped bars (DF_SC). These are illustrated in the Figure 6, as well as the detailed core-description, core photos, and well-log types (modified from Butterworth *et al*., 2001; Lambiase *et al*., 2017; Riadi *et al*., 2018).

Figure 7 demonstrates the best quality of sandstone's litho facies are dominated by FLU_SX of both M50M45 and M45M40 sections, while small part of this category is represented by the litho facies DC_SX of M50M45 and DF_SC of M45M40. The detailed description of these litho facies characterized by upper medium- to lower coarse-grained sublitharenite sandstones that have cross-bedding structures, overall blocky to upwards fining succession, but relatively massive textures (non-laminated), moderately to well sorting, subangular to subrounded grains, none to traces porefilling cements/ overgrowth of quartz (<1.5%), carbonate (<10% siderite), and clay materials (<5% of kaolinite).

Common sedimentary structures associated with concretion-rich layers are parallel laminae and trough cross-bedding with high-energy that closely relate to insignificant fall of relative sea level. The other high-energy features are illustrated by planar and trough cross beddings (Chiarella & Longhitano, 2012, Longhitano *et al*.,2014 both *in* Ghaznavi *et al*., 2019). The coarse-grained sediments suggest a range of moderate to high energy depositions (Boggs, 2009; *in* Ghaznavi *et al*., 2019), while the well-sorted and subrounded grains are devoid of matrix, also indicating a high-energy beach subenvironment (Ghaznavi *et al*., 2019). The low-carbonate cements had usually been observed in the high-energy deposition like the distributary channels (Werdaya *et al*., 2017). These references suggest the FLU_SX, DC_SX, and DF_SC of the Middle Miocene (M50M45 and M45M40) sandstone's litho facies had been associated with the high-sedimentation rate (Morley *et al*., 2016; shown in the Figure 2), which might potentially be related to the relative sea-level fall (Nugrahanto *et al*., 2021).

In contrast to the best sandstone reservoir aforementioned, the bottom-left corner of Figure 7 displays the poor quality of sandstone's litho facies DF_SC (M45M40), DC_SX (M50M45 and M65M50), FLU_SX (M50M45), and DC_SB (M50M45). This category reflects high variation in the litho facies, however the most distinctive aspects that set them into poor quality are mixed medium-to fine-grained and mainly laminated sandstones with more pore filled with cements such as calcite and dolomites (trace – up to 10%), and quartz (1.5% - 8%), in addition to the siderite and kaolinite within the best reservoir quality. This study also observed the increase of rigid materials (feldspar and lithics). However, normalized lithics incremental of >10% - up to 30% looks more significant than the feldspar, which are both higher than the one at best-quality sandstone's litho facies.

Ahmad *et al*. (2013 *in* Ghaznavi *et al*., 2019) found that a low-energy environment is represented by the gypsiferous shale and siltstone to sandstone facies. Werdaya *et al*. (2017) suggested the Early Miocene sandstones are mainly composed by ductile to rigid detrital minerals associated with low-energy of deposition, which may potentially be sensitive to the depth of burial. Likewise, the porosity of the sandstones dramatically reduce to <5% when the carbonate cement exceeds >6%, and the permeability down to 0.1 mD to become non-reservoir rock. In line with these citations, the increase of burial depth in the study area may damage the DF_SC, DC_SX, FLU_SX, and DC_SB litho facies even if they were medium-grained sandstones. Along with the depth of burial aspect, higher quartz cement would definitely reduce these litho facies into none reservoir quality; in particular the DF_SC litho facies that demonstrate <5% core porosity and <0.1 mD core permeability (Figure 7).

The ternary diagram in Figure 6 shows five group of rock samples: (a) the samples from LR and PA wells demonstrate the older strata (M40M33) in the southern drainage system is dominated by the shallow-marine sandstones. They have dominant lithic arkose to feldspathic litharenite classification. (b) The remaining M40M33 samples from NA, NB, and P wells in the northern drainage are mainly sublitharenite to litharenite composition. The decreasing of feldspar and lithic contents in the younger strata of M45M40 can be subdivided into two sub classifications: (c) a wide range from sublitharenite, feldspathic litharenite, and litharenite at the SE and P wellbores representing the northern drainage, and (d) subarkosic dominant as shown in the samples from PR and PA wells representing the southern drainage. (e) The uppermost Middle Miocene samples of M50M45 have less feldspar and lithic contents than the previous two intervals at both the northern (NA and NB wells) and the southern (MA and MB wells) drainages.

The ternary diagram in Figure 8 shows the opposite trend from the older (M65M50) to the younger

(M80M70) sections, where (a) to (d) reflects the decrease of quartzarenite and sublitharenite compositions to become more feldspathic litharenite and litharenite.

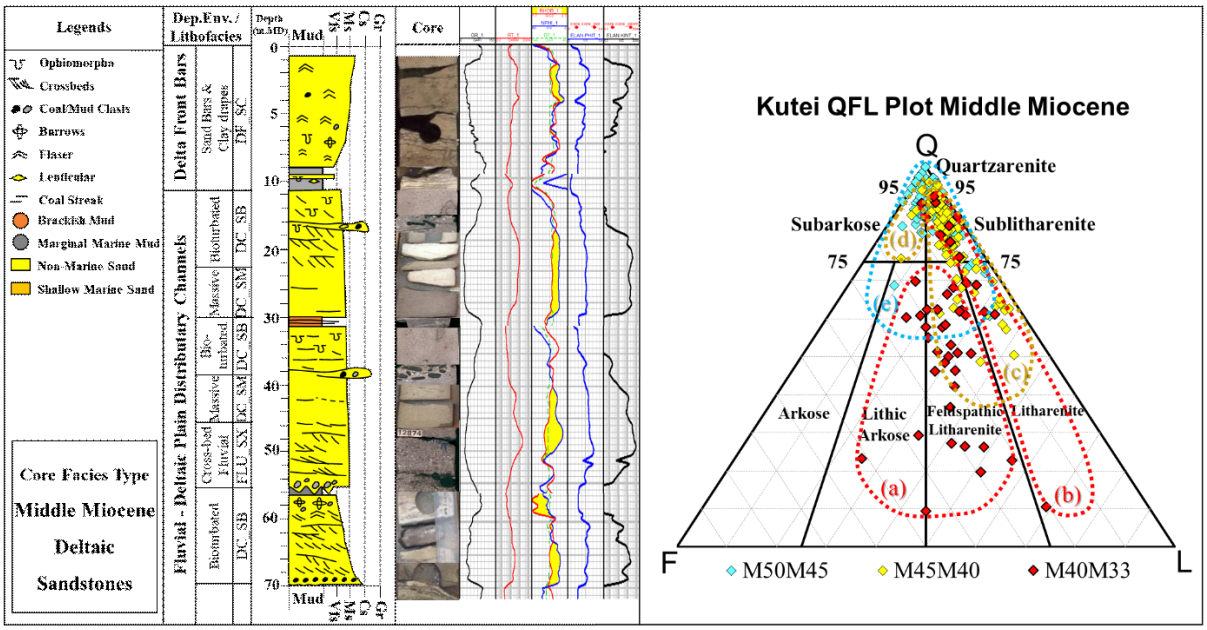

Figure 6. Core-facies Type of the Middle Miocene deltaic sandstones (modified from Butterworth *et al*., 2001; Lambiase *et al*., 2017, and Riadi *et al*., 2018), along with their QFL grouping in the ternary diagram.

It is important to notice that the best sandstone's litho facies of FLU_SX commonly has blocky and / or upwards fining (bell-shaped) GR-log. Contrarily, the poor sandstone's litho facies of DF_SC, DC_SX, FLU_SX, and DC_SB are various in the well-log types due to mixed descriptions of grain size (fine to medium), depth of burial, and cementations. The lowest core porosity and permeability values are mainly observed in the DF_SC litho facies that usually has upwards coarsening (funnel-shaped) GR log (Figures 6 and 7).

Late Miocene's Mineralogy, Litho Facies, and Reservoir Quality

The Late Miocene's samples from ten wellbores located offshore have been evaluated in order to characterize the depositional environment of the sandstone reservoirs. It is noteworthy most of these rock samples do not reach the lowest part of the Late Miocene (M65M50) interval except three wellbores in the northern drainage. Regrettably, there have been none of conventional core data representing the deep-water slope to basin floor settings in the M65M50. Therefore, this study refers to Saller *et al*. (2008) who had described the core data of Gendalo Late Miocene 1020 sandstone (7–8 Ma). This is equivalent to the M70M66 marker, which is associated with the highest sedimentation rate or maximum progradation throughout the Kutai Basin (Figure 2). The coherency attribute from 3-D seismic data (Saller *et al*., 2008) and regional isopach map (Nugrahanto *et al*., 2021) had defined the northwestern feeder system as the source of sediments for the deep-water slope fans in this specific area.

There are four litho facies had been reported is Saller *et al*. (2008): 1) High net-to-gross (NTG) ratio of 65%-100% sand, called Ta – the fine-grained massive sandstone with good porosity (20%-30%) and permeability (100-2,000 mD) that has an average individual sand beds of <1.0 feet, but rarely amalgamated. 2) Medium NTG ratio of 30%-65% sand, assigned Tb and Tc – the Tb is fine-grained and parallel laminae sandstone with coal-organic matters; while the Tc is very fine-grained rippled sandstone. 3) Low NTG ratio of 10%-30% sand (Tc); and 4) Non-reservoir with NTG ratio of <10%, which are mainly shale and debrites (Figure 8). The sandstones are generally dark color as they comprise abundant carbonaceous-organic matters that are commonly revealed within the parallel-laminated sandstones (Tb); Saller *et al*. (2006 *in* Saller *et al*., 2008).

This study had observed deep-water's litho facies in relationship with their reservoir quality; as shown at Figure 9: (i) a group of high porosity (>22%) with moderate (>35 mD) to high (>100 mD) permeability, which is predominantly well-sorted, fine to medium-grained sandstones; (ii) another group of moderate porosity (17%-22%) with moderate (>11-100 mD) to high permeability (>100 mD) that shows well-sorted, fine-grained sand-

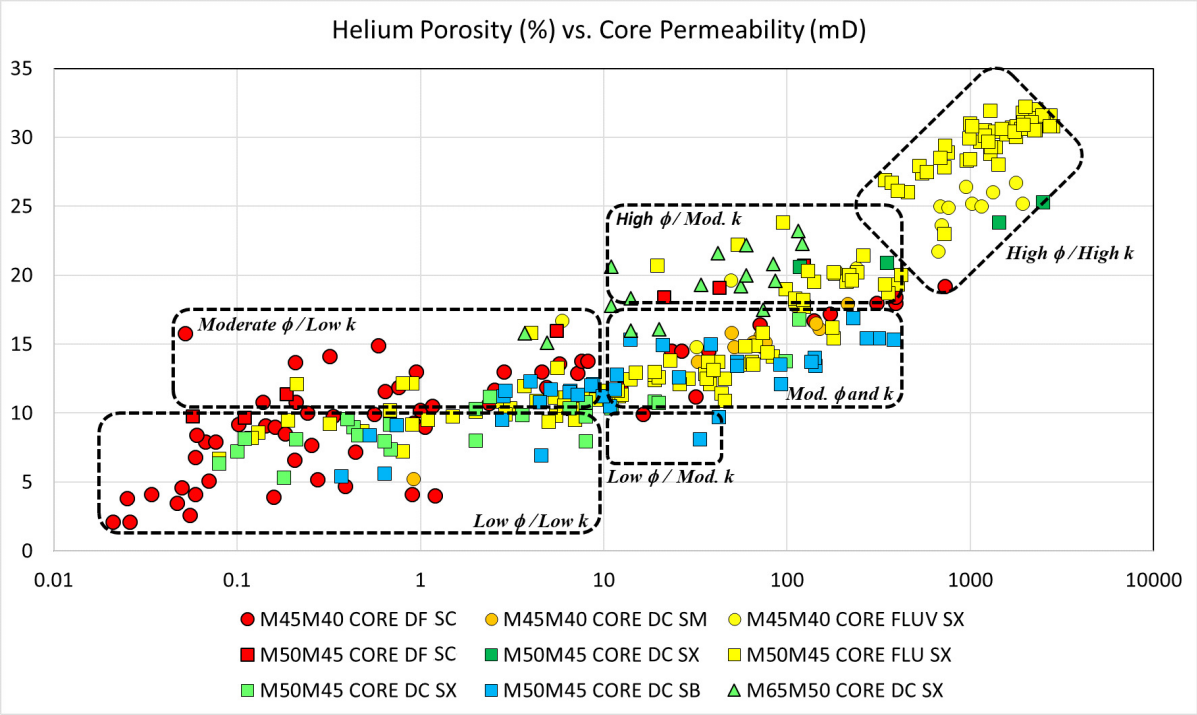

Figure 7. A cross plot of core-porosity vs. core-permeability in relation to the sandstone's litho types in the Middle Miocene section.

stone. Both group (i) and (ii) are mainly well-sorted sandstones (SSWS) with minor exception from medium-grained, poorly-sorted sandstones (SSPS) that have negligible clay matrix, but slightly high cements (>10%); and from fine- to medium-grained, poorly-sorted muddy sandstone (MSPS) that contains low clay matrix (none to <15%) and low cements (<6%). The last group (iii) is low to moderate porosity (up to 26%) with low permeability (<11 mD) poorly sorted sandstone (SSPS), and poorly sorted muddy sandstone (MSPS) with little anomaly from well sorted sandstone (SSWS) and well-sorted muddy sandstone (MSWS); where all containing high-clay matrix of >16% - up to 50%. Important to note the core porosity and permeability data @ambient condition is selected to represent more samples (than @overburden condition) since the difference of both conditions are considerably small; 1% to 4%.

Aligning the NTG-based (Saller *et al.*, 2008) and sorting-based (this study, 2021) of the deep water's lithofacies grouping, conclude that high-NTG ratio is closely related to well-sorted sandstone litho facies; while lower NTG-ratio is associated with poorly-sorted sandstone litho facies.

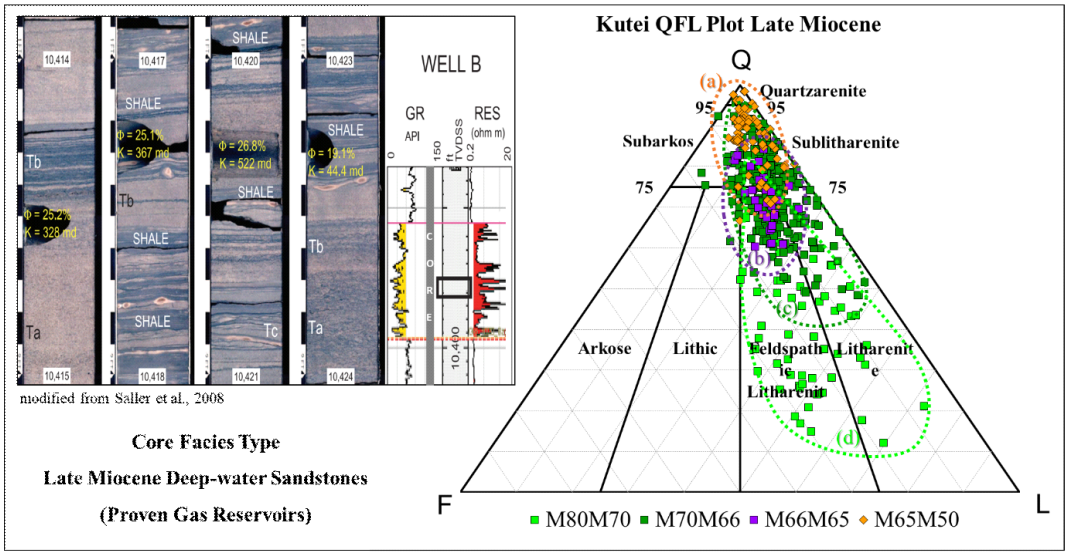

Figure 8. Core-facies Type of the Late Miocene deep-water sandstones (modified from Saller *et al.*, 2008) with the ternary diagram showing the QFL grouping of the Late Miocene interval.

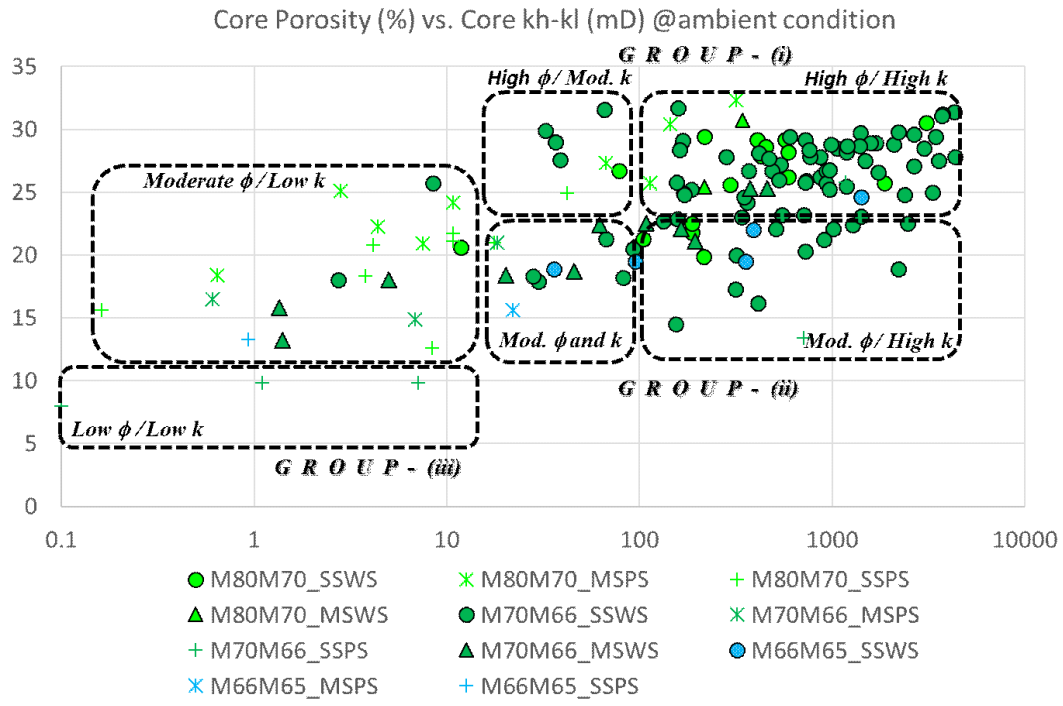

Figure 10. A cross plot of core-based helium porosity (%) versus the maximum burial depth (in feet), which is below mudline (bml) for the offshore wellbores. The circles are the Late Miocene, while the square ones are the Middle Miocene's rock samples data point.

The overall samples in the Late Miocene stratas have negligible arkosic content and predominantly litharenitic as seen on the right hand side of the ternary diagram. Opposite to the Middle Miocene's QFL trend, the Late Miocene's shows incremental lithic but reduction in quartz contents toward the younger strata from M65M50 (a) to M80M70 (d) strata (Figure 8).

Predicting the Reservoir Quality

Relational trends of the core-based porosity with maximum-burial depth and their associated litho facies are illustrated in the Figure 10. The rock samples are from conventional core data in the wellbores located onshore and offshore where the circles are the Late Miocene's deep-water facies, and the squares are the Middle Miocene's deltaic facies data point. Three permeability cut-off trends are plotted to classify the quality of reservoirs, which have been divided into none-poor (<10 mD), moderate-good (10-100 mD), and excellent (>1000 mD) reservoir quality. As discussed earlier, the Middle Miocene's deltaic FLU_SX, DC_SX, and DC_SM litho facies represent the excellent reservoir quality, while the DF_SC litho facies dominates the none-poor ones. The excellent reservoir quality of the Late

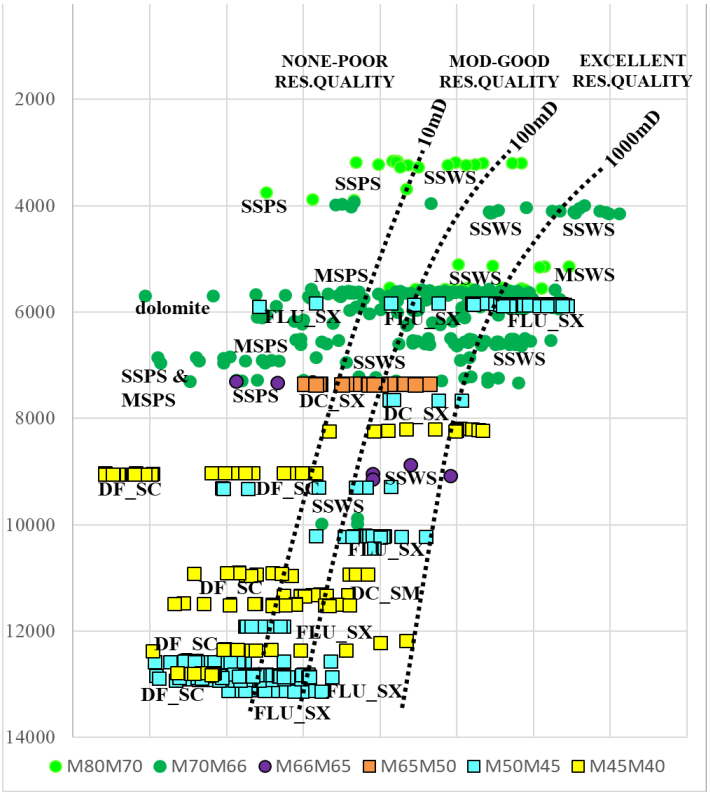

Figure 10. A cross plot of core-based helium porosity (%) versus the maximum burial depth (in feet), which is below mudline (bml) for the offshore wellbores. The circles are the Late Miocene, while the square ones are the Middle Miocene's rock samples data point.

Miocene's deep-water reservoir has been dominated by the SSWS lithofacies, while the none-poor ones are portrayed by the SSPS and MSPS litho facies.

The cross plot of the core-based porosity versus depth in Figure 10 shows a general trend of decreasing porosity with increasing of depth. One thing that stands out most when the decrease of core-based permeability's trend line with depth is not as much as the other two permeability trend lines. It is clearly seen that the reservoir's litho facies of clean (low clay matrix and cements), fine to medium-grain size, and well sorting is able to maintain its quality against the depth of burial.

Comprehensive seismic and well-based GDE mapping is considerably very important to assess and locate the litho facies variation especially the ones associated with the high-energy deposition. Extracting the litho facies information from the GDE map would be able to predict the porosity and permeability of the unpenetrated Middle Miocene's deep-water reservoirs.

CONCLUSIONS

The Middle to Late Miocene (M40 to M70 markers) rock samples reveal a strong correlation between the high quartz and low feldspar-lithics trend with the high peaks of sedimentation-rate package, which is much higher than any peaks within the Late Miocene to the modern-day Mahakam. The proto Mahakam River has been widely considered as the Neogene's drainage systems that delivered most of the sediments toward the Kutei and North Makassar basins. Thicker isopach provided paleo-drainage systems of either incised-valley fill and / or sedimentary pods in the deltaic to marine-shelf settings, and led the potential high-energy deposition of clastic-reservoirs further into the deep-water slope and basin floor settings.

Contrarily to the M40 to M70 interval, low-quartz but high content in rigid materials (feldspar and lithics) are exhibited in the rock samples from the onshore wellbores of the older Middle Miocene (M40M33) to Early Miocene (M33 and older), as well as the uppermost part of Late Miocene (M80M70). The M40M33 in the southern-drainage system is dominated by lithic arkose to feldspathic litharenite, while the rock samples in the northern drainage are mainly sublitharenite to litharenite composition.

The Middle Miocene FLU_SX deltaic litho facies that commonly has upwards fining (bell-shaped) to blocky GR-log is identified the best reservoir quality among the rock samples from the onshore wellbores. The Middle Miocene DF_SC, DC_SX, DC_SB, and even the FLU_SX deltaic litho facies are observed poorer in reservoir quality due to huge variation in finer grain size, depth of burial, as well as the carbonate cementation. The upwards coarsening (funnel-shaped) GR log of DF_SC litho facies is commonly found the worst in reservoir quality.

In the absence of deep-water facies rock samples; especially the conventional core data from the Middle Miocene age, this study has classified the Late Miocene's deep water litho-facies into groups and found the alignment between NTG-based with the sorting-based litho facies. It summarizes that the best deep-water sandstone reservoir has high-NTG ratio and good sorting, while oppositely the lower NTG-ratio and poorly-sorted ones represent the worst reservoir quality. The Late Miocene rock samples reveal negligible arkosic with predominantly litharenitic contents, and exhibits the increase in lithic but reduction in the quartz contents toward the younger strata from M65M50 (a) to M80M70 (d) strata.

The litho facies of fine-to medium-grained, and well-sorted sandstone reservoirs that contain negligible-to-low clay matrix and cements would be able to preserve its quality against the burial depth. The cross plot exhibits the decrease of the excellent permeability's trend line with depth is not as aggressive as the other two permeability trend lines. The GDE mapping is very essential to afford the important information of the litho facies that go along with the high-energy deposition, which may be able to provide the excellent reservoir quality.

ACKNOWLEDGEMENTS

The authors would like to thank the Faculty of Geological Engineering of the University of Padjadjaran (Unpad), as well as the Centre of Data and Information Technology (Pusdatin), which is under the Ministry of Energy and Mineral Resources (ESDM) of Indonesia. The supporting data from, and the technical consultation with the Exploration New Ventures Team at Upstream Subholding Pertamina Hulu Energi (PHE SHU), Pertamina Hulu Sanga Sanga (PHSS), Pertamina Hulu Kalimantan Timur (PHKT), and Pertamina Hulu Mahakam (PHM) have been really constructive. Without all of these continuing supports, this study would have not been completed. Our gratitude is also conveyed to every parties whose contribution were significant in this study, which is Kuntadi Nugrahanto's thesis at the magister program of Unpad. This study is the authors' personal view hence do not represent all the above-mentioned organizations.

REFERENCES

Advokaat, E.L., Marshall, N.T., Li, S., Spakman, W., Krijgsman, W., and van Hinsbergen, D.J.J., 2018.

Cenozoic Rotation History of Borneo and Sundaland, SE Asia Revealed by Paleomagnetism, Seismic Tomography, and Kinematic Reconstruction. *Tectonics July 2018*, p.1-27.

Baryati, F. D., Setiawan, T., Meilany, Y., Assalam, A., 2019. The Progressive Illitization Process, Diagenetic Mechanism and Its Effect on Reservoir Quality Based On SEM, Burial History, and Simultaneous Multi-Well Analysis: A Case Study in The Sanga-Sanga Block, Kutai Basin, East Kalimantan. *Proceedings Indonesian Petroleum Association 43rd Annual Convention and Exhibition, October 2019*.

Butterworth, P.J., Cook, P., Dewanto, H., Drummond, D., Kiesow, U., McMahon, I.T., Ripple, R.A., Setoputri, A., and Sidi, F.H., 2001. Reservoir Architecture of an Incised Valley-fill from The Nilam Field, Kutai Basin, Indonesia. *Proceedings Indonesian Petroleum Association 28th Annual Convention and Exhibition, October 2001*.

Corelab, 2003. Kutei Basin Regional Evaluation, Chapter 6: Reservoir Quality, Section 6.3: Petrographic Analysis of Diagenetic Effects. Internal Report of Unocal Indonesia, unpublished.

Duval, B.C., de Janvry, G. C., Loiret, B., 1992. *Offshore Technology Conference*, 4-7 May, Houston, Texas.

Ghaznavi, A. A., Quasim, M. A., Ahmad, A. H. M., Ghosh, S. K., 2019. Granulometric and facies analysis of Middle-Upper Jurassic rocks of Ler Dome, Kachchh, western India: an attempt to reconstruct the depositional environment. *Geologos 25, 1 (2019)*: 51-73.

Hall, R. and Sevastjanova, I., 2012. Australian Crust in Indonesia. *Australian Journal of Earth Sciences*, 59: 827-844).

Hall, R., 2013. The Palaeogeography of Sundaland and Wallacea Since the Late Jurassic, *J. Limnol.*, 72(s2): 1- Geological History. DOI: 10.4081/ jlimnol.2013.s2.e2

Heins, W. A., Kairo, S., 2007. Predicting sand character with integrated genetic analysis. *Geological Society of America Special Papers 2007*; 420; 345-379. DOI:10.1130/2006/2420(20) downloaded from specialpapers.gsapubs.org on June 22, 2015.

Lambiase, J. J., Riadi, R. S., Nirsal, N., Husein, S., 2017. Transgressive successions of the Mahakam Delta Province, Indonesia. From: Hampson, G. J., Reynolds, A. D., Kostic, B. & Wells, M. R. (eds) 2017. Sedimentology of Paralic Reservoirs: Recent Advances. *Geological Society, London, Special Publications, 444*, 335 –348.

McClay, K., Dooley, T., Ferguson, A., and Poblet, J., 2000. Tectonic Evolution of the Sanga Sanga Block, Mahakam Delta, Kalimantan, Indonesia. *The American Association of Petroleum Geologists (AAPG) Bulletin*, 84(6): 765-786.

Metcalfe, I., 2011. Tectonic Framework and Phanerozoic Evolution of Sundaland. *Gondwana Research*, 19: 3-21.

Metcalfe, I., 2013. Gondwana Dispersion and Asian Accretion: Tectonic and Palaegeographic Evolution of Eastern Tethys. *Journal of Asian Earth Sciences*, 66: 1-33.

Morley, J.M., Morley, H.P., and Swiecicki, T., 2016. Mio-Pliocene Palaeogeography, Uplands and River Systems of the Sunda Region Based On Mapping Within A Framework of VIM Depositional Cycles. *Proceedings, Indonesian Petroleum Association 40th Annual Convention and Exhibition, May 2016.*

Moss, S.J., Chambers, J., Cloke, I., Satria, D., Ali, J.R., Baker, S., Milsom, J., and Carter., 1997. New Observation on the sedimentary and tectonic evolution of the Tertiary Kutai Basin, East Kalimantan. *in* Fraser, A. J., Matthews, S. J., and Murphy, R. W. (Eds.). *Petroleum Geology of Southeast Asia*. Geological Society Special Publication, 126: 395-416.

Nugrahanto, K., Syafri, I., Muljana, B., 2021. Depositional Environment of Deep-Water Fan Facies: A Case Study of the Middle Miocene Interval at the Kutei and North Makassar Basins. *Journal of Geology and Mineral Resources*, Vol. 22. No. 1 Februari 2021 hal 45-57.

Riadi, R. S., Permana, R. C., Setoputri, A., Andaryani, S., 2018. Fresh Outlook of Reservoir Understanding and Implication for Further Development Strategy of Mature Fields, Case Study from Semberah and Mutiara Fields, Kutei Basin, Indonesia. *Proceedings: Indonesian Petroleum Association 42nd Annual Convention and Exhibition, May 2018.*

Saller, A.H., and Vijaya, S., 2002. Depositional and Diagenetic History of the Kerendan Carbonate Platform, Oligocene, Central Kalimantan, Indonesia. *Journal of Petroleum Geology*, 25(2): 123-150.

Saller, A., Werner, K., Sugiaman, F., Cebastiant, A., May, R., Glenn, D., and Barker, C., 2008. Characteristics of Pleistocene Deep-water Fan Lobes and Their Application to an Upper Miocene Reservoir Model, Offshore East Kalimantan, Indonesia. *The American Association of Petroleum Geologists Bulletin*, 92(7): 919–949.

Shanmugam, G., 2013. New Perspectives on Deep-water Sandstones: Implications. *Petrol. Explor. Develop.*, 40(3): 316–324.

Shanmugam, G., 2015. Lithofacies Palaeogeography and Sedimentology - Submarine Fans: A Critical Retrospective (1950-2015). *Journal of Palaeogeography*, 5(2):110-184 (00095).

Shanmugam, G., 2017. Contourites: Physical Oceanography, Process Sedimentology and Petroleum Geology. *Petroleum Exploration and Development*, 44: 183–216.

Shuang Li, S., Yang, X., Sun, W., 2015. The Lamandau IOCG deposit, southwestern Kalimantan Island, Indonesia: Evidence for its formation from geochronology, mineralogy, and petrogenesis of igneous host rocks. *Ore Geology Reviews 68* (2015) 43-58.

Soeria-Atmadja, R., Noeradi, D., Priadi, B., 1999. Cenozoic magmatism in Kalimantan and its related geodynamic evolution. *Journal of Asian Earth Sciences 17 (1999),* 25-45.

Supriatna., S., Sukardi, and Rustandi, E., 1995. *Geological Map of Samarinda Sheet, 1:250,000*. Geological Research and Development Center, Bandung, Indonesia.

Tanean, H., 1994. Petrology and Provenance of the Miocene Sediments in the Kutai Basin, Appendix 8.1: Reservoir Studies – Hondiro Tanean. File/ Report No. GR.950601, Map No.: 1405-20. Virginia Indonesia Company (VICO), unpublished.

Tanean, H., Paterson, D. W., Endharto, M., 1996. Source Provenance Interpretation of Kutei Basin Sandstones and The Implications for The Tectono-Stratigraphic Evolution of Kalimantan. *Proceedings Indonesian Petroleum Association 25th Silver Anniversary Convention and Exhibition, October 1996.*

Werdaya, A., Alexandra, M., Nugrahanto, K., Anshori, R., Pradipta, A., Armitage, P., 2017. Comprehensive Evaluation of Reservoir Quality in the Early Miocene, Kutei Basin, Onshore East Kalimantan. *Proceedings Indonesian Petroleum Association 41st Annual Convention and Exhibition, May 2017.*

Witts, D., Davies, L., Morley, R., 2014. Uplift of the Meratus Complex: Sedimentology, Biostratigraphy, Provenance, and Structure. *Proceedings Indonesian Petroleum Association 38th Annual Convention and Exhibition, May 2014.*

Witts, D., Davies, L., Morley, J.M., and Anderson, L., 2015. Neogene Deformation of East Kalimantan: A Regional Perspective. *Proceedings Indonesian Petroleum Association 39th Annual Convention and Exhibition, May 2015*.

DISTRIBUTION OF SUBSURFACE SEDIMENTATION AS A POTENTIAL MINERAL PLACER DEPOSITS IN SOUTH BINTAN ISLAND WATERS

SEBARAN SEDIMENTASI BAWAH PERMUKAAN SEBAGAI POTENSI ENDAPAN MINERAL PLACER DI PERAIRAN SELATAN PULAU BINTAN

Muhammad Zulfikar[1,2], Nazar Nurdin[2], Noor Cahyo Dwi Ariyanto[2], Ildrem Syafri[3], Budi Mulyana[3], Andi Agus Nur[3]

[1]Study Program of Master, Faculty of Geological Engineering, Padjadjaran University
Jl. Raya Jatinangor Km. 21 Bandung, Indonesia
[2]Marine Geological Institute of Indonesia
Jl. Dr. Djunjunan No.236 Bandung, Indonesia
[3]Faculty of Geological Engineering, Padjadjaran University
Jl. Raya Jatinangor Km. 21 Bandung, Indonesia

Corresponding author: muhammad20389@mail.unpad.ac.id; muhammad.zulfikar@esdm.go.id

(Received 7 June 2021; in revised from 18 June 2021; accepted 26 July 2021)

ABSTRACT: Bintan Island is one of the areas traversed by the Southeast Asian granitoid belt which is known to have the potential for heavy mineral placer deposits. Due to the dwindling presence of heavy mineral placer deposits in land areas, it is necessary to explore in water areas. Delineation of deposits accommodation of heavy mineral placer in the defined area are requires subsurface imaging investigations. The method used in this subsurface mapping is a single channel seismic method with a total of 179 lines from northeast-southwest and west - east directions. The results of this seismic record are then interpreted as the boundaries of the seismic facies unit and distributed using the kriging method. Furthermore, the thickness calculates by using the assumption velocity of 1600 m/s.

Based on the facies unit boundaries that have been interpreted, the quaternary sediments that formed in the study area are divided into 2 types of units, namely: Unit 2 which is estimated to be fluvial - transitional sediment, and Unit 1 which is estimated to be transitional - shallow marine sediment. There is also a difference in thickness patterns in these two units, where Unit 2 shows a pattern of sediment thickening that resembles a paleochannel trending northeast - southwest, while Unit 1 is relatively uniform.

From the results of this study, it can be said that the area that has potential of heavy mineral placer deposits is in the west-center of the southern waters of Bintan Island. Where the potential for heavy mineral placer deposits should be in the paleochannel deposits that are part of Unit 2.

Keywords: Quaternary Sediments, Heavy Mineral Placer Deposits, Rare Earth Elements, Southern Waters of Bintan

ABSTRAK: *Pulau Bintan merupakan salah satu wilayah yang dilalui oleh jalur granitoid Asia Tenggara yang dikenal memiliki potensi keterdapatan mineral berat plaser. Akibat keberadaan mineral berat plaser di wilayah daratan semakin menipis, maka dilakukan pencarian potensi tersebut di wilayah perairan. Delineasi wadah mineral berat plaser pada area ini memerlukan penyelidikan citra bawah permukaan.*

Pemetaan bawah permukaan ini menggunakan metode seismik single channel dengan jumlah lintasan sebanyak 179 lintasan dari timurlaut - baratdaya dan barat - timur. Hasil rekaman seismik ini kemudian diinterpretasi batas-batas unit fasiesnya dan disebar dengan menggunakan metode kriging. Selanjutnya dihitung ketebalannya dengan menggunakan asumsi cepat rambat 1600 m/s.

Berdasarkan batas unit fasies yang telah diinterpretasi sedimen kuarter yang terbentuk di daerah penelitian terbagi menjadi 2 jenis unit yaitu: Unit 2 yang diperkirakan merupakan sedimen fluvial - transisi, dan Unit 1 yang diperkirakan sebagai sedimen transisi - laut dangkal. Terlihat pula adanya perbedaan pola ketebalan sedimen pada kedua Unit ini, dimana Unit 2 menunjukkan adanya pola penebalan sedimen menyerupai paleochannel berarah timurlaut - baratdaya sedangkan pada Unit 1 relatif terlihat seragam.

Dari hasil penelitian ini dapat disimpulkan bahwa daerah yang memiliki potensi endapan mineral berat plaser berada di Barat ke tengah daerah perairan selatan Pulau Bintan. Dimana potensi endapan pembawa mineral berat plaser seharusnya berada pada endapan paleochannel yang merupakan bagian dari Unit 2.

Kata Kunci: *Sedimen Kuarter, Endapan Mineral Berat Plaser, Unsur Tanah Jarang, Perairan Selatan Bintan*

INTRODUCTION

Southeast Asia is one of the areas traversed by the granitoid route that carries economically heavy minerals. Where this granitoid line stretches for 3000 km from Burma to West Kalimantan, not passing through Bintan Island and the surrounding waters (Cobbing, 2005). As it is known that the distribution of these granitoids is not only on land, but also spreads to the waters (Zulfikar et al., 2020). The presence of placer-heavy minerals on land through which the Southeast Asian granitoid route passes is limited. This forces geological explorers to look for new reserves in territorial waters. The mineral placer deposits exploration is intrinsically linked with the mineral deposit accommodation. We need to find this heavy minerals placer deposit accomodation that contain fairly large mineral placer accumulation.

The objectives of this study are to investigate the presence of accommodation of heavy mineral and rare earth elements deposits in South Bintan Island Waters based on subsurface sedimentary pattern by using single-channel seismic data interpretation. Data analysis was performed by identifying reflector configuration patterns and those continuity. Where sediment units that are estimated to have the potential for placer mineral deposits are generally sediment units located just above the acoustic basement (granite??) or unit 2 with a paleovalley or paleochannel shape. These characterizes (paleovalley/ paleochannel) showed alluvial deposits and generally has potential to contain placer minerals (Arifin, 2011; Raharjo, 2007).

The study area is located in the southern waters of Bintan Island, part of East Bintan District, Bintan Regency, Riau Islands Province. It lies within the latitude 86,874.34 mN to 93,664.28 mN and the longitude 441,499.37 mE to 456,751.02 mE (Figure 1). Geographically, it is part of northern hemisphere UTM Zone 48 N.

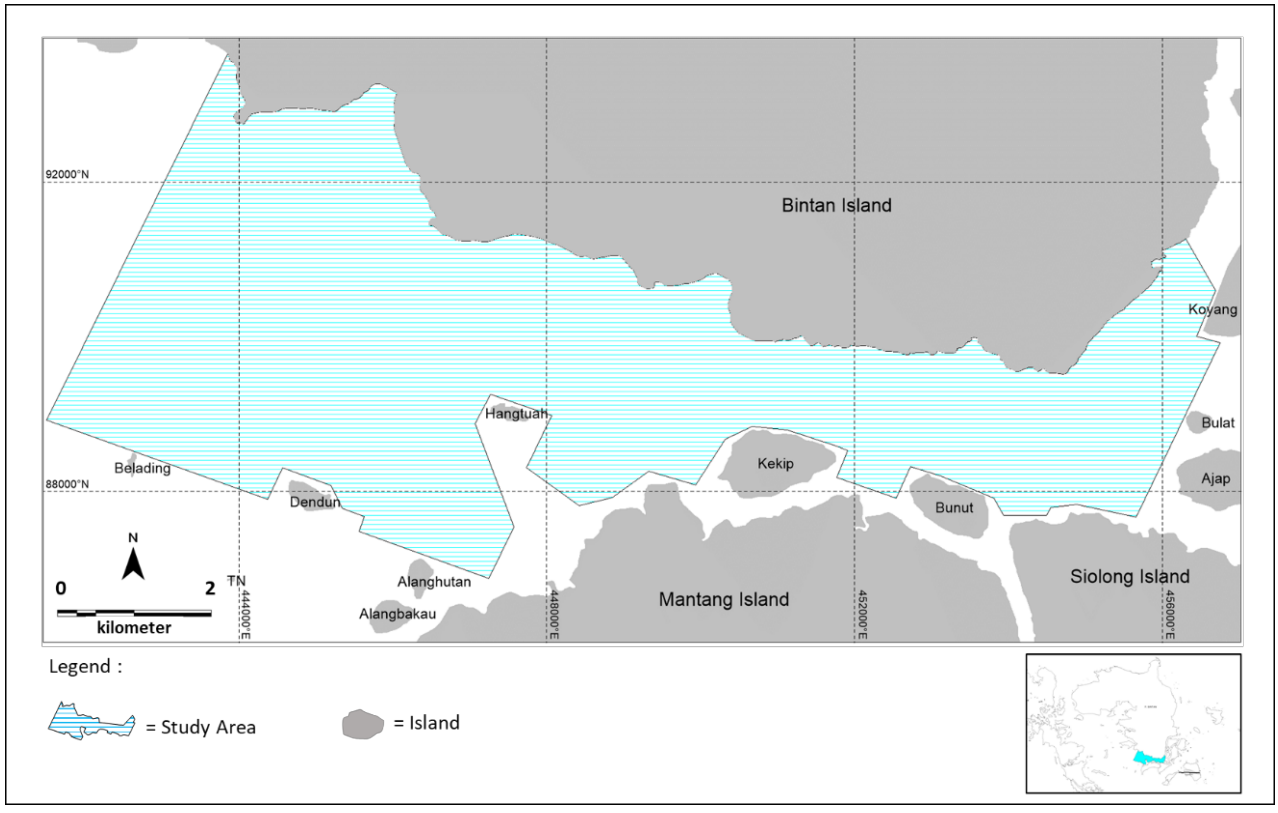

Figure 1. Study area

Geology of Bintan Island and its surroundings

According to Kusnama (1994) Bintan Island and its surroundings are part of the Riau Archipelago which is generally composed of intrusive igneous rocks in the form of granite and diorite of pre-tertiary (Triassic) age. This breakthrough rock is the oldest rock on the mainland of Bintan Island with enough to dominate about 40% of the total land on Bintan Island (Figure 2).

In a small part in the southwest part of Bintan Island, the Goungon Formation is deposited which dominates almost all parts of the mainland of Bintan Island. The Goungon Formation is composed of white tuffaceous sandstone, fine to medium grained, has a parallel laminated structure. In addition, there are also siltstones and dacitan tuff and feldspathic lithic tuff, smooth, white in color and locally interspersed with tuffaceous sandstones. This formation was deposited in a fluviatile environment and is Pliocene - Pleistocene in age. Then

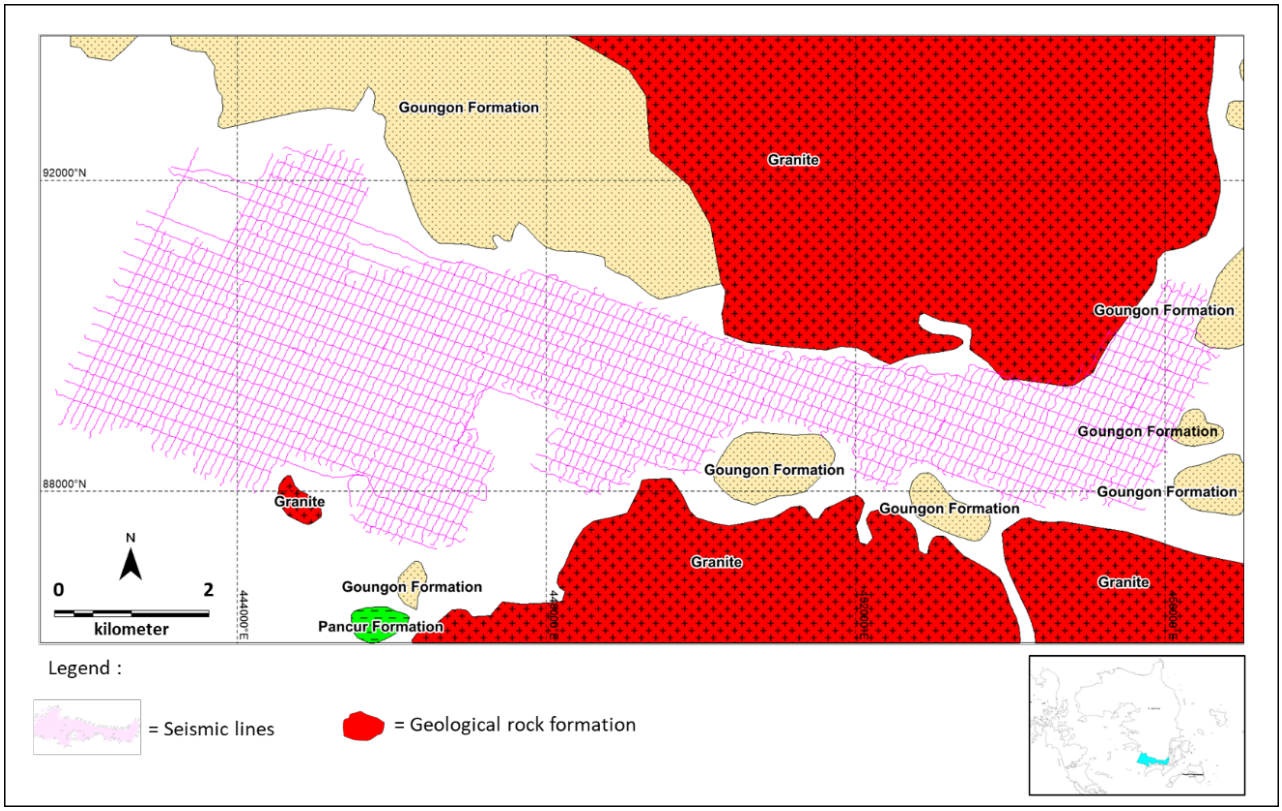

Figure 2. Geological rock formation (Kusnama, 1994) and seismic lines map

sedimentary rocks of Cretaceous age were found, namely the Pancur Formation and the Semarung Formation. The Pancur Formation is composed of claystone/shale with a reddish color with a pencil structure, in some places there are inserts of well-layered and well-separated quartz sandstone. This formation is not aligned with the granite rock which is thought to be the acoustic bedrock in the Bintan Island area. Meanwhile, the Semarung Formation is composed of medium-coarse grained arcose sandstones, well consolidated and there are claystone inserts with light gray color and thin layers. The Semarung Formation was deposited in a terrestrial environment until the transition which also overlaps with the Pancur Formation.

Above the Triassic-aged granite, andesite rocks are formed with the composition of plagioclase, hornblende, and biotite. This rock has a porphyritic texture with a base mass of micro-crystalline feldspar and is generally fresh rock. This andesite rock is estimated to be in the Early Miocene to Late Miocene age. Above these andesite rocks above the Goungon Formation, alluvium of Holocene age was deposited which was composed of sand, yellowish red with a composition of quartz, feldspar, hornblende and biotite which is a remnant of granite erosion. This alluvium unit is the result of river and coastal deposits that cover unconformably above the Goungon Formation or older rocks. All rock formations in the study area are shown in the regional stratigraphic table (Figure 3).

Quaternary Sediments of Bintan Island and its surroundings

At the age of the quarter around 12,000 - 15,000 years ago during the Last Glacial Maximum (LGM), Bintan Island was still part of the Sunda Shelf which stretched from China to Madura Island and East Kalimantan. At that time, the waters of Bintan Island and its surroundings were still in the form of land, around which many ancient river patterns developed that flowed into the South China Sea (Hanebuth et al., 2002; Molengraaff & Weber, 1921; Pucha?a et al., 2011;

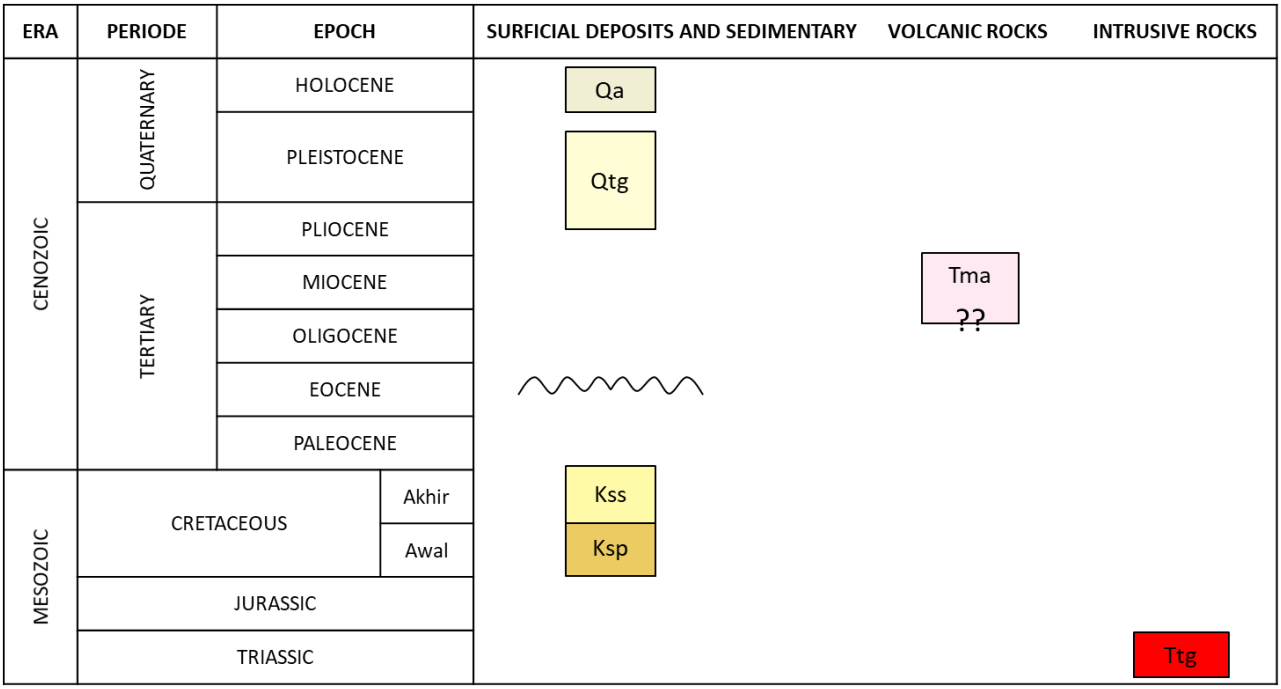

Figure 3. Regional stratigraphy of Bintan Island and surroundings (Kusnama, 1994)

Sathiamurthy & Rahman, 2017; Solihuddin, 2014; Voris, 2000).

Pre-quaternary rocks that located on Bintan Island and its surroundings are dominated by Triassic-aged granite. This granite rock is thought to be a large batholith body. In some places, the body of this batholith were intruded again by andesite at the Oligocene - Miocene age. All of these rocks then undergo a weathering process and were eroded by the drainage system or the evolving fluvial system. Thus, all of the eroded materials were transported and deposited. The sedimentary materials that transported from the previous rock were accumulate in deposit trap (valley). These area have a relatively low morphology compared to the source rock. This process continues until the Last Glacial Maximum occurs and causes global land sinking by sea level rise.

The sinking that occurred during the Last Glacial Maximum caused sea levels rise to covered fluvial depositional patterns. The sea level which was originally under 120 meters from the sea level today, tends to rise until the depositional environment which was originally a terrestrial environment turns into a marine environment. This includes the southern waters of Bintan Island and its surroundings. Terrestrial depositional facies, which were originally rocks older than the quarter, were later covered by transitional and marine facies.

Heavy Minerals and Rare Earth Elements Potential on Bintan Island

The entire area that traversed by Southeast Asian granitoid belt has potential for presence heavy mineral placer deposits. These deposits were formed from fragments of granitoid rocks that carry heavy minerals. Cobbing (2005) classifies that the Granitoids in Bintan Island are I-type granitoids. Genetically, Winter (2001) considers that this I-type granite is a granite that formed by partial melting of mafic mantle igneous material from subduction zones which results in the formation of breakthrough rock with a distinctive chemical composition.

Previous research stated that the I-type granitoids have heavy mineral potential such as Cu and Mo, which were formed from volcanic arc granite (Pearce et al., 1984). Moreover, Setiady and Sarmili (2005) stated that seabed sediments and coastal sediments in the waters around Batam Island and the western part of Bintan Island contain various metallic minerals. These heavy minerals are magnetite, ilmenite, monazite, cassiterite, hematite, etc. This is allegedly due to the deposition of placer minerals resulting from the breakdown of granite rocks on Batam Island and Bintan Island.

In addition, as is well known, most of Bintan Island is rich in bauxite content. Where this bauxite is found in clay from weathered granite with a high alumina content (Rohmana et al., 2007; Yusuf et al., 2005). The formation of bauxite is due to very intense weathering, causing the lateritized zone of granite to be enriched by bauxite and deposited above the source rock. Even in the northern and eastern parts of Bintan Island, a rock structure in the form of Corestone is formed which is a sign of fairly massive granite weathering (Hutabarat et al., 2016).

In addition to the potential for heavy minerals, Bintan Island also has a high potential for rare earth elements. Irzon and Abidin (2017) mention that granite rocks in the north of Bintan Island have a high content of rare earth elements. Where regionally, Kusnama (1994) stated that, the granite in the north of Bintan Island has

similarities with the granite in the south of Bintan Island. The identification of placer mineral deposits using a seismic stratigraphic interpretation approach in the waters will provide clues to the drilling target and delineation of the boundary of the placer mineral deposits (Batchelor, 1979). Batchelor's succeeded in exploring placer minerals (in this case offshore tin), with the concept that the potential of placer minerals deposits is not only in young alluvium valleys (which are the result of onshore source rock deposits). But it is also located in the old sedimentary facies which is a subsurface heavy mineral-bearing rock deposit. These event occurred before the last glacial maximum period, when Sundaland still exist. So the thickness stratigraphic unit distribution becomes important.

METHODS

The subsurface geological conditions in this study were identified using shallow reflected seismic. The total number of lines acquired as a result of 179 routes stretching from the western waters of the south of Bintan Island and the east of the southern waters of Bintan Island, while the northern and southern parts of the research area are located in the strait between the south of Bintan Island and the north of Mantang Island. The intervals between lines are range from 100 - 200 m with the main line direction relative to the northeast - southwest as many as 135 lines and a cross-section with a west - east direction as many as 44 lines. The length of each track ranges from 150 meters - 4400 meters.

Single-channel seismic reflection using a typical single plate boomer sound source with a total power of 300 joules to produce sound waves at every 0.5 seconds of shot interval. Such waves propagate towards the seabed and are reflected back to the streamer hydrophone. Parameter of these wave propagation contains information about the properties of the subsurface. Seismic recording executed by using Sonarwiz 5 software with the ouput of digital data recorded in the SEG-Y format (filename extension .sgy)

The data outputting from seismic acquisition has been further processed to enhance the quality of seismic images by denoising technique using band-pass filtering. These band pass filtering processes was settings with following frequency limitation: low cut frequency 20 Hz, low pass frequency 750 Hz, high cut frequency 150 Hz and high pass frequency 1500 Hz. All of these processed are used over a range of 256 samples. To sharpen the resolution of the seismic image we used a gain setting of 3x10-4 dB.

From there on, we did the interpretation of sedimentary unit boundaries (horizon) based on characteristics of seismic facies that derived from reflector configuration of seismic profile (Mitchum, et al., 1977 in Veeken, 2007). After that, we created an isopach map that illustrates the stratigraphic thickness pattern between an upper and lower horizon. We consider kriging as a fitted geostatistical method to be used in predicting spatial distribution of these horizons. Furthermore, to determine the distribution of sediment unit thickness in meters (isopach), we used a time to depth conversion with a velocity assumption around 1540 m/s for seabed (water velocities) and 1600 m/s for subsurface sediment (Puchala, 2011) . The whole processing and interpretation was performed by Sonarwiz and Petrel software.

RESULTS

Total of 179 seismic lines that have been interpreted in this study area. The track consists of a main line with a northeast - southwest direction, and a crossline with a west - east direction. Based on the reflector configuration analysis from the seismic records, there are 3 seismic horizons that bounded 2 seismic facies units above the acoustic basement with various thickness patterns and markedly different distribution patterns. These 3 horizons are presumed to be quaternary sediments consists of the seabed (horizon 1), bottom unit 1 (horizon 2) and acoustic basement (horizon 3).

Seismic Correlation Surface and Seismic Facies Unit

Seismic Correlation Surface

The interpretation of the three horizons then correlated as a surface, which were distribute throughout the entire area. The result of this seismic horizon interpretation shows the paleogeographic pattern in the area. Each horizon has a difference pattern, horizon 3 shows a depth pattern that is relatively different from the recent bathymetry. This surface shows the steep highs countours and the other place shows a continuous valley. Meanwhile, horizon 2 does not show a significant difference in depth pattern from horizon 1 which is the current bathymetry.

Seismic Facies Unit

Based on the results of the correlation between the surface area boundaries, the study area is divided into 3 seismic facies units, namely:

Facies Unit 3 / Acoustic Basement

This facies unit is the oldest facies in the study area. Top of this unit overlain by the surface of bottom unit 2 and the bottom boundary of these unit appear clear despite the used of maximum penetration during seismic acquisition.

The reflector characteristics in the entire seismic records of this unit shows a weak frequency, subparallel - chaotic, and moderate amplitude. Based on the reflector pattern, this unit can be divided into 2 types, namely acoustic basement which is estimated as bedrock (granitoid?) and sedimentary rock. Acoustic basement is generally dominates the whole area characterized by chaotic and hyperbolic reflector patterns (Figures 4 and 5). Meanwhile, facies unit 3 which is a sedimentary rock appears relatively subparallel - chaotic reflector pattern. The thickness range of this facies unit cannot be identified because the lower boundaries of this unit cannot be known.

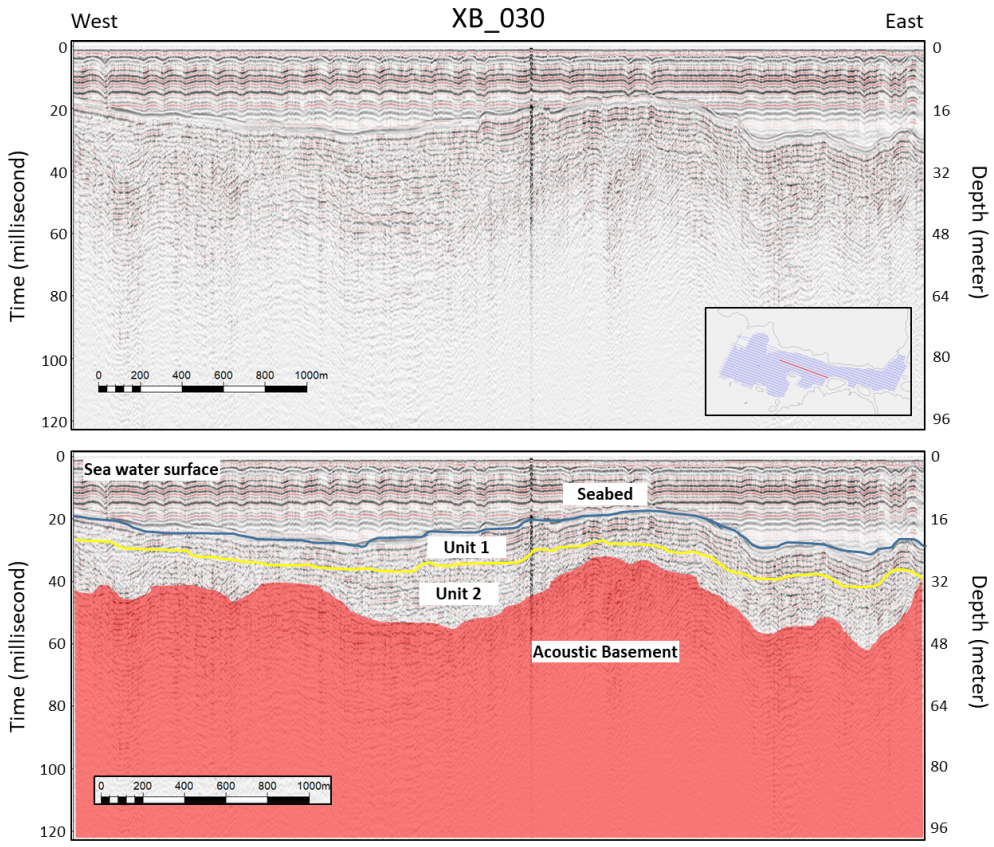

Figure 4. Interpretation of seismic line XB_030

records of this unit shows a moderate frequency, subparallel - chaotic, and medium amplitude. It is estimated that the sediment deposited is a medium-coarse fraction sediment resulting from the previous rocks weathering whose transportation process is not too far from the source rock. In some places, continuous valley that forming a paleochannel were also found (Figures 6 and 7). The depositional pattern that developed in this unit is thought to be a fluvial - transitional depositional facies. The thickness range of this facies unit is quite high, ranging from 0.75 - 30 meters.

Facies Unit 2

This facies unit is a sedimentary facies whose top is bounded by the surface of the bottom unit 1/top unit 2 (horizon 2) and the bottom is bounded by surface of bottom unit 2/top unit 3 (horizon 3) which is presumably sedimentary rock. In some places there are directly adjacent to the acoustic basement with reflector patterns in the form of chaotic and relatively hyperbolic shapes sticking up like granitoids.

The reflector characteristics in the entire seismic

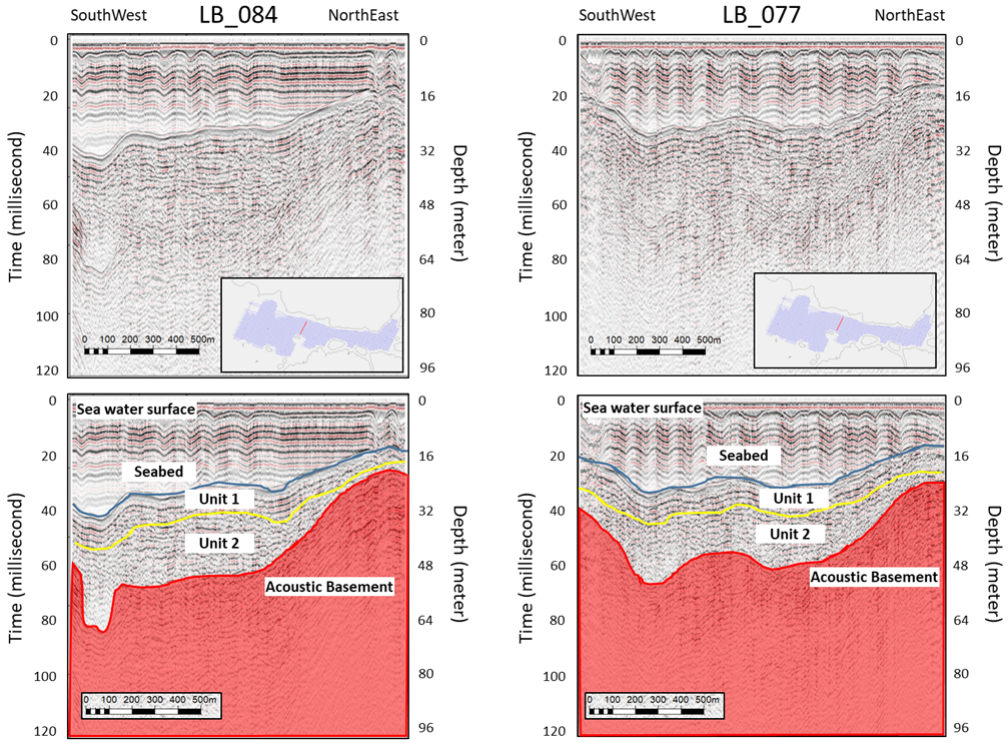

Figure 5. LB_084 and LB_077 seismic lines interpretation

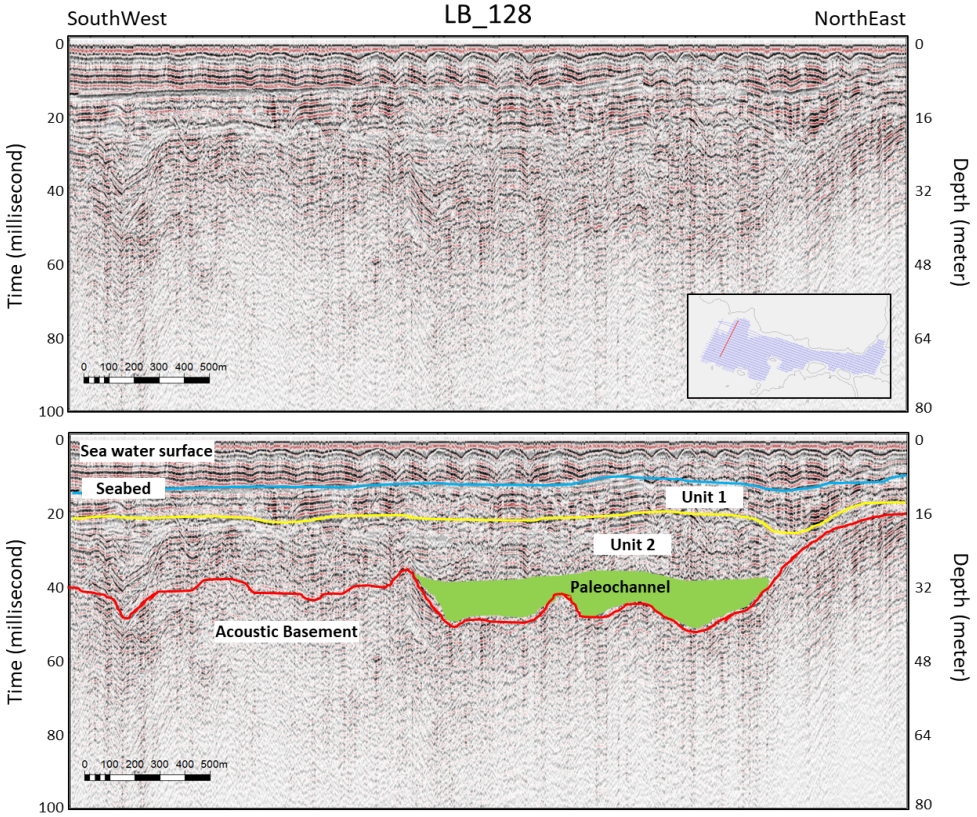

Figure 6. LB_128 seismic line interpretation

Facies Unit 1

This facies unit is the youngest facies unit or recent sedimentary facies which is bounded at the top by the seabed and at the bottom by the bottom unit 1/top unit 2.

This unit has the characteristics of high frequency, the dominant reflector pattern is simple parallel continuous with a small part there is subparallel, and the amplitude is medium - high. This is allegedly due to the sediment deposited at this time is sediment resulting from the deposition of a shallow marine environment which tends to be influenced by tides and waves and has not been well compacted.

The sediments in this unit are estimated to be dominated by fine fraction sediments and in some places there are also sediments dominated by shell fragments (Nurdin et al., 2020). This is due to the good lighting and nutrition of the environment, making it a good place for molluscs and coral reefs to grow. In addition, this also shows that the depositional environment in the area is dominated by tides and waves where this environment is in a

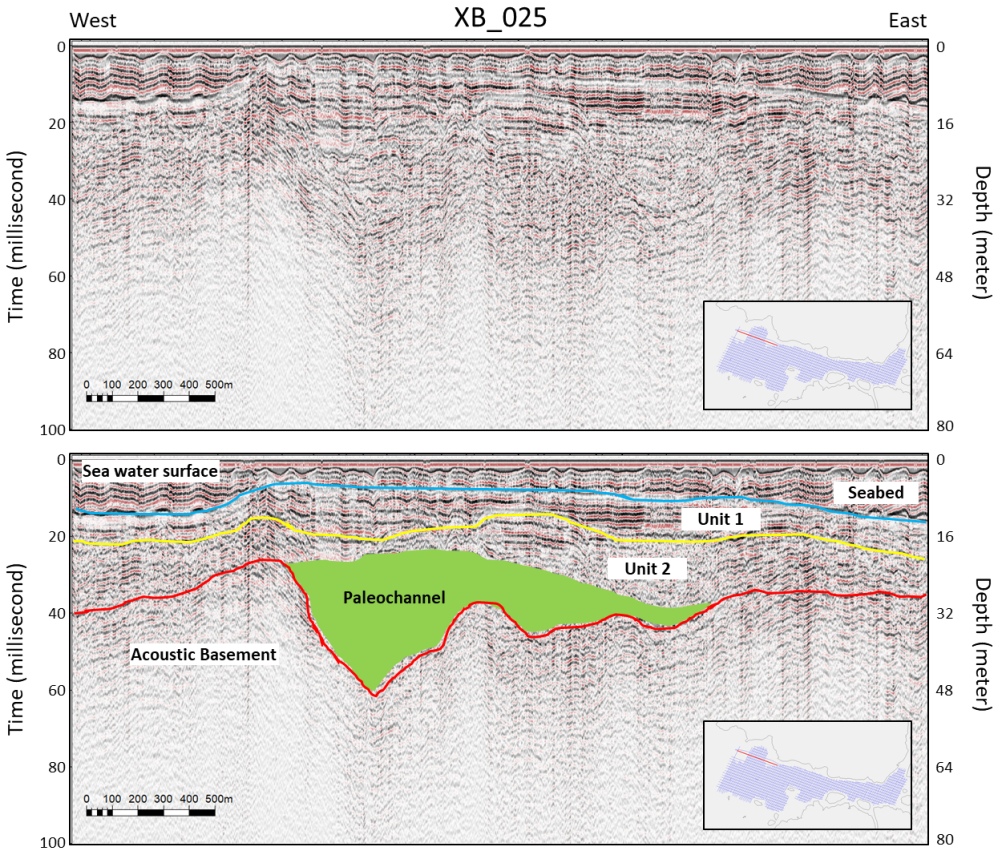

Figure 7. XB_025 seismic line interpretation

coral reefs do not like places where the water is cloudy, which is a dominant feature of fluvial deposition. The thickness range of this unit ranges from 1 - 13.5 meters.

DISCUSSIONS

Sediment Distribution Pattern in the Southern Waters of Bintan Island

The distribution of quaternary sediments in the Southern Waters of Bintan Island shows patterns of thinning and thickening of sediments in unit 1 and unit 2. However, the tendency of sediment thickening or thinning in unit 1 and unit 2 is different. This is because the depositional facies in each unit are different, so the depositional patterns are different.

Quaternary sediments Unit 2

Unit 2, which is estimated to be a fluvial-transitional depositional facies unit, shows a varied thickness pattern with a wide range ranging from 0.75 - 30 meters (Figure 8). If we look at the pattern of unit 2 sediment thickness formed in the study area, there are differences in the pattern between the west - center of the study area and the east - center of the study area.

The farther from the mainland, the thickness pattern is relatively uniform. While there is also sediment thinning up to 2 meters, this is allegedly due to the acoustic basement in the area being closer to the surface. However, the sediment in central to eastern study area more thinner than central to western study area. This can be seen from the influence of rock resistance to weathering. So that the fluvial sedimentation that is formed is not well developed. In regionally, Kusnama (1994) provides a formation boundary in the south of Bintan Island between the west and the east. The western part is dominated by the Goungon Formation (Qtg), while the eastern part is dominated by Triassic-aged granite (Trg).

Overall, the thickness pattern in unit 2 shows a relatively diverse sediment thickness. Where in the central - western part of the study area, thickening of the sediment is seen with patterns resembling paleochannels which are closely related to fluvial deposits. Meanwhile, in the center - east study area sediment depletion is seen. Which is estimated to be in this area a relatively high level that is still resistant to weathering. This indicates the unit of this part is terrestrial depositional system. Where the terrestrial

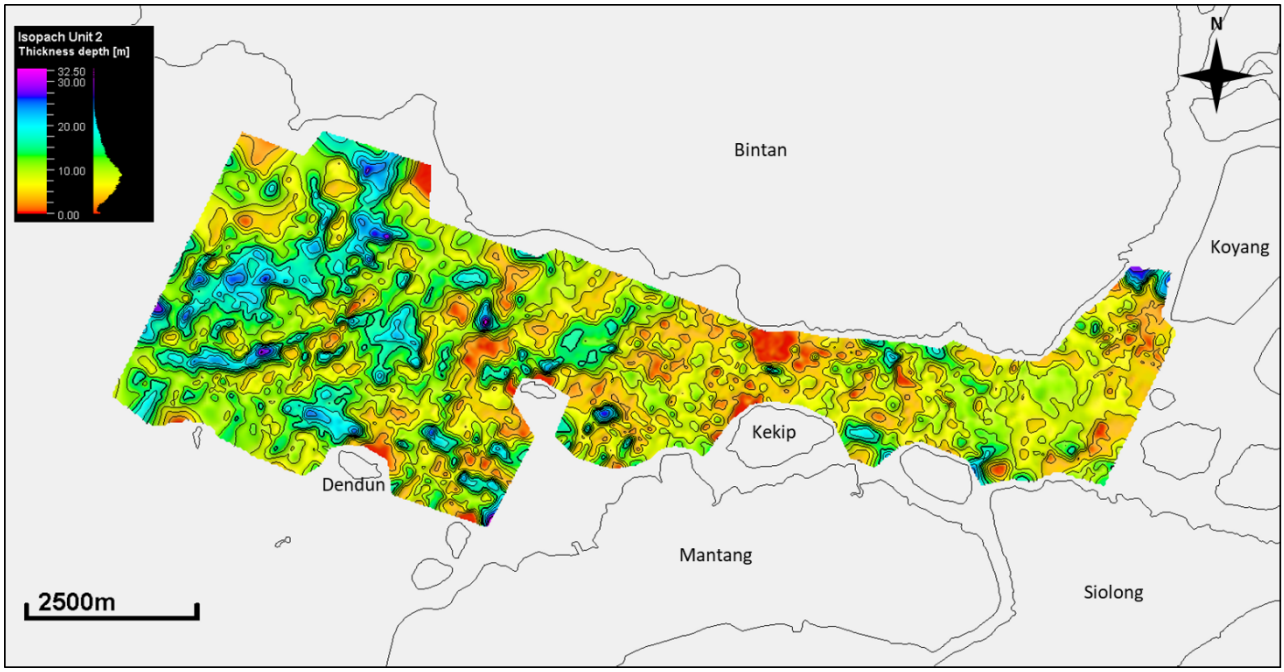

Figure 8. Unit 2 isopach map

In the central to western part of the study area, sediment thickening occurs with a pattern resembling a paleochannel. The sediments formed were relatively thickened towards southwest of the study area. This paleochannel is thought to be a fluvial deposit-forming groove which then continues to the larger main river.

In the central to eastern part of the study area, the dominant sediment thickness pattern ranges from 3 - 7.5 meters. In some places close to the mainland, there is a thickening of up to 20 meters, this is allegedly due to the influence of sedimentation from rivers on the mainland.

depositional system allows the formation of paleochannel patterns.

According to Voris (2000), in the period before last glacial maximum, there were 4 large rivers formed in Southeast Asia, namely the North Sunda River, Siam River, Malaca River and South Sunda River. Sediments originating from these large rivers flow from the highlands and then head towards the open sea. The presence of paleochannels seen in the study area is estimated to lead to one of the two major rivers, namely the North Sunda River

or the Siam River. Judging from its geographical location, this paleochannel tends to join the North Sunda River to the South China Sea.

Quaternary Sediment Unit 1

This unit is interpreted as a transitional - marine facies unit. It has simple parallel - subparallel reflector patterns which show a non-varied thickness pattern with a shorter range that ranging from 1 - 13.5 meters (Figure 9). The thickness pattern in this Unit 1 sediment shows a different pattern in the middle - east part of the study area compared to the western part of the study area.

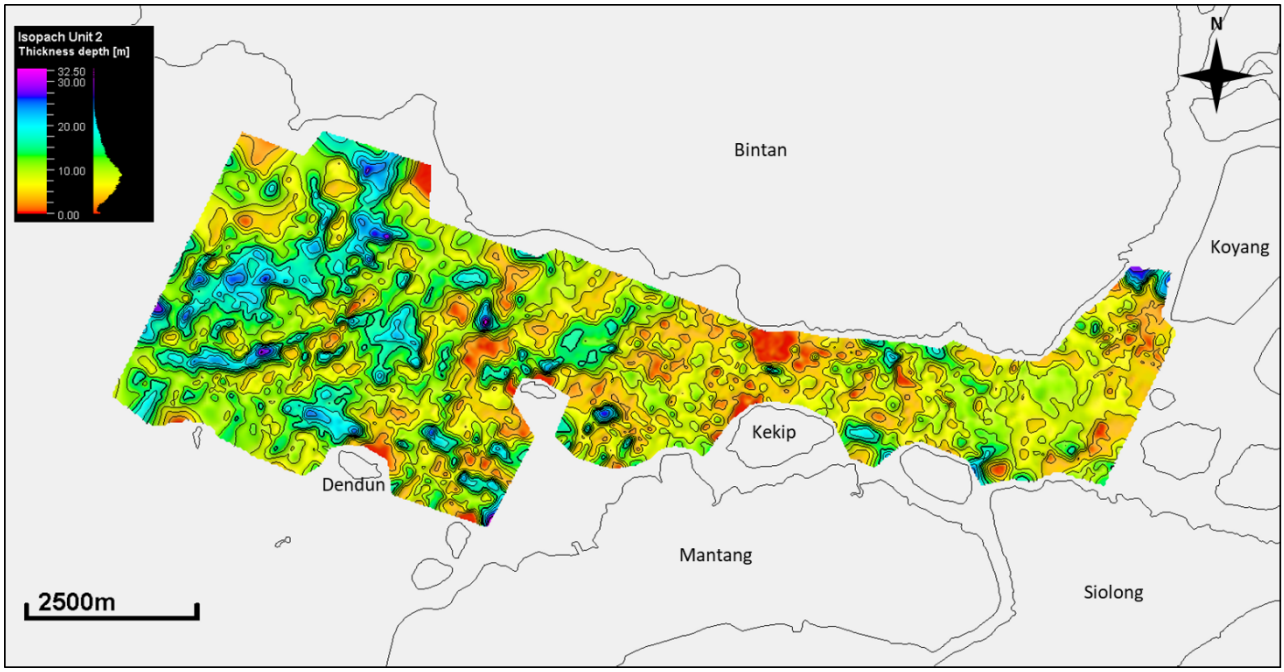

Figure 9. Unit 1 isopach map

The pattern of sediment thickness in the middle - west of the study area shows a dominant thickness with range between 4 - 8 meters. However, in west and central part there are close to the main river in Bintan Island or Mantang Island has a sediment thickening pattern up to 12 meters. This is allegedly due to the influence of sedimentation from the rivers. The farther from these river has a uniform thickness pattern. On the other hand there is also sediment depletion up to 3 meters. This is allegedly due to the basement acoustics in the area closer to the surface. Thus, the accommodation space for the sediment is getting shallower.

Meanwhile, in the central - eastern part of the study area has a thinner pattern than central - west study area with dominant pattern of sediment thickness ranges from 3 - 6 meters. However, in some places that are close to river in mainland showing the same pattern as the mid-west area. It can be seen from a thickening up to 12 meters. We interpreted there cause of the sedimentation from the main rivers on the mainland affects the sedimentation pattern. The farther from the mainland, shows a uniform thickness pattern. In addition, there is also sediment depletion up to 1 meter. This is presumably due to the reduced accommodation space caused by the basement acoustics getting closer to the surface. This pattern is relatively similar to the thickness pattern in Unit 2. Where the sediment tends to follow the shape of its accommodation space (same as its Unit 2).

Overall, the thickness pattern in unit 1 shows a fairly wide spread of sediment. It is shows these unit is a part of shallow marine depositional system (same as the current environmental conditions). Where this shallow marine deposition system is dominated by tides and waves.

The Potential of Heavy Mineral Placer Deposits or Rare Earth Elements in the Southern Waters of Bintan Island

Based on consideration of sediment thickness and paleochannel pattern in Unit 2, which develops in a northeast-southwest direction with acoustic basement that shallow to the surface. The area that has greater potential is in central to west area. Where in this area Unit 2 has paleochannel as a mineral placer deposit accommodation, even more location of the source rock (acoustic basement) not too far away from the deposits. Regarding the type and amount of mineral content, further research is needed using drill data and laboratory analysis.

ACKNOWLEDGEMENTS

We would like to thank the Head of Marine Geological Institute and all the team members who involved during data acquisition, as well as those who contributed to the success of this research program.

CONCLUSION

- Quaternary sediment deposits in the Southern Waters of Bintan Island consist of 2 units, namely: Unit 1 which is shallow marine sediments with a predominance of fine fractions and Unit 2 which is fluvial - transitional sediments with a dominance of medium - coarse fractions.
- Areas that have the potential for heavy mineral placer deposits are the western – central areas of the Southern Waters of Bintan Island. The potential for this heavy mineral placer deposit is in the paleochannel deposits which are part of Unit 2.

REFERENCES

Arifin, L., 2011. Identifikasi Alur Sungai Purba dan Endapan Plaser di Perairan Lembar Peta 1612 Kalimantan Selatan. Jurnal Sumber Daya Geologi.

Batchelor, B.C., 1979. Geological Characteristics of Certain Coastal and Offshore Placers as Essential Guides for Tin Exploration in Sundaland, Southeast Asia. Geol. Soc. Malaysia, pp.283-313.

Cobbing, E. J., 2005. Granites. In Sumatra: Geology, Resources and Tectonic Evolution (Vol. 31, pp. 54-62). Geological Society.

Hanebuth, T. J., Stattegger, K., & Saito, Y., 2002. The stratigraphic architecture of the central Sunda Shelf (SE Asia) recorded by shallow-seismic surveying. Geo-Marine Letters, 22(2), 86-94. https://doi.org/10.1007/s00367-002-0102-1.

Hutabarat, J., Syafri, I., Sulaksana, N., Sukiyah, E., Fauzielly, L., & Sudradjat, A., 2016. Fenomena Pelapukan Granit "Corestones" di Daerah Bagian Timur dan Utara Pulau Bintan. Seminar Nasional Ke - III Fakultas Teknik Geologi Universitas Padjadajran.

Irzon, R., & Abidin, H. Z., 2017. Kandungan Unsur Tanah Jarang pada Granit Putih Kemerahan dari Daerah Lagoi dan Perbandingan dengan Batuan Sejenis di tempat lain. Jurnal Geologi Dan Sumberdaya Mineral, 18(3), 137-146.

Molengraaff, G. A. F., & Weber, M., 1921. Proceedings Royal Academic Amsterdam. XXIII, 395-427.

Nurdin, N., Zulfikar, M., Kamiludin, U., Setiady, D., Mustafa, M. A., Setyanto, A., Widiatmoko, H. C., Setiadi, I., Hans, D. Z., Piranti, S. A., Aryanto, N. C. D., & Haryanto, A. D. (2020). Upaya Penambahan Potensi Cadangan Mineral Strategis Kelautan di Jalur Granitoid Tahap-1 (Lokasi: Bintan Selatan dan Sekitarnya, Kabupaten Bintan, Provinsi Kepulauan Riau). Pusat Penelitian dan Pengembangan Geologi Kelautan, Bandung, Badan Penelitian dan Pengembangan Energi dan Sumberdaya Mineral, Kementerian Energi dan Sumberdaya Mineral. Internal report, 88p. Unpublished.

Pearce, J. A., Harris, N. B. W., & Tindle, A. G., 1984. Trace element discrimination diagrams for the tectonic interpretation of granitic rocks. Journal of Petrology, 25(4), 956-983. https://doi.org/10.1093/petrology/25.4.956.

Pucha?a, R. J., Porbski, S. J., ?liwi?ski, W. R., & August, C. J., 2011. Pleistocene to Holocene transition in the central basin of the Gulf of Thailand, based on geoacoustic survey and radiocarbon ages. Marine Geology, 288(1-4), 103-111. https://doi.org/10.1016/j.margeo.2011.08.007.

Raharjo, P., & Arifin, L., 2007. Identifikasi Alur Purba Berdasarkan Seismik Pantul Dangkal di Perairan Bangka Utara Lembar Peta 1114. Jurnal Geologi Kelautan. Vol. 5 (2), 165-176.

Rohmana, Djunaedi E.K, & M.P, P., 2007. Inventarisasi Bahan Galian. Proceeding Pemaparan Hasil Kegaitan Lapangan Dan Non Lapangan, 1-14. http://psdg.bgl.esdm.go.id/kolokium 2007/KONSERVASI/Prosiding-Bintan.pdf.

Sathiamurthy, E., & Rahman, M. M., 2017. Late quaternary paleo fluvial system research of sunda shelf: A review. Bulletin of the Geological Society of Malaysia, 64(December), 81-92. https://doi.org/10.7186/bgsm64201708.

Setiady, D., & Sarmili, L., 2005. Keterdapatan Beberapa Mineral Berat Di Perairan Pulau Bintan Dan Sekitarnya Sebagai Hasil Rombakan Dari Sedimen Holosen Asal Paparan Sunda. Jurnal Geologi Kelautan, 3(3), 1-7. https://doi.org/10.32693/jgk.3.3.2005.126.

Solihuddin, T., 2014. A Drowning Sunda Shelf model during Last Glacial Maximum (LGM) and Holocene: A review. Indonesian Journal on Geoscience, 1(2), 99-107. https://doi.org/10.17014/ijog.v1i2.182.

Veeken, P. C. H., 2007. Handbook of Geophysical Exploration: Seismic Exploration. In Elsevier (Vol. 37). https://doi.org/10.1016/S0950-1401(07)80025-5.

Voris, H. K., 2000. Maps of Pleistocene sea levels in Southeast Asia: Shorelines, river systems and time durations. Journal of Biogeography, 27(5), 1153-1167. https://doi.org/10.1046/j.1365-2699.2000.00489.x.

Winter, J. D., 2001. An Introduction to Igneous and Metamorphic Petrology. Prentice Hall.

Yusuf, A. F., P, M. R., Sayekti, B., & Awaludin., 2005. Inventarisasi dan Penyelidikan Bahan Galian Industri Kabupaten Kepulauan Riau, Provinsi Kepulauan Riau. Proceeding Pemaparan Hasil Kegiatan Lapangan Dan Non Lapangan, 1-5.

Zulfikar, M., Aryanto, N. C. D., Nur, A. A., & Syafri, I., 2020. Study of Granitoid Distribution at Toboali Waters, Bangka Belitung Province: Seismic data interpretation approach. Bulletin of the Marine Geology, 35(2), 53-64. https://doi.org/10.32693/bomg.35.2.2020.681

ASSESSMENT OF POTENTIAL MARINE CURRENT ENERGY IN THE STRAITS OF THE LESSER SUNDA ISLANDS

KAJIAN POTENSI ENERGI ARUS LAUT DI SELAT-SELAT KEPULAUAN SUNDA KECIL

Ai Yuningsih[1] and Mario D. Saputra[1]

[1]Marine Geological Institute of Indonesia
Jl. Dr. Djunjunan No.236 Bandung, Indonesia

Corresponding author: ai.yuningsih@esdm.go.id

(Received 11 May 2021; in revised from 28 May 2021; accepted 7 September 2021)

ABSTRACT: The Lesser Sunda Islands extend from Bali to Timor and consist of two geologically distinct parts formed by a subduction system of oceanic crust along the Java-Timor Trench. The northern part which includes Bali, Lombok, Sumbawa, Flores, Wetar, Pantar and Alor, is volcanic in origin; whilst the southern part is non-volcanic, encompassing the islands of Sumba, Timor and Rote. The straits along the Lesser Sunda Islands are formed as a result of very complex geological processes and tectonics in this area. These straits are the most important cross-sections in the southern part of the Indonesian Throughflow (ITF), functioning as outlets for the mass flows of seawater from the Pacific Ocean to the Indian Ocean through the Flores and the Savu Seas. In these straits, relatively high current speeds are occurred, not only caused by the ITF but also due to its geometry, the influence of tidal flow, and monsoonal currents.

Site study and ocean current measurement were conducted by using an echosounder, a pair of Acoustic Doppler Current Profilers (ADCP), and other supporting equipment. In general, the average of most ocean current speeds is less than 1.5 m/s with a duration flow of 8 -12 hours a day, and the maximum speed reaches up to 3 m/s. The tidal types in almost all the straits are mixed semidiurnal tides, in which two high waters and two low waters occur twice a day, with the high and low tides differ in height.

The Lesser Sunda Straits were selected as the potential sites for ocean current power plant because their current speeds are relatively high and their characteristics are more predictable compared with other straits from other regions. Based on the results of bathymetry survey and current characteristics from the deployed ADCP at a fixed (stationary) location on the seabed, the best location for the current power turbines is at the depth of 15-30 m where the seabed gently sloping.

Keywords: Ocean Current, Sunda Lesser, Renewable Energy

***ABSTRAK**: Kepulauan Sunda Kecil membentang dari Bali ke Timor yang terbagi menjadi dua bagian yang Kepulauan Sunda Kecil membentang dari Bali ke Timor yang terbagi menjadi dua bagian yang berbeda secara geologis dan terbentuk karena subduksi kerak samudera di sepanjang Palung Jawa-Timor. Bagian utara Kepulauan Sunda Kecil, yang meliputi Bali, Lombok, Sumbawa, Flores, Wetar, Pantar dan Alor, merupakan kepulauan busur vulkanik, sedangkan pulau-pulau di bagian selatannya adalah pulau non-vulkanik yang mencakup Sumba, Timor dan Rote. Selat-selat di sepanjang Kepulauan Sunda Kecil adalah bentukan dari proses geologi dan tektonik yang kompleks yang terjadi di daerah ini. Selat-selat tersebut menjadi perpotongan yang paling penting pada bagian selatan Arus Lintas Indonesia (Arlindo) dan berfungsi sebagai alur keluar aliran massa air laut dari Samudera Pasifik yang melintas melalui Laut Flores dan Laut Sawu hingga ke Samudra Hindia. Kecepatan arus di selat-selat tersebut relatif tinggi. Hal ini tidak hanya disebabkan oleh adanya Arlindo, tetapi juga karena adanya pengaruh geometri, siklus pasang surut dan arus Muson.*

Studi lokasi dan pengukuran arus laut telah dilakukan dengan menggunakan alat perum gema, sepasang Acoustic Doppler Current Profiler (ADCP) dan peralatan pendukung lainnya. Secara umum kecepatan arus laut rata-rata kurang dari 1.5 m/detik dengan durasi aliran 8 -12 jam per hari, dan kecepatan maksimum bisa mencapai lebih dari 3 m/detik. Jenis pasang surut di hampir semua selat perairan Sunda Kecil adalah pasang surut campuran harian ganda, yaitu dalam satu hari terjadi dua kali pasang naik dan dua kali pasang surut yang berbeda tinggi.

Selat-selat di perairan Sunda Kecil dapat dijadikan pilihan sebagai lokasi potensial untuk pembangkit listrik arus laut karena kecepatan arusnya yang relatif tinggi dan karakteristik dari arus yang lebih dapat diprediksi dibandingkan dengan selat-selat di lain daerah. Berdasarkan hasil survei batimetri dan karakteristik arus dari ADCP stasioner di dasar laut, lokasi terbaik untuk pembangkit listrik saat ini adalah pada kedalaman 15-30 m yang memiliki kemiringan dasar laut yang landai.
Kata Kunci: *Arus Laut, Sunda Kecil, Energi Terbarukan*

INTRODUCTION

The possibility of generating electrical power from the ocean current in Indonesia has been recognized for many years. It started since 2007 when the Ministry of Energy and Mineral Resources established Nusa Penida Island as the selected Renewable Energy Village for renewable energy development program (Lubis and Yuningsih, 2012). However, significant research and development of renewable energy from the ocean such as ocean current, tidal, wave and ocean thermal energy conversions in this area has only started recently.

Currently, ocean current power demonstrates as a possible and significant energy resources for developing renewable energy. There are several advantages of ocean current energy utilization compared to other energy generation. The production of electricity generated from ocean currents is renewable, more predictable and more environmentally friendly. An important initial step in exploring ocean energy is to characterize and to map the resources of ocean currents for generating electrical energy. The utilization of ocean currents to produce electricity, however, is still not developed favorably and need to study in more depth (Hidayati et al., 2016). Hence, site study and ocean current resources observation has been conducted by Marine Geological Institute in the selected straits of the Lesser Sunda Islands, such as Bali and East Nusa Tenggara area (Figure 1).

The Lesser Sunda Islands are a group of islands located between the waters of Southeast Asia and Northern Australia. The Lesser Sunda Islands is a volcanic strip of the Sunda Arc, consists of two geologically distinct parts formed by a subduction system of oceanic crust along the Java-Timor Trench. The northern part of the Lesser Sunda Island are active volcanic in origin consists of the islands of Bali, Lombok, Sumbawa, Flores, Wetar, Pantar and Alor. Meanwhile, the islands in the southern part, such as the islands of Sumba, Timor and Rote, are non-volcanic archipelagos which are geologically derived from the Australian plate. Geologically, Flores Sea is a morphostructure feature, coinciding a back arc basin due to the collision between the Nusa Tenggara island arc and the Australian continent (Prasetyo and Sarmili, 1994). The geological structure of this area is quite complex. Compression tectonics in the Flores Basin to Timor High resulted in the formation of a horizontal fault and a rising fault along the Lesser Sunda Islands. The intersections of the fault zones in the Lesser Sunda Islands formed straits, connecting the Flores Sea and the Savu Sea. These straits become the most important cross section of the Indonesian Through Flow (ITF), further function as an outlets for the mass flow of seawater from the Pacific Ocean through the Flores Sea to the Savu Sea and then to the Indian Ocean (Gordon A.L., 2005), In these straits, relatively high current speeds occur, not only

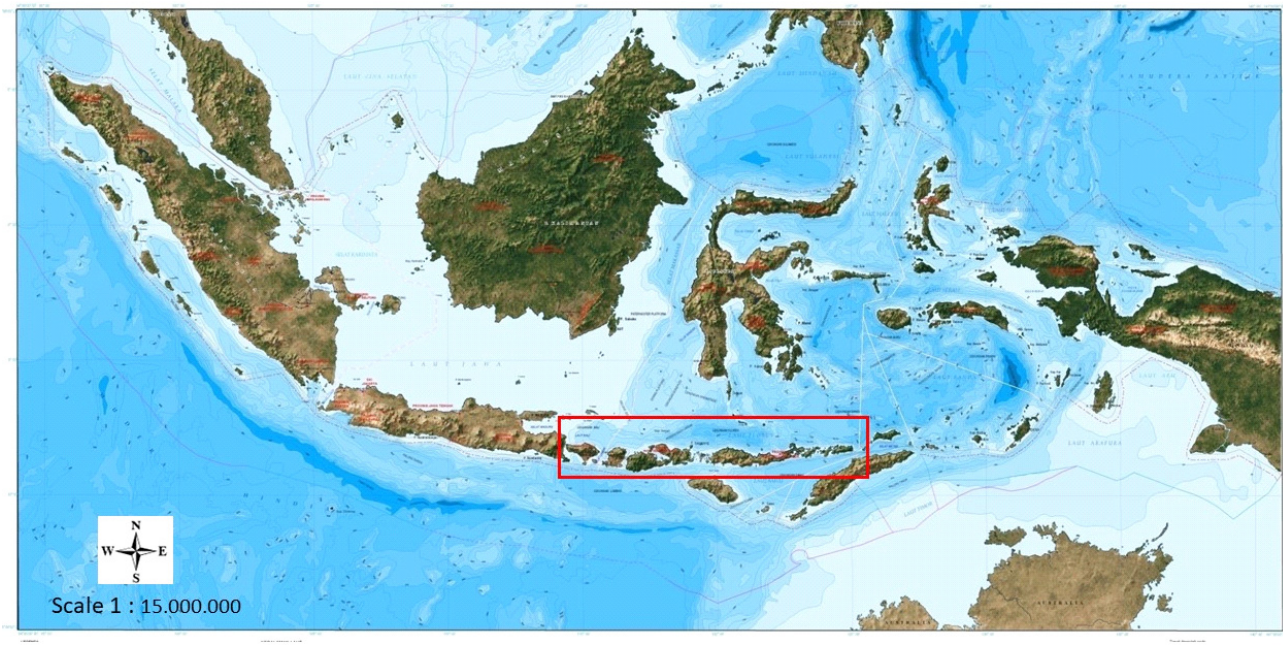

Figure 1. Site study area located at the straits of Lesser Sunda Islands, Indonesia.

caused by the ITF but also due to its geometry, the influence of the monsoon currents, and the South China Sea - Indonesian Seas Transport/Exchange (SITE). The locations of ITF, SITE and Trades influences are shown in Figure 2.

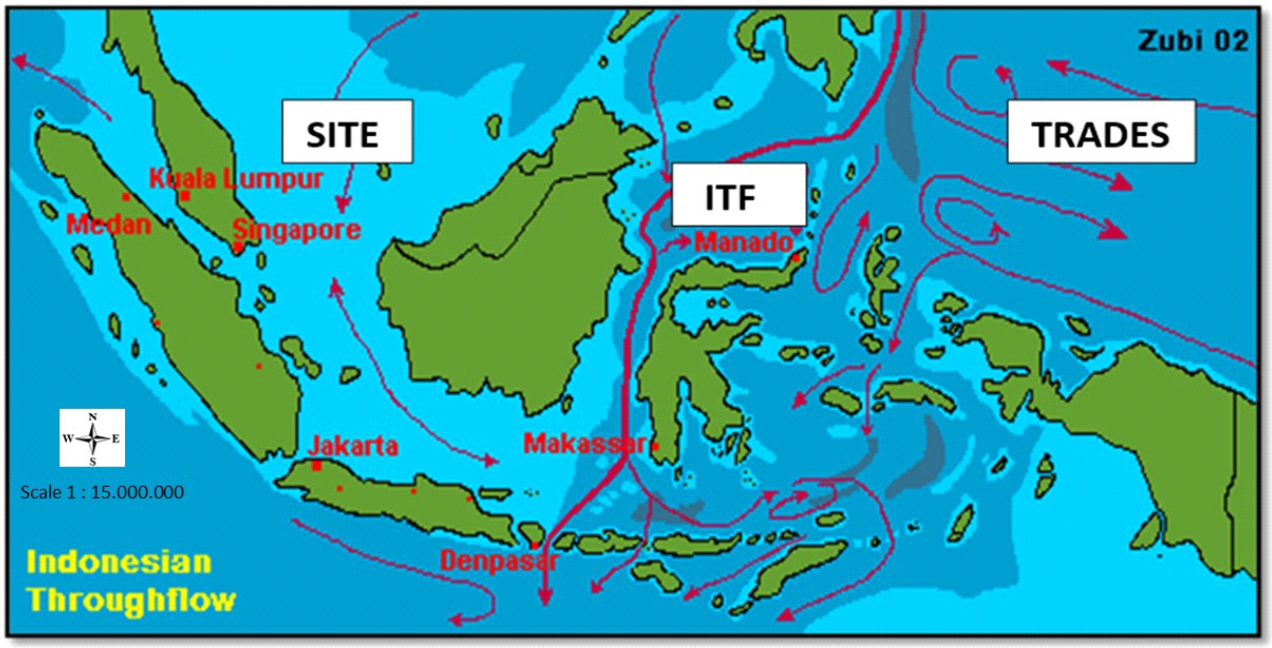

Figure 2. The influences of ITF, SITE, and Trades (monsoon currents) in Indonesian water area (after Susanto, et al., 2000).

In general, the electricity distribution in Bali and Nusa Tenggara is still insufficient for the entire islands, resulting electrical blackout arrangements in some settlements for more than 6 hours per day. To hinder insufficiency of electricity, PT PLN, the national electricity company, has been hiring more diesel generators to increase the supply of electricity. Based on data issued in 2013, the ratio of settlement electrification facilitated by PT PLN in the islands is still quite low at only less than 45 %. This number is much less below the national average electricity consumption which reached 60 - 80 % at the same year.

The purpose of the study is to identify the characteristics of ocean currents in the straits of the Lesser Sunda Islands in order to observe the potential of ocean currents as renewable energy resources in the strait areas. Research was conducted to collect data from the selected sites by determining the seabed morphology and the hydro-oceanographic characteristics.

METHODS

Survey methods applied during field works at the strait of the Lesser Sunda Islands from 2008-2015 were measurement of currents, tidal observation, observation of meteorological parameters, conditions of the seabed morphology, seabed nature and the coastal characteristics. Additionally, some methods of observations were applied to collect field data to assess the selected site and the proper type of ocean current power turbine for generating sufficient electricity. Referring to the ocean current turbine site selection criteria from Marine Current Turbine Ltd., a decent location to develop ocean current power generation must be located not far from the beach, be closed to the power grid, have an ocean current speed of 2.0 - 3.0 m/s (depending on the turbine type), and have relatively flat seabed morphology (Ainsworth and Thake, 2006).

In this study, Tidal Range Observation was measured by using an Electronic Tide Gauge and a tidal harmonic analysis was carried out by applying Royal Admiralty method. To obtain the tidal characteristics, this measurement was also necessary in order to determine the Chart Datum for bathymetric survey result correction and to obtain correlating data with the current observations.

Ocean Current Characteristics was measured by using an Acoustic Doppler Current Profiler (ADCP). There were two survey methods applied, such as Transect and Stationary Surveys. A transect survey is carried out by towing an ADCP instrument to measure the currents under a moving boat. A static survey is so called because it engages the deployment of a sea current measurement device (ADCP) at a site to moor on the seabed. Typically, ADCP measurements of the tidal currents must be taken for at least 30 days. This allows a tidal harmonic analysis of the flow to be completed (EMEC, 2009).

Bathymetric survey was conducted using a single beam echosounder (SBES) with spacing of sounding lines approximately 50 - 100 meters. Mobile ADCP and Single Channel Echosounder equipment were integrated by Global Positioning System (GPS) device. Both equipment recorded data of current speeds and ocean depths according to survey ship trajectories. The ocean depth data was then correlated with the result stream data from the recording of mobile ADCP to infer the relationship

between the morphology of the seabed and the current velocity distribution.

Ocean Current Data recorded from mobile ADCP and static ADCP was correlated with the tidal data to indicate pattern movements of the ocean currents at high and low tide conditions.

Weather Observation was conducted by using an Automatic Weather Station (AWS) during the field works. The AWS measures weather parameters, such as air temperature, humidity, wind speed and directions, air pressure, and rainfall. Weather conditions can change the current flow. Large pressure system may enhance or reduce the current flow, and storm surges can cause strong flow that can damage the turbines. Weather can also affect deployment and maintenance by limiting access to the site (EMEC, 2009).

Current Data obtained from field measurements were presented in time graph series, scatter plots, stick plots, and current rose.

In this study the current energy conversion calculated from the current speed data is indicated in the form of power density unit (watt/m^2). We adopt the formula from Fraenkel (2002), the power density can be obtained through the following equation:

$$P/A = \frac{1}{2} \times \rho \times V^3 \quad \ldots\ldots\ldots\ldots\ldots\ldots\ldots\ldots (1)$$

where P is power (Watt); ρ is the density of seawater (kg/m^3); A is the cross-sectional area of the turbine location (m^2); and V is the speed of the ocean current (m/s). The density value of seawater used here is the same as 1025 kg/m^3. The turbine cross-sectional area (A) is considered to be 1 m^2 so that the most influential variables in the conversion calculation process into electric current are the current velocity and the turbine area (Fraenkel, 2002).

tide, while the neap tide has shorter time length. Have the spring tide shown the slope of the water level at high and low tides, this condition will be followed by an increased current speed. Thus, the current speed will reach its maximum condition.

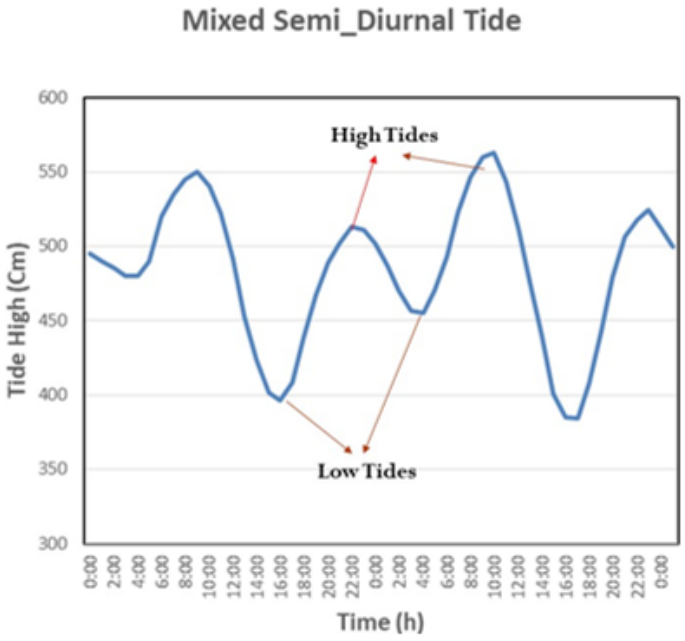

Figure 3. A 50-hour plot of the tidal range at Toyapakeh Strait, Nusa Penida

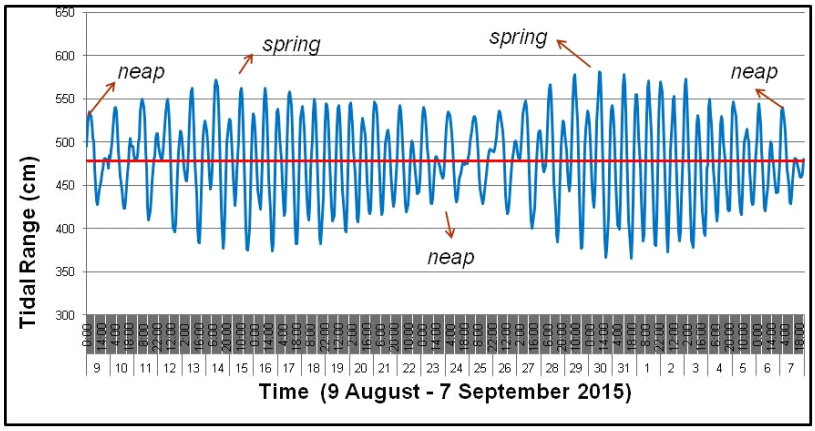

Figure 4. Tidal curve of 30-day cycle at Toyapakeh Strait, Nusa Penida (Yuningsih et al., 2015)

RESULTS AND DISCUSSION

3.1. Tidal Characteristics

Based on the harmonic tidal analysis using the Royal Admiralty method, the tidal type in almost all of the straits are mixed semidiurnal tides, with two high tides and two low tides each day. The high and low tides variability can be seen in Figure 3. The tidal curve of 30-day cycle at Toyapakeh Strait (Figure 4) shows the tidal current pattern in which two high tides and two low tides occurs within 24 hours with a maximum water level of 2.15 m. This situation causes the time length during high tide and low tide conditions are about 6-7 hours on average in the spring

3.2. Current Speed and Direction.

The Lesser Sunda Straits were selected as the potential site for sea current power plant due to their relatively high current speeds and their more predictable characteristics. The route of the current exchanges reveals that owing to the narrow straits of the Lesser Sunda Islands, inflow waters are trapped here before flowing to the Indian Ocean. This is the reason why the current speeds of the straits are relatively high.

Table 1 shows the range of current velocities for certain depths. The current velocity in this table is the minimum and maximum velocities recorded by a device during high and low tides at up to 27 m depth. The maximum velocity is above 2 m/s, particularly above 3 m/s from 3 m to 22 m depth where the greatest speed is at the depth of 5 m. Based on the current distribution data and the performance of continuous long-term current measurements, one can estimate the best position and depth for the placement of the ocean current power plant equipment/turbine.

The result of stationary current measurement and current transect survey during high and low tides indicates that in high tide conditions the current direction tends toward the northeast; and during the low tide conditions the current tends to flow to southwest direction (Yuningsih and Lubis, 2011). The current speed and direction at Larantuka Strait with the two conditions, i.e. during the high and low tides, are shown in Figure 5; whereas the distribution of the current speed derived from the ship-mounted ADCP survey during the field work are shown in Table 1.

Table 1. The range of current velocities for each depth at Larantuka Strait based on current transect survey during spring tide

Depth (m)	Minimum Speed (m/s)	Maximum Speed (m/s)
3	0.011	3.436
5	0.004	3.676
7	0.011	3.531
9	0.016	3.462
11	0.015	3.441
13	0.014	3.505
15	0.026	3.527
17	0.014	3.350
19	0.014	3.283
21	0.006	3.087
23	0.010	3.105
25	0.019	2.928
27	0.015	2.381

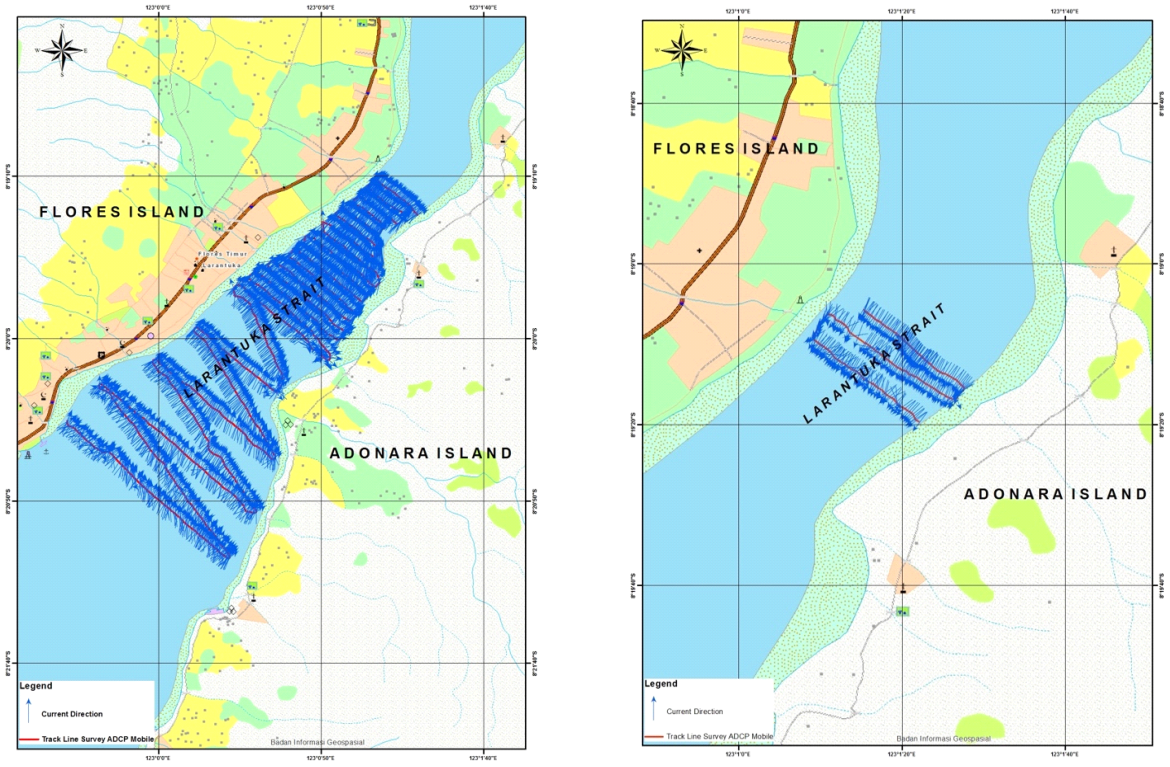

(a) During high tide, northeastward current (b) During low tide, southwestward current

Figure 5. Tidal currents tend to flow northeastward during the high tide (a) and southwestward during the low tide (b).

Specifically for the Toyapakeh Strait - Nusa Penida, the current direction has a unique pattern. The results of field measurements and observations during the survey are plotted in a current rose diagram. It shows the dominant current direction to the southwest in all the high and low tides conditions, as well as in all the conditions of the spring and neap tides (Figure 6).

Based on the results of current data processing using World Current 1.03 after Leverani et al. (2016), the types of currents in Toyapakeh Strait are tidal currents. The current direction describes the movement of two directions (bi-directional current), namely southwest - northeast direction. The direction of the current is formed due to the changes in water level elevation and seabed morphology.

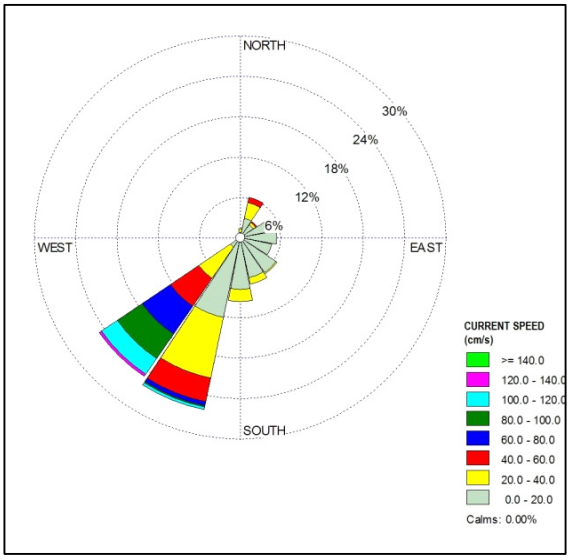

Figure 6. Current Rose diagram from field measurement results

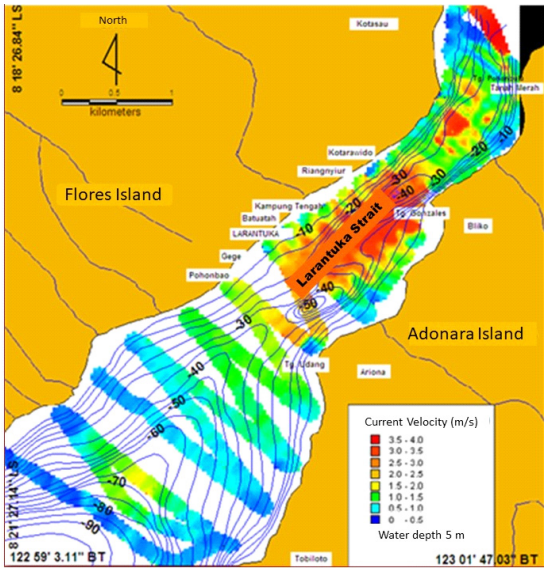

Figure 8. Bathymetry and horizontal distribution of current speed along the ship-mounted ADCP survey at 5 meters depth at Larantuka Strait (Yuningsih and Masduki, 2011)

3.3. Bathymetry

Vertically and horizontally, the current velocity distribution in the straits of the Lesser Sunda Island are not only influenced by the tidal conditions, but also by the condition of seabed morphology, the width of the strait and the depth of the sea. Based on data from several trajectories of the ship-mounted ADCP, the current velocity in these strait correlates with the depth of the sea, where the current speed is relatively high. The highest current velocity occurs in the deepest and narrowest part of the strait channel during the high and low tides (Figure 7 and Figure 8).

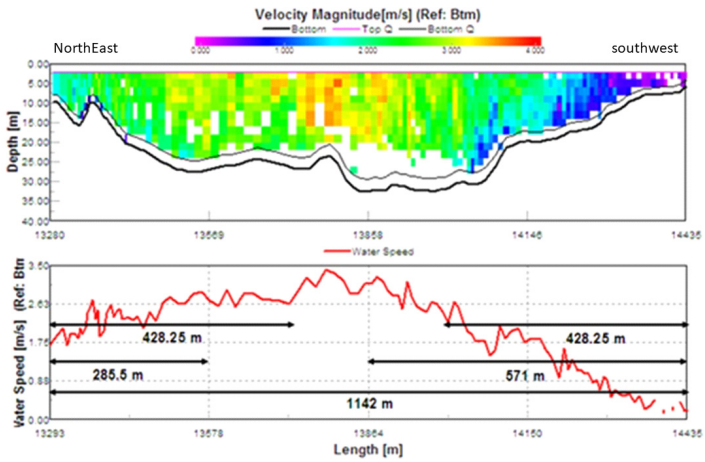

Figure 7. Correlation between vertical and horizontal distribution of current velocity and sea depth

In general, potential energy of ocean current that is possible to harvest depends on both parameters, i.e. the current speed and the swept area of the marine turbine blades (Thomas, 1991; Fraenkel, 1999). Another important consideration that has a significant impact to the ocean current power plant is the right position of turbine installation at the proper depth where the optimal current speed occurs.

The basic technical factors that may affect the assessment of a site for turbine deployment are the site must have a large enough current speed between 0.5 m/s - 3.0 m/s with relatively uniform velocity from the surface to the bottom, the site must be not too far from the beach (ideally less than 1 km), the sea depth must be ranging from 15 m - 50 m, and the morphology of the seabed must have a gentle slope.

The water depth at the Toyapakeh Strait and Boleng Strait generally ranges between 5-50 meters in the outer channel with a gentle seabed morphology, whereas in the middle channel the depth is increasing gradually to more than 200 meters (Figure 9 and 10). Bathymetric contour pattern from both straits shows a steep and narrow morphology. Some closed-pattern contours are found at the depth up to 200 meters, indicating several deep hole morphologies. Herein, some of the closed bathymetric contour patterns of more than 100 meters depth have the potential to cause a vortex of ocean currents.

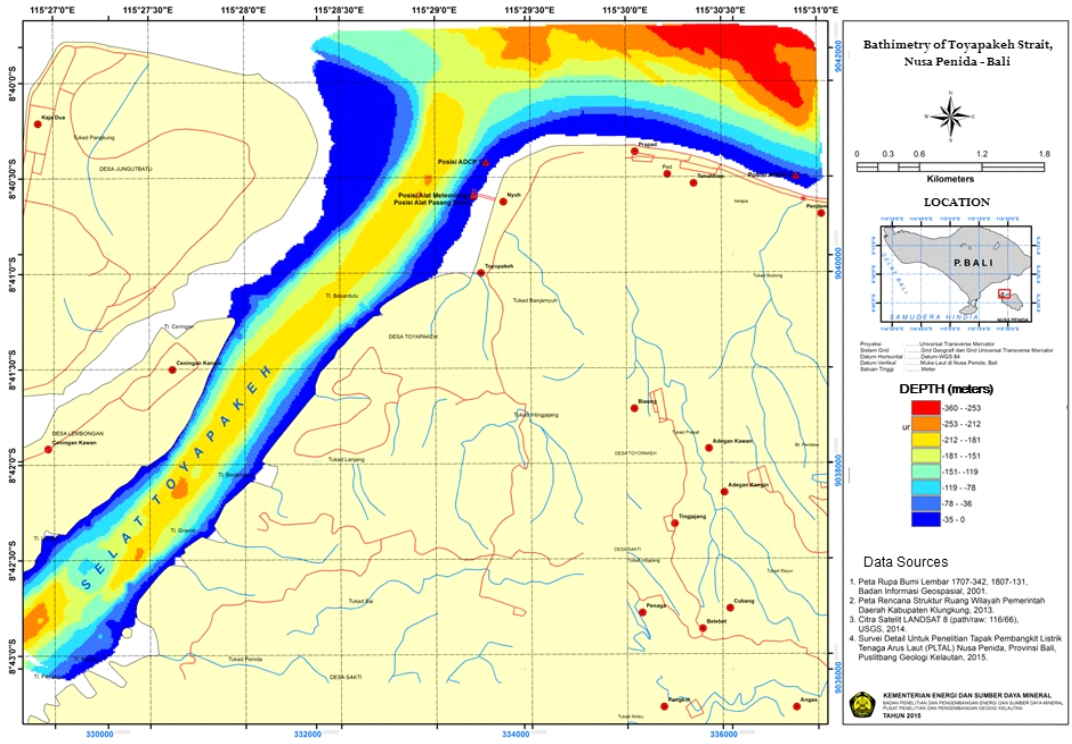

Figure 9. Bathymetry of Toyapakeh Strait - Nusa Penida, Bali (Yuningsih et al., 2015)

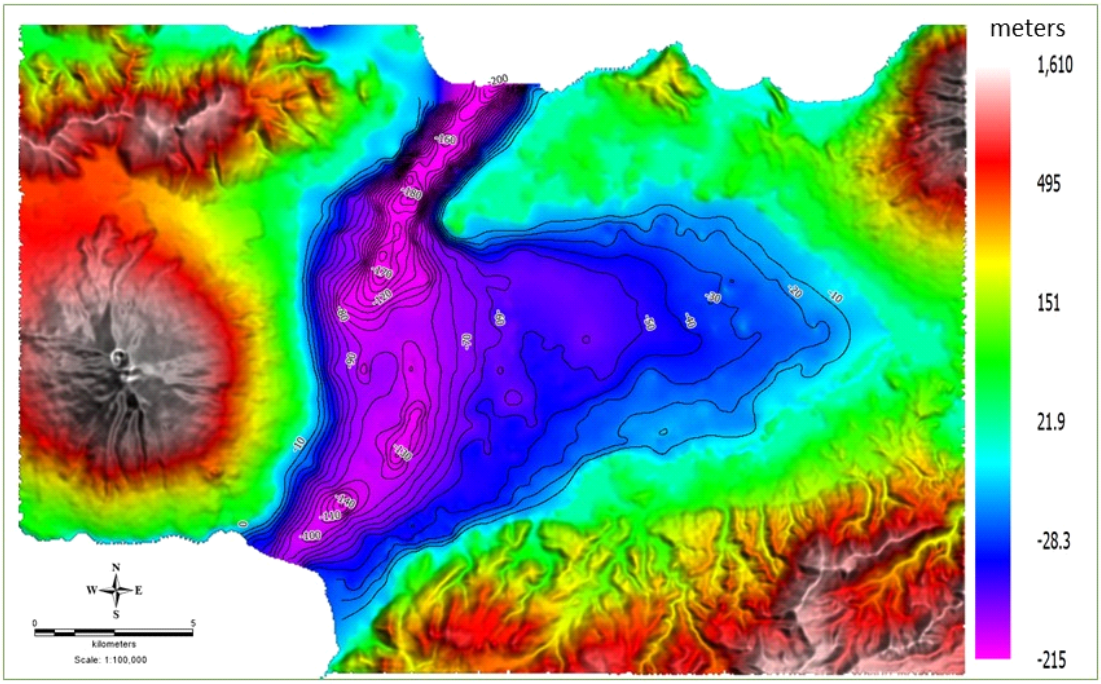

Figure 10. Depth contour and seabed morphology of Boleng Strait (Yuningsih et al., 2012).

The bathymetry of almost all straits reflects the tectonic activity in the area, which is characterized by a deep channel in the middle and a small shallow platform in the outer channel on a gentle seabed morphology. This condition gives rise to a strong tidal current that can be utilized to generate electricity. One of various information from the area for designing an ocean current turbine is the sediments that composed the seafloor and coastal area (Kurnio et al., 2018).

At the Larantuka Strait, the water depth ranges from 5 to 80 meters on a gentle slope morphology (Figure 8). Observing the strait width, the bathymetric contour pattern, the depth, and the seabed morphology, there is a possibility for a fast channeling of the mass flow of seawater to occur from the Flores Sea to the Savu Sea, especially of the surface ocean currents. No potential for a vortex of ocean currents was found. The current pattern in the Larantuka strait is also more predictable than other straits. From some of these technical aspects, the Larantuka Strait is more preferable to be selected as a site for ocean current power plant compared to other straits.

3.4 Current Energy Conversion

Based on ocean current characteristic and the territorial water profile, the straits of the Lesser Sunda Islands have a great potential for the utilization of ocean current power plants. Although the ocean current power is not widely implemented at present in Indonesia, it has an important potential for future renewable electricity generation, especially in remote coastal areas.

There are many selected sites of the straits of the Lesser Sunda Islands that have potency to generate electricity due to the significant current speed of more than 2.5 m/s. In general, the average of sea current speeds in the Lesser Sunda Straits are less than 1.5 m/s with the duration flow of 8-12 hours a day. The maximum speed reaches 2.5 m/s up to more than 3.0 m/s with the duration flow of 2-3 hours a day.

The calculation result of ocean current energy using Fraenkel formulation (2002) in the several straits of the Lesser Sunda Islands, e.g. Toyapakeh Strait, Larantuka Strait, and Boleng Strait, is shown in Table 2. The ocean current power calculated from the current speed data is indicated in the form of power density unit (W/m^2).

Table 2. The calculation results derived from current speed data at several straits of Sunda Lesser.

	Toyapakeh Strait	Larantuka Strait	Boleng Strait
Current speed from seabed mounted ADCP	0.5-3.4 m/s	0.5-2.83 m/s	0.5-2.0 m/s
Current speed from Transect Survey	0.5-2.5 m/s	0.5 - 3.67 m/s	0.5 - 3.4 m/s
Maximum Power Density	13.8 kW/m^2	25.5 kW/m^2	20.8 kW/m^2

CONCLUSION

The study conducted in the Lesser Sunda Straits draws some conclusions as follows:

- The straits through Bali and Nusa Tenggara namely the Lesser Sunda Straits can be selected as the potential sites for the sea current power plant due to the strong current speeds between 0.5 m/s to more than 3.0 m/sec.
- In general, the current direction tends toward the northeast during the high tides and toward the southwest during the low tides.
- Based on several moving ADCP trajectories data, the relatively high current velocity in these straits is correlated with the depth of the sea. The highest current velocity occurs in the deepest and narrowest part of the strait channel during high tide and low tide conditions.
- From some of the technical aspects, i.e. the tide, the current speed, the bathymetry and the seabed morphology, the Larantuka Strait is more preferable to be the selected site for developing ocean current power plant.
- Based on the speed and the duration of the flowing current, the ocean current turbine technology suitable to apply in the waters around Bali-Nusa Tenggara is the technology which requires a minimum speed to move (low cut in speed, 0.5 - 1 m/s) to obtain sufficient electrical power.

ACKNOWLEDGEMENTS

The authors would like to especially thank Mr. Hedi Hidayat as the Director of Marine Geological Institute. The authors appreciate all the team members from the marine renewable energy research group for their dedication, assistance and support, both in the field and during data processing. Special thanks is also addressed to Mr. Subaktian Lubis for his precious suggestions and continuous support. We thank Godwin Latuputty for his help in drawing the maps. Finally, the quality of this paper is also enhanced by the reviews and valuable input from the reviewer and our colleagues.

REFERENCES

European Marine Energy Centre Ltd (EMEC), 2009. *Assessment of Tidal Energy Resource*, United Kingdom, ISBN 978-0-580-65642-2

Fraenkel, P.L. 2002. Power from Marine Currents. *Proceedings of the Institution of Mechanical Engineers, Part A: Journal of Power and Energy*, 216(1): 1-14. DOI: 10.1243/09576502760024782

Gordon, A.L. 2005. Oceanography of the Indonesian Seas and their Throughflow. *Oceanography*, 18:14–27.

Hidayati, N., Mahmudi, M., Saputra, D.K., Musa, M., Purnawali, H.S., 2016. Ocean Currents Energy for Electricity Generation and Its Potential in East Java Water, *Journal of Environmental Engineering & Sustainable Technology,* vol. 03(02): 104-111.

Kurnio, H., Yuningsih, A., Zuraida, R., 2018. Characteristics of Boleng Strait Sediments, East Nusa Tenggara, and its Relationship with Current Velocity. *Bulletin of the Marine Geology,* vol. 33(1): 15-28.

Lubis, S. and Yuningsih, A., 2012. Sea Current Patterns in the Straits of Lesser Sunda as a Possible Location for Renewable Energy Developments, presented at *METI International Conference*, Bali, Indonesia. *(unpublished paper).*

Prasetyo, H. and Sarmili, L., 1994. Structural and Tectonic Development of West-East Indonesian Backarc Transition Zone: Implication for Hydrocarbon Prospect. *Bulletin of the Marine Geological,* vol. 9(2): 23-69.

Rachmat, B., Yuningsih, A., and Astjario, P. 2013. Preliminary Research on Installation of Sea Current Energy for Electricity Turbin from Current and Seafloor Morphology data of Boleng Strait, Eastern Lesser Sunda Islands. *Jurnal Geologi Kelautan*, 11:17-32 (in Bahasa Indonesia).

Susanto, R.D., Gordon, A.L., Sprintall, J. and Herunadi, B., 2000. Indonesian Throughflow, Intraseasonal variability and Tides in Makassar Strait, *Geophysical Research Letters,* vol. 27(10): 1499-1502.

Syarif, A,I., Yuningsih, A., Syafiudin A.S. Wardhani, 2016. The Study of Tidal Energy Selection - The Case of Toyopakeh Strait, Nusa Penida, Bali, Presented and Proceeding at International Conference on Ocean, Mechanical and Aerospace for Scientist and Engineer, 7 - 8 November 2016, Universiti Malaysia Terengganu). Proceeding p. 439-445.

Thomas, K., 1991. Low Speed Energy Conversion from Marine Currents, *Comprehensive Summaries of Uppsala Dissertations from the Faculty of Science and Technology* 287, ISBN 978-91-554-7063-0

Wyrtki, K., 1961. *Physical oceanography of the Southeast Asian Waters. Naga* Rep. 2: The University of California La Jolla. California. p. 26.

Yuningsih, A, Sujono, E.H., Rachmat, B. Lubis, S., 2010. Prospek Energi Arus Laut sebagai Sumber Tenaga Listrik di Selat-selat Perairan Nusa Tenggara, Indonesia, *Prosiding Seminar Nasional Energi 2010*, Universitas Padjadjaran, ISSN : 2087 – 7471.

Yuningsih, A. And Masduki, A., 2011. The Potential of Ocean Current Energy for Electric Power Plants in the Coastal Area of East Flores, *Journal of Tropical Marine Science and Technology*, ISOI – IPB, ISSN Cetak : 2087 - 9423, ISSN Elektronik : 2085 – 6695.

Yuningsih, A. and Lubis, S., 2011. Nusa Penida Strait, a Prospect Location for Developing Electrical Corrent Power as Reliable Renewable Energy Source. *Proceeding International Congress on Ocean Energy and Deep Ocean Water Application.* DOWA Japan. Bali, Indonesia.

Yuningsih A, Rachmat, B., Kurnio, H., Surachman, M., Suryoko, M.A., and Nurdin, N., 2012. Ocean Current Energy Research as a Renewable Energy Source at Boleng Strait, East Nusa Tenggara. *Pusat Penelitian dan Pengembangan Geologi Kelautan, Badan Penelitian dan Pengembangan Energi dan Sumberdaya Mineral, Departemen Energi dan Sumberdaya Mineral, Internal Report*, 183p, Unpublished.

Yuningsih, A., 2015. Measurement of Ocean Current Characteristics in the Toyapakeh Strait, Nusa Penida, to Support PLTAL's Detailed Engineering Design (DED), *Mineral and Energy Magazine*, vol. 13(10): p.95-103, (in Bahasa Indonesia).

Yuningsih A, Rachmat, B., Yosi, M., Saputra, M.D., Raharjo, P., Lugra, I.W., and Rahardiawan, R. 2015. Site Characterization and Resource Observation for Ocean Current Power Plant at Toyapakeh Strait - Nusa Penida, Bali, *Pusat Penelitian dan Pengembangan Geologi Kelautan, Badan Penelitian dan Pengembangan Energi dan Sumberdaya Mineral, Departemen Energi dan Sumberdaya Mineral, Internal Report*, 151p, Unpublished.

THE SEAWATER AND FRESHWATER INFLUENCE ON EXPANSIVITY BEHAVIORS OF CLAY MINERALS

PENGARUH AIRLAUT DAN AIRTAWAR TERHADAP DAYA KEMBANG SUSUT MINERAL LEMPUNG

Dian Agus Widiarso[1], Nurakhmi Qadaryati[1], Wiyatno Haryanto[2]

[1]Department of Geological Engineering, Universitas Diponegoro, Jl. Prof. Soedharto, SH., Tembalang, Semarang, Indonesia
[2]Indonesian Society of Geotechical Engineering, Jakarta, Indonesia

Corresponding author: dianagus@lecturer.undip.ac.id

(Received 07 July 2021; in revised from 22 July 2021; accepted 22 September 2021)

ABSTRACT: Semarang City subsurface geology is characterized by an intercalating of loam-silt and clayey units. The behavior of clay materials are their expansivity potency of their volume when in contact with water. Some problems in the presence of tidal flooding appears when the seawater ingress to the shoreland that causes severe damage to infrastructures. This research attempts to reveal the influence of both seawater and freshwater on the expansivity behaviors of the clayey materials based on its mineral composition. In order to observe expansivity potency of clay minerals, 28 samples from four drill hole samples were soaked in seawater and freshwater for twenty-four hours. The initial volume of each samples were then compared with the samples volume after being soaked.X-Ray Diffraction (XRD) analysis was also conducted on selected samples to determine their mineral composition. The ANOVA test was then introduced to distinguish the influence of certain mineral types and composition to the clay expansivity behaviors. Confidence level and alpha (α) are about ninety-five percent and about five percent, respectively. The result of this research has proven that montmorilonite is clay mineral type that is most affected by expansivity behaviors when immersed in seawater and freshwater compared to kaolinite and illite minerals.

Keywords: Clay minerals, montmorillonite, expansivity, seawater, freshwater, tidal flooding.

***ABSTRAK**: Kota Semarang tersusun dari satuan lanau dan lempung. Mineral lempung memiliki sifat kembang susut dari segi volumenya ketika mengalami kontak dengan air. Permasalahan yang timbul akibat terjadinya peristiwa banjir pasang di perkotaan, adalah masuknya air laut menuju ke pantai dan daratan yang dapat merusak infrastruktur. Penelitian ini bertujuan untuk menunjukkan dampak yang ditimbulkan oleh air tawar maupun air laut terhadap kembang susut mineral lempung berdasarkan komposisi mineralnya. Untuk mengamati perubahan volume dalam mineral lempung, sebanyak 28 sampel dari empat sampel sumur bor direndam dalam air tawar dan air laut selama 24 jam. Kemudian volume awal setiap sampel dibandingkan dengan volume sampel sesudah dilakukan perendaman. . Uji X-Ray Diffraction (XRD) juga dilakukan pada sampel pilihan untuk mengetahui komposisi mineral sampel tersebut. Uji ANOVA dengan tingkat kepercayaan 95% dan alpha (α) 5% diterapkan untuk mengetahui pengaruh tipe dan komposisi mineral lempung tertentu terhadap kembang susut yang terjadi. Penelitian ini berhasil membuktikan bahwa montmorilonit merupakan jenis mineral lempung yang paling terpengaruh oleh sifat kembang susut di daerah penelitian ketika direndam dengan air tawar dan air laut, dibandingkan dengan kaolinit dan ilit.*

***Kata Kunci:** Mineral lempung, montmorilonit, kembang susut, air laut, air tawar, banjir pasang*

INTRODUCTION

In general, a clayey material is an important part of the soil, which mostly involves chemical weathering of rock-forming minerals and will change in some engineering behaviors when it contacts seawater (Aksoy et al., 2008). Some research on mineralogical and geotechnical approaches in coastal areas with a predominance of clay lithology has been performed widely in several countries. For example Veerasingam et Al.(2014) studied mineralogy and geotechnic for a construction planning in Lianyungang – a region of China that requires some investigative data regarding the origin of rocks, and some geotechnical studies of the clay minerals onsite by Liu et al. (2011). Similar case from the Changi project in Singapore within Quaternary sediment, which are composed of soft marine clay recognized as problematic soil for geotechnical engineering purposes (Bo et al., 2015). The major decision in construction process involves selecting a suitable site with the best soil conditions (Manimaran et al., 2019).

Based on geological setting, Semarang City is a part of the Holocene sediment which is composed of a river, flood-plain, swamp, tidal, and coastal deposits (Thanden et al., 1996). The sediment is characterized by intercalating of a dominant loam-silt and clay units and constituted normally consolidated clays with a soft and very soft consistency (Widiarso et al., 2019). This city is the capital city of Central Java Province, located in a large coastal deposit area with significant environmental issue. One problem such as tidal flooding in which the seawater ingresses frequently to the shoreland area during a high tide period (Wahyudi, 2007), causes serious damage in infrastructures and residential areas (Marfai and King, 2008; Muslim et al., 2019). The quality of the circumference decreases due to being influenced by tidal flooding (Sulaksana et al., 2019). One of the most important goals of disaster management teams is to protect the assets and infrastructures of the community from natural disasters such as floods (Darani and Bashiri, 2018).

Based on previous research, it was explained that claystone which has montmorillonite mineral composition more than 72% may indicate a reduction in the expansivity of the clay material when mixed with seawater, conversely, it exhibits less expansive when mixed with freshwater (Elmashad and Ata, 2014). Supporting that study result, other studies explained that the clay minerals such as kaolinite, chlorite, and mixing of other clay minerals have a lower reaction (low reactivity) than montmorillonite mineral when mixed with seawater (Aksoy et al, 2008). Therefore, the authors intend to present this research to study the influence of seawater and freshwater on the expansivity behaviors of clay materials based on particular mineral composition.

Clay Minerals Overview

Soil is defined as a constituent mineral with or without organic material left over from plants and fauna that are weathered, structured, and textured. It is useful as a construction material in various kinds of civil engineering works. As addition, the land also functions as a support for building foundation (Das, 2008). Based on the cohesivity, soils can be distinguished as cohesive and non-cohesive soils, fine-grained or coarse-grained soils (Bowles, 2015).

The abundance of clay minerals in the soils varies greatly, influenced by various things, including the type of origin rock, weathering, and diagenesis process, which cause variations both vertically and laterally. The most influential factor that determines soil types is the particle size distribution (Kareem et al., 2020). Clay materials with particle sizes smaller than 0.002-mm can be divided into three subgroups of clay minerals, are kaolinite, illite, and montmorillonite (Dunn et al., 1980).

Tidal Flood

Tidal flood is a flood that inundating the lowland areas on the coast, including estuaries and deltas, resulting in salty/brackish groundwater (Marfai, 2004). The underlying problem of tidal flooding affecting shoreland and coastal area is that the land level is lower than the high tide level. Furthermore, human activities include excessive groundwater extraction, dredging on the shipping lines, coastal reclamation, etc., are some factors contribute the tidal flooding.

METHODS (AND MATERIALS)

The research area is in Semarang City, especially on the alluvium and flood plains as referring to the Geological Map of Magelang and Semarang, Java (Thanden et al., 1996). The soil mechanics laboratory tests are performed on 28 clay soil samples, selected from 4 (four) drill hole samples (BM01, BM03, BM04, and BM05 in Figure 1). The depths of the drill hole samples are 60m, 40m, 30m, and 30m, respectively. The samples were then soaked d in seawater and freshwater for twenty-four hours. The samples volume were measured prior and after the soaking test. During the time, we observed the changes in their volumetric parameters. The difference of the lithologic volume is a product of the reduction between a final volume and the initial volume. The freshwater and seawater used in the soaking tests have been analyzed in terms of chemical and physical properties in Groundwater Utilization Sector, Geological Agency, Ministry of Energy and Mineral Resources, Bandung. (Table 1).

Table 1. The results of chemical analysis of fresh water and seawater sample

Type of Water	Indicators (mg/L)					
	Ca^{2+}	Mg^{2+}	K^{+}	Na^{+}	Cl^{-}	SO_4^{2-}
Seawater	315	749,5	248,5	7293,5	13393,9	246,5
Freshwater	25,4	6,4	6	19,1	14,4	1

X-Ray Diffraction (XRD) tests were performed on the similar samples as the soaking test. The purpose of this analysis is to determine the clay mineral type of the samples. The results were then processed by using X-pert Highscore and Siroquant software. The software is used to obtain the quantitative data on the diffraction pattern of a sample. ANOVA was then performed to observe the effect of mineral types and composition on the clay mineral expansivity. It is also used as an analytical tool to test the hypothesis by assessing whether there are any differences among the groups. Hypothesis testing is performed at a ninety-five percent confidence level and alpha (α) five percent.

RESULTS AND DISCUSSION

The result of the soaking test is shown in Table 2, it is observed that 3 samples were broken after soaking in both seawater and freshwater (BM 05-2, BM 05-5, BM 05-6). Therefore, these three samples were not taken into account for statistical ANOVA test. In addition to these three samples, one sample BM 05-3 was also broken after soaking in freshwater. Meanwhile, the result of XRD (X-ray diffraction) analysis in the clay mineral compositions is demonstrated in Table 3.

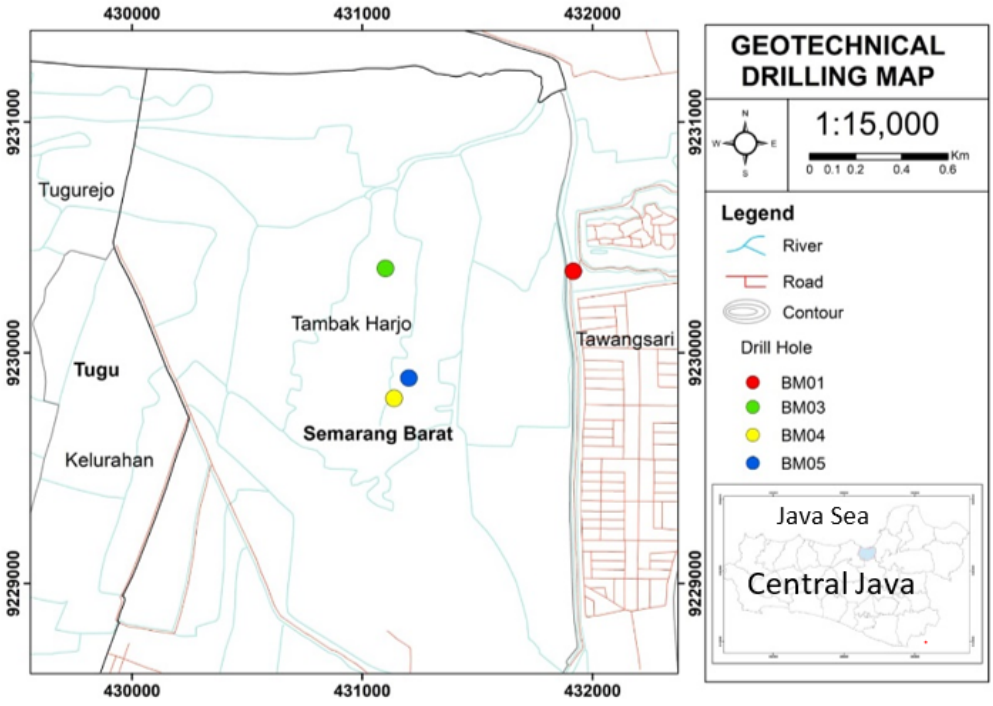

Figure 1. Geotechnical Drilling Map

Table 2. Test parameters of soaking

No	Code	Depth	Soaking in Sea Water		Soaking in Fresh Water	
			Initial Volume (cm^3)	End Volume (cm^3)	Initial Volume (cm^3)	End Volume (cm^3)
1	BM 01-1	5 - 6	166	263	133	120
2	BM 01-2	11 - 12	113	140	113	148
3	BM 01-3	15 - 16	113	159	113	135
4	BM 01-4	23 - 24	113	119	107	159
5	BM 01-5	25 - 26	90	453	90	509
6	BM 01-6	31 - 32	73	145	84	428
7	BM 01-7	41 - 42	113	127	113	137
8	BM 01-8	51 - 52	106	133	106	136
9	BM 01-9	59 - 60	129	154	129	145
10	BM 03-1	5 - 6	113	176	113	206

11	BM 03-2	11 - 12	73	122	113	161
12	BM 03-3	15 - 16	109	168	113	183
13	BM 03-4	21 - 22	107	139	140	190
14	BM 03-5	25 - 26	127	468	127	171
15	BM 03-6	29 - 30	113	144	106	146
16	BM 03-7	39 - 40	159	200	172	170
17	BM 04-1	5 - 6	113	146	113	176
18	BM 04-2	11 - 12	99	129	99	154
19	BM 04-3	15 - 16	109	134	109	166
20	BM 04-4	21 - 22	95	117	79	76
21	BM 04-5	25 - 26	95	142	79	956
22	BM 04-6	29 - 30	113	662	113	708
23	BM 05-1	5 - 6	113	108	55	163
24	BM 05-2	11 - 12	104	broken	104	broken
25	BM 05-3	15 - 16	132	190	112	broken
26	BM 05-4	21 - 22	119	468	79	179
27	BM 05-5	25 - 26	119	broken	119	broken
28	BM 05-6	25,5 - 26	98	broken	95	broken

Statistical Test on Soaking in Seawater

The independent variables in the statistical test with ANOVA were the mineral content in the sample, which are kaolinite, montmorillonite, and illite. Statistical tests were carried out by observing changes in the sample volume before and after soaking without considering the soil water content. The coefficient of significance value (α) is determined at 0.05. The significance or probability column of the ANOVA test results indicate the level of significance. The significancevalue (sig value) is used as a cut-off model to determine if the independent variable affects or does not affect the dependent variable. The independent variable is considered to affect the dependent variable if the sig value is lower than 0.05.

Table 3. Percentage of identified mineral from XRD analysis

No	Code	Depth	Identified minerals (%)			
			Quartz	Kaolinite	Illite	Montmorillonite
1	BM 01-1	5 - 6	54.97	40.56	4.47	0
2	BM 01-2	11 - 12	57.33	35.09	7.58	0
3	BM 01-3	15 - 16	59.69	39.54	0	0.76
4	BM 01-4	23 - 24	42.35	48.53	9.12	0
5	BM 01-5	25 - 26	29.48	43.98	0	26.54
6	BM 01-6	31 - 32	28.47	40.95	0	30.58
7	BM 01-7	41 - 42	35.71	0	63.77	0.52
8	BM 01-8	51 - 52	40.48	13.42	33.55	12.54
9	BM 01-9	59 - 60	28.54	44.23	0	27.23
10	BM 03-1	5 - 6	47.26	20.15	31.70	0.89
11	BM 03-2	11 - 12	48.36	17.41	33.18	1.04
12	BM 03-3	15 - 16	47.98	22.34	28.34	1.35
13	BM 03-4	21 - 22	43.62	33.87	0	22.51
14	BM 03-5	25 - 26	27.03	0	60.36	12.61
15	BM 03-6	29 - 30	23.82	47.83	0	28.35
16	BM 03-7	39 - 40	28.06	44.60	0	27.34
17	BM 04-1	5 - 6	72.61	0	26.11	1.27

18	BM 04-2	11 - 12	64.78	28.85	0	6.37
19	BM 04-3	15 - 16	45.72	29.01	22.06	3.21
20	BM 04-4	21 - 22	50.19	49.05	0	0.76
21	BM 04-5	25 - 26	33.84	0	59.44	6.72
22	BM 04-6	29 - 30	28.04	38.10	0	33.86
23	BM 05-1	5 - 6	60.04	34.40	0	5.56
24	BM 05-2	11 - 12	48.12	25.29	24.71	1.88
25	BM 05-3	15 - 16	94.37	0	0	5.63
26	BM 05-4	21 - 22	59.62	0	0	40.38
27	BM 05-5	25 - 26	12.80	0	87.20	0
28	BM 05-6	25,5 - 26	63.55	35.81	0	0.65

Based on Table 4, it shows that the sig value is 0.024, smaller than 0.05 (α), suggests that the model passed and can be used to specify the influence of the mineral contents in samples on sample volume changes after soaked in seawater. The probability value (significance) is below 0.05, indicates all independent variables influence the dependent variable and vice versa.

Tabel 4. ANOVA test result on soaking in seawater

Model	df	Mean square	F	Sig.
Regression	3	48961.1	3.897	0.024[b]
Residual	20	12563.6		
Total	23			

a. Dependent variable: after soaked in seawater

b. Predictors: (constant), montmorillonite, kaolinite, and illite.

Afterwards, the F-count value (F in table 4) is then compared to the F-table parameter. The F-table is obtained by calculating the number of df (degree of freedom). The df of multiple regression consists of df1 and df2 with the following formula:

df1=k-1.....……(1)

df2=n-k.....…….(2)

under following condition:

n = number of samples

k = number of independent variables

For this statistical tests, 25 samples were analyzed. As has been mentioned before, from total 28 samples, 3 samples (BM 05-2, BM 05-5, and BM 05-6) were broken after being soaked in seawater, therefore were not considered for the statistical test. The soaking test in seawater has k value = 3 and n = 25. Hence, the values of df1 = 2 and df2 = 22 are obtained. Based on F distribution table at 0.05 sig level, the F-table value is 3.443 (Nuryadi et al., 2017), which is smaller than F-count (3.897). Therefore, it can be concluded that all independent variables influence the dependent variable. The test results of the coefficient value on the soaking in seawater is displayed in Table 5.

In Table 5, t value is the benchmark to see the influence of variable (partial) by comparing their each t value to the t-table value. When the value of t-count is greater than the t-table value, denotes the variable has an impact. By calculating the number of df (degree of freedom), t-table is obtained with the following formula:

df=n–(k–1)....……(3)

under the following condition:

n = number of samples

k = number of independent variables

The calculation of df (degree of freedom) = 25 – (3–1) = 23.

Based on t-table value for multiple regression df 23 at sig 0.05 is 1.71387 (Nuryadi et al., 2017). T-count value of montmorillonite mineral reveals a value of 3.303 (Table 5), which is greater than t-table value. In contrast, t-count value of kaolinite and illite are -0.375 and 0.568, respectively, which are lower than t-table (1.71387). It is concluded that montmorillonite mineral has the most influence on the changes in sample volumetric when it is soaked in seawater compared to kaolinite and illite minerals.

The sig column in Table 5 represents the significance level of each independent variable to determine whether the variables influence the dependent variable or not. When sig value is smaller than 0.05 (α), signify that there is significant impact, in contrast, when it is greater than 0.05 (α), then there is no influence at all. The result reveals that only sig value of montmorillonite mineral has a lower value than 0.05 (0.004). So, montmorillonite mineral has the most influence on changes in sample volume compared to kaolinite and illite minerals when soaked in seawater.

Statistical Test on Soaking in Freshwater

The data is processed using multiple regression analysis methods with the dependent variable is the percentage of difference between the initial volume with the sample final volume, after soaked in freshwater for

Tabel 5. Coefficient test result of soaked in seawater

Model	t	Sig.
(Constant)	1.503	0.148
Kaolinite	-0.375	0.712
Illite	0.568	0.576
Montmorillonite	3.303	0.004

twenty-four hours. The ANOVA test result shown in Table 6 with the sig value of about 0.249.

Tabel 6. ANOVA test result on soaked in freshwater

Model	df	Mean square	F	Sig.
Regression	3	93014.1	1.484	0.249[b]
Residual	20	62688.1		
Total	23			

Dependent variable: after soaked in freshwater

Predictors: (Constant), montmorillonite, kaolinite, and illite

The value is greater than 0.05 (α), so the model is considered failed, and cannot be used to determine the influence of sample's mineral content in the changes of sample volume after being soaked in freshwater. The probability value (significance) is above 0.05, suggests not all independent variables have an affect on the dependent variable and vice versa.

Only 24 out of 28 samples were analyzed in the statistical tests after being soaked in freshwater because four samples (BM 05-2, BM 05-3, BM 05-5, BM 05 -6) were broken after being soaked. The soaking test in freshwater has a value of k = 4 and a value of n = 24, so that the values of df1 = 3 and df2 = 21 are obtained. Based on the F distribution table at the 0.05 sig level, the F-table value is 3.072 (Nuryadi et al., 2017), greater than the F-count amounting to 1.484 (Table 6). It can be concluded that not all independent variables have an influence on the dependent variable.

Table 7. Coefficient test result of soaked in freshwater

Model	t	Sig.
(Constant)	-0.012	0.990
Kaolinite	0.364	0.719
Illite	1.304	0.207
Montmorillonite	1.837	0.081

The df value for the soaking test in freshwater is = 24–(4–1) = 21. Based on the t-table value for the multiple regression df 21 at sig 0.05 is 1.72074 (Nuryadi, et al., 2017). The t-count value of the montmorillonite mineral in Table 7 shows a value of 1.837, so the montmorillonite mineral has the most influence in the changes of sample volume compared to the kaolinite and illite minerals when soaked in freshwater.

Based on a comparison of the ANOVA difference test for soaking of the clay minerals in seawater and freshwater, it is obtained that the F value is 3.897 with a sig of 0.024, while the results of soaking in freshwater, the F value is 1.484 with sig value 0.24. Hence, it is suggested that seawater has a more significant influence on the expansion process of the clay minerals compared to freshwater.

Montmorillonite is a mineral formed by two sheets of silica and one sheet of aluminium. The octahedral sheet is located between two silica sheets with the ends of the tetrahedra. Tetrahedra is mixed with hydroxyl of the octahedral sheet to form an aluminium single layer by magnesium. Due to the weak Van der Waals bonding forces (bonds due to changes in the number of electrons at any time in one part of the atomic nucleus) between the ends of the silica sheet and the lack of negative charge in the octahedral sheet, water (H_2O) and moving ions can enter and separate the layers (Ariesnawan, 2015). This, results in high swelling properties. The ionic content of seawater which is higher than that in fresh water, induces the swelling properties of mineral montmorillonite to be more developed when exposed to seawater than when exposed to fresh water.

CONCLUSSIONS

It is proven that montmorillonite mineral is the most influential in changing the volumetric expansivity of soil when the soil is soaked in seawater and freshwater compared to kaolinite and illite minerals. The montmorillonite minerals have more effect on volumetric changes when the clay minerals are immersed in seawater than when they are immersed in freshwater. This study provides an understanding that it is also necessary to have a good knowledge regarding the composition of clay minerals in the planning, especially when the land area is dominated by clay material and affected by tidal flooding. Engineering geological planning should not only observe the physical properties of lithology, they must consider the chemical properties of lithology as well.

ACKNOWLEDGEMENTS

This paper is a part of Research Development and Implementation Research (RPP) Fund Sources Apart from the Diponegoro University State Budget for the 2021 Fiscal Year. The authors are grateful to all those who have supported and helped during the research process.

REFERENCES

Aksoy, Y. Y., Kaya, A., Oren, A. H., 2008. Seawater effect on consistency limits and compressibility characterisics of clays. *Engineering Geology*, 102: 54-61.

Ariesnawan, R. A., 2015. The Mechanic And Dynamic Characteristic of Tuban Clay Shale Due To Changes of Water Content. Thesis. Institut Teknologi Sepuluh Nopember Surabaya.

Bo, M. W., Arulrajah, A., Sukma, P., Horpibulsuk, S., 2015. Mineralogy and Geotechnical Properties of Singapore Marine Clay at Changi. *Soils and Foundation*, 55: 600- 613.

Bowles, J. E., 2015. *Physical and Geotechnical Properties of Soils*. McGraw-Hill International Book Company.

Darani, S. K., Bashiri, M., 2018. A Multi-district Asset Protection Problem with Time Windows for Disaster Management. *International Journal of Engineering*, 31(11):1929-1934.

Das, B. M., 2008. *Advanced Soil Mechanics, Third Edition*. Taylor & Francis Group.

Dunn, I. S., Anderson, I. R., dan Kiefer, F. W., 1980. *Basics of Geotechnical Analysis, First Edition*. IKIP Semarang Press.

Elmashad, M. E., and Ata, A. A., 2014. Effect Of Seawater On Consistency, Infiltration Rate And Swelling Characteristics Of Montmorillonite Clay. *Housing and Building National Research Center*, 12: 175-180.

Kareem, K. W. A, Fattah, M. Y., Khaled, Z. S. M., 2020. Assessment of Changes in Shear Strength Parameters for Soils below Circular Machine Foundation. *International Journal of Engineering*, 33(8):1491-1498.

Liu, S. Y., Shao, G. H., Du, Y. J., Cai, G. J., 2011. Depositional and Geotechnical properties of Marine Clays in Lianyungang, China. *Engineering Geology*, 121:66-74.

Manimaran, A., Seenu, S., Ravichandra, P. T. N., 2019. Stimulation Behaviour Study on Clay Treated with Ground Granulated Blast Slag and Groundnutshell Ash. *International Journal of Engineering*, 32(5):673-678.

Marfai, M. A., 2004. Tidal Flood Hazards Assessment: Modelling in Raster GIS, Case in Western Part of Semarang Coastal Area. *Indonesian Journal of Geography*, 36(1):25-28.

Marfai, M. A. and King, L., 2008. Potential Vulnerability Implications if Coastalinundation Due Sea Level Rise for The Coastal Zone Of Semarang City, Indonesia. *Journal Environmental Geology*, 54:1235-1245.

Muslim, D, Haerani E., Muslim F. N. and Muslim G. O., 2019. Toward the Safe Live-able Built Environment around Ciletuh-Palabuhanratu Geopark Area in Sukabumi Regency, Indonesia. *IOP Conf. Series: Earth and Environmental Science*, 248: 012036. doi:10.1088/1755-1315/248/1/012036.

Nuryadi, Astuti, T. D., Utami, E. S., Budiantara, M. 2017. Dasar-dasar Statistik Penelitian. Sibuku Media. Yogyakarta.

Sulaksana, N., Iskandarsyah, T. Y.W.M., Rifai, A., Rendra, P.P.R. and Sulastri, M., 2019 Prospective Zone Area for Agriculture and Residential Based on Geological Disaster Potentials in South Bandung Region. *Journal of Geological Sciences and Applied Geology*, 3(1): 26-37.

Thanden, R. E., Sumadirdja, H., Richards, P. W., dan Sutisna, K., 1996. *Peta Geologi Lembar Magelang dan Semarang, Jawa skala 1:100.000*. Pusat Survey Geologi.

Veerasingam, S., Venkatachalapathy, R., Ramkumar, T., 2014. Distribution of Clay Minerals in Marine Sediments of Chennai, Bay of Bengal, India: Indicators of Sediment Sources and Transport Processes. *International Journal of Sediment Research*, 29:11-23.

Wahyudi, 2007. Tingkat Pengaruh Elevasi Pasang Laut Terhadap Banjir dan Rob di Kawasan Kaligawe Semarang. *Jurnal dalam Riptek*, 1(1):27-34.

Widiarso, D. A., Haryanto, W., Muslim, D., Zakaria, Z. and Iskandarsyah, T. Y., 2019. Potential Consolidation Settlement Due to Load Stresses of Building Structures. *International Journal of GEOMATE*, 17(60):204-210.

PETROPHYSICAL ANALYSIS AND SEISMIC STRATIGRAPHY INTERPRETATION TO DETERMINE HYDROCARBON RESERVOIR IN TARAKAN BASIN, BUNYU ISLAND WATERS

ANALISIS PETROFISIKA DAN INTERPRETASI SEISMIK STRATIGRAFI UNTUK MENENTUKAN RESERVOAR HIDROKARBON DI CEKUNGAN TARAKAN, PERAIRAN PULAU BUNYU

Daffa Dzakwan Shiddiq[1], Eleonora Agustine[1], Tumpal Bernhard Nainggolan[2], Imam Setiadi[2] and Shaska Zulivandama[2]

[1]Geophysics Department, Faculty of Mathematics and Natural Sciences, Universitas Padjadjaran, Jl. Raya Bandung Sumedang KM. 21, Jatinangor, 45363

[2]Marine Geological Institute, Jl. Dr. Djundjunan No. 236, Bandung, 40174

Corresponding author: daffadzakwan2202@gmail.com

(Received 14 June 2021; in revised from 18 June 2021; accepted 27 October 2021)

ABSTRACT: Tarakan Basin area of Bunyu Island Waters is known to have hydrocarbon potential with complex geological structures. This study aims to determine reservoir characterization and to obtain prospect of hydrocarbon reservoir zones based on petrophysical and seismic stratigraphy analysis with reference to Well DDS-1 and 2D seismic Line S88. Petrophysical analysis results 3 zones that have potential as hydrocarbon reservoirs. Based on petrophysical quantitative analysis, Zone 1 has values of 52.25% for shale volume, 18.48% for effective porosity, 39.84% for water saturation and 13.03 mD for permeability. Zone 2 has values of 54.66% for shale volume, 10.27% for effective porosity, 40.9% for water saturation and 1.14 mD for permeability. Zone 3 has values of 49.22% for shale volume, 9.33% for effective porosity, 56.33% for water saturation and 0.22 mD for permeability. Out of these three reservoir zones in Well DDS-1, Zone 1 has the prospect of hydrocarbons which is supported by the net pay value. Based on seismic stratigraphy interpretation, the reservoir zone is correlated to the Tabul Formation, which comprises calcareous clay and limestone.

Keywords: hydrocarbon reservoir, petrophysical analysis, seismic stratigraphy, Tabul Formation, Tarakan Basin

***ABSTRAK**: Wilayah Cekungan Tarakan pada Perairan Pulau Bunyu dikenal memiliki potensi hidrokarbon dengan struktur geologi yang kompleks. Studi ini bertujuan untuk mengetahui karakteristik reservoar dan mendapatkan prospek zona reservoar hidrokarbon berdasarkan analisis petrofisika dan seismik stratigrafi. Dalam analisis petrofisika dan seismik stratigrafi, digunakan data sumur DDS-1 dan seismik 2D lintasan S88. Pada hasil analisis petrofisika, ditunjukkan adanya 3 zona yang berpotensi sebagai zona reservoar hidrokarbon. Berdasarkan perhitungan petrofisika, Zona 1 memiliki nilai volume shale 52.25%, porositas efektif 18.48%, saturasi air 39.84% dan permeabilitas 13.03 mD. Zona 2 memiliki nilai volume shale 54.66%, porositas efektif 10.27%, saturasi air 40.9% dan permeabilitas 1.14 mD. Zona 3 memiliki nilai volume shale 49.22%, porositas efektif 9.33%, saturasi air 56.33% dan permeabilitas 0.22 mD. Dari ketiga zona reservoar pada sumur DDS-1, Zona 1 memiliki prospek adanya hidrokarbon yang didukung oleh nilai net pay. Berdasarkan interpretasi seismik stratigrafi, zona reservoar sebanding dengan Formasi Tabul yang menunjukkan keterdapatan batulempung karbonatan dan batugamping.*

***Kata Kunci:** reservoar hidrokarbon, analisis petrofisika, seismik stratigrafi, Formasi Tabul, Cekungan Tarakan*

INTRODUCTION

To measure hydrocarbon reserves in Bunyu Island Waters, an integrated method is needed to detect the presence of hydrocarbons in reservoir rocks to obtain and produce hydrocarbons. The objective of this research is to determine hydrocarbon potential in reservoir rocks based on petrophysical and seismic stratigraphy analysis. Petrophysical analysis is used to determine the ability of rocks to store and release fluids based on the parameters of shale volume, porosity, water saturation, permeability, net reservoir and net pay of reservoir rocks (Darling, 2005). Seismic stratigraphy analysis is used to analyze the presence of reservoir rocks based on rock lithology and stratigraphy obtained from seismic and well log data (Veeken, 2007).

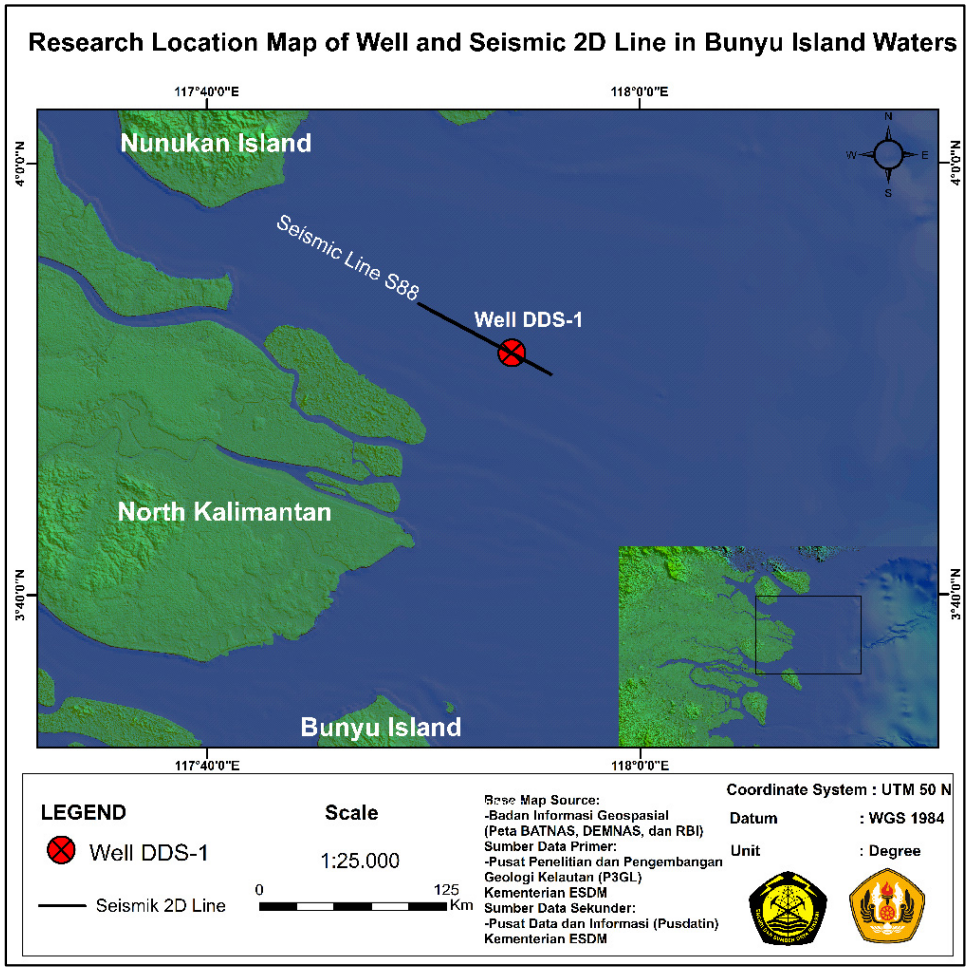

Figure 1. Map of Research Location in Bunyu Island Waters

GEOLOGICAL SETTINGS

Tarakan Basin is one of the three main Tertiary basins in the eastern part of Kalimantan Island, which is characterized by the presence of clastic sedimentary rocks as the dominant constituent with fine to coarse grained sandstones and several calcareous deposits (Setyowiyoto et al., 2019). Tarakan Basin is bordered by Sekatak Berau Ridge to the west, Suikerbrood Ridge and Mangkalihat Peninsula to the south, Sempurna Peninsula to the north, and Sulawesi Sea to the east. Tarakan Basin is located in the middle of the estuary of the Sajau River (Figure 2).

Stratigraphically, the Tarakan Basin is divided into two sedimentary systems, i.e., the older (non-deltaic) main sediments and the younger deltaic sediments. The non-deltaic sedimentary systems occurs during the Eocene to Early Miocene. This sedimentary system contains volcanic material, distributed from the deep sea to the mainland. This sediment is detected above the basement complex of metamorphic-igneous rock which was deformed by faults. The lithostratigraphy of the non-deltaic sedimentary systems can be identified as the Sembakung, Sajau, Seilor, Mangkabua, Tempilan, Tabalar, Mesaloi, and Naintupo Formations. Meanwhile, the delta sedimentary system occurs during the Middle Miocene to the Quaternary. This system consists of

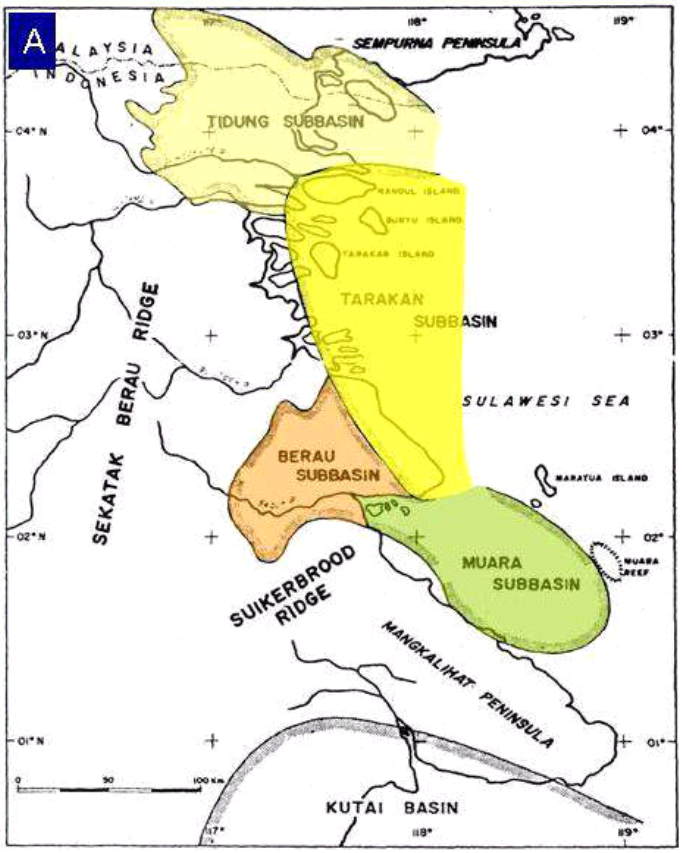

Figure 2. Regional Geology of Tarakan Basin (modified from Achmad and Samuel, 1984)

interfingering between deltaic deposits and prodelta deposits of the Naintupo Formation. The clastic material of the delta was originated from the western part of the Tarakan Basin, which is known as the Central Kalimantan Mountains or the Kuching Plateau. The general stratigraphy of the Tarakan Basin can be seen in Figure 3.

DATA AND METHODS

The study uses one well data (Well DDS-1) and one post-stack time migration 2D seismic line data (Line S88). Well data is used for quantitative petrophysical analysis and lithological identification, while post-stack time migration 2D seismic data is used for seismic stratigraphy interpretation to provide lithological and stratigraphic information on the subsurface area. The flow chart of this research can be seen in Figure 4.

Reservoir Zone Identification

Reservoir zone identification is conducted by analyzing the lithology logs of gamma ray and spontaneous potential, the resistivity logs of Lateralog Deep (LLD), Lateralog Shallow (LLS), Micro Spherically Focused Log (MSFL) which provides fluid information, and the porosity logs of density, neutron and sonic (Nopiyanti et al., 2020). The identification of the reservoir zone is derived from the curve pattern of lithology logs which shows the depth of sandstone or carbonate rocks. The

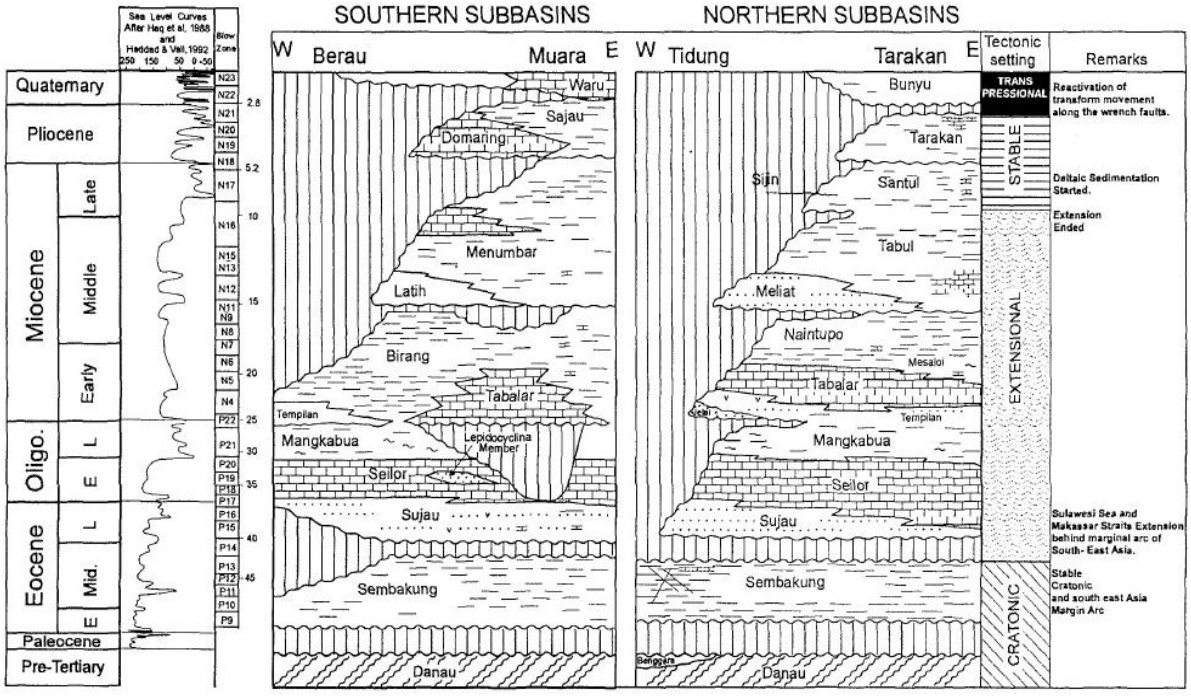

Figure 3. Regional Stratigraphy of Tarakan Basin (Lentini and Darman, 1996)

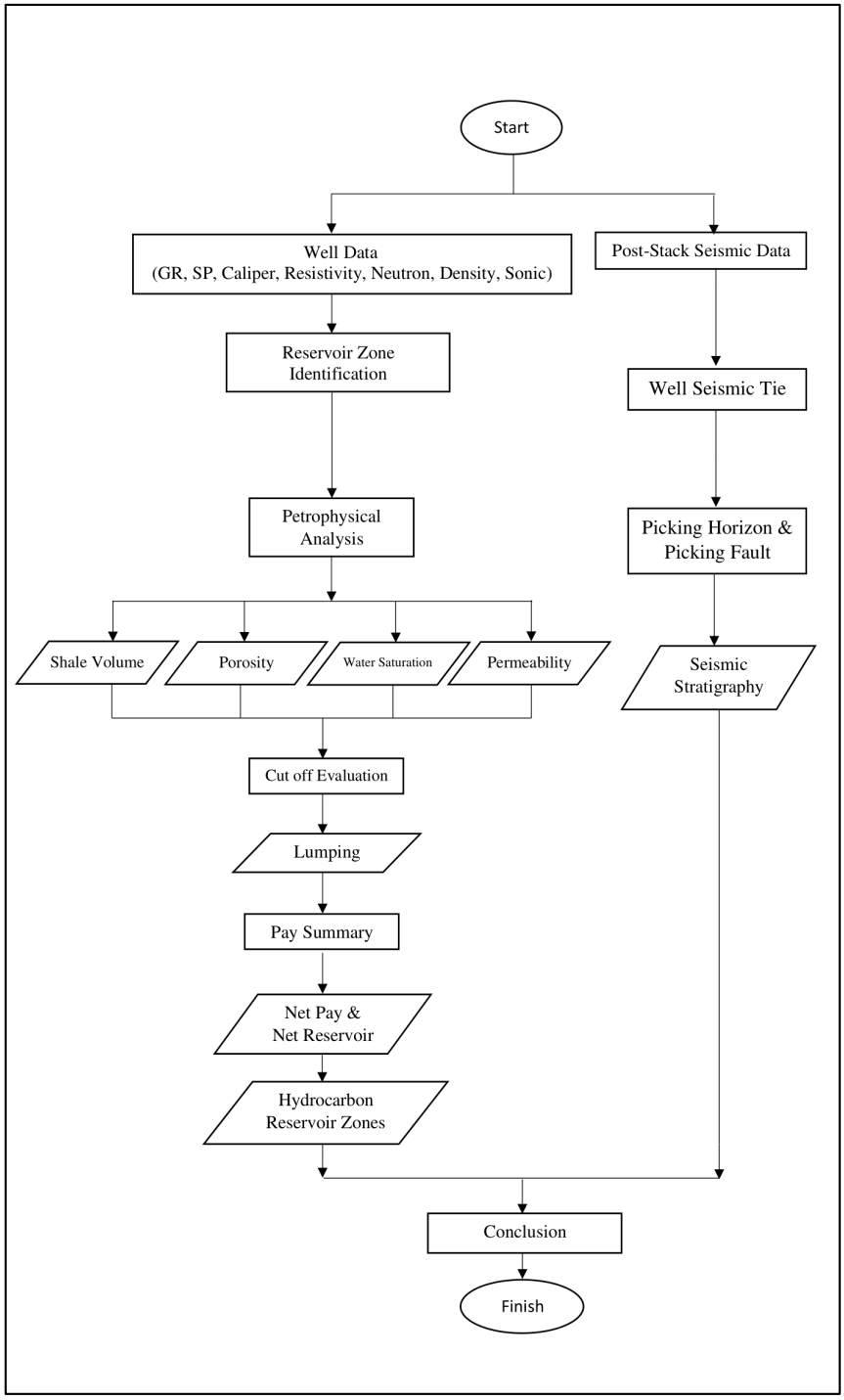

Figure 4. The flowchart of petrophysical and seismic stratigraphy analysis

resistivity log shows a fairly high resistivity value indicated by its hydrocarbons and fresh water contents. The porosity log shows the porosity of the rock formation (Purba et al., 2020).

Shale Volume

Shale volume is the volume of shale fraction in the formation determined by the volume of clay content over the total volume of the formation. Shale volume calculation which is based on gamma-ray log uses a linear method (Asquith & Krygowski, 2004) with the following equation:

$$Vsh = IGR = \frac{GR_{log} - GR_{clean}}{GR_{shale} - GR_{clean}} \quad (1)$$

where:
Vsh = Shale Volume (%)
IGR = Gamma Ray Index (%)
GRlog = Gamma ray log reading (API)
GRclean = Log response in shale-free zone
GRshale = Log response in the shale zone

Porosity

Porosity is the size of the pore space in the rock which functions as a storage area for fluids (water, oil, and gas). The porosity intended to obtain from this research is effective porosity because it shows the properties of rock pores that are interconnected, allowing the fluid to flow. Rock pores that are unable to transmit fluid are not included in the type of effective porosity (Asquith & Krygowski, 2004). In this study area, the Wyllie Sonic Porosity equation is used because the time acoustic parameters, lithology of rock type (Δtma), and fluid type of pore filler (Δtf) are known to show lithology and fluid content in the zoning area. According to Wyllie (1958), the porosity equation can be written as follow:

$$(\Phi) = \frac{\Delta t\,\mathrm{sh} - \Delta t\,ma}{\Delta t\,fl - \Delta t\,ma} \qquad (2)$$

where:
(Φ) = Porosity (%)
Δtma = Interval transit time in the rock matrix (msec/ft)
Δtsh = Interval transit time in the shale zone (msec/ft)
Δtfl = Interval transit time in the fluid in formation (msec/ft)

The porosity value in equation (2) is the value of total porosity, while the porosity value used in this research is the effective porosity. Krygowski (2003) used the following equations to obtain the value of effective porosity:

$$\Phi e = \Phi t - (\mathrm{Vsh} * \Phi sh) \qquad (3)$$

$$\Phi sh = \frac{(\rho_{\mathrm{Dsh}} - \rho_{\mathrm{sh}})}{(\rho_{\mathrm{Dsh}} - \rho_{\mathrm{fl}})} \qquad (4)$$

Where:
Φe = Effective porosity (%)
ρ_{sh} = Shale density (g/cc)
Vsh = Shale Volume (%)
Φt = Total porosity (%)
ρ_{fl} = Fluids density (g/cc)
Φsh = Total porosity in the shale zone (%)
ρ_{Dsh} = Dry shale density (g/cc)

Water Saturation

Water saturation (Sw) is the part of the pore space filled with water, while the part filled with hydrocarbons is called hydrocarbon saturation (Sh) which has a value of (1 - Sw) (Harsono, 1997). In this study area, the Indonesia equation is applied to acquire the value of water saturation because this equation considers the shale effect on the basis of shale volume (*Vsh*), as well as the resistivity of shale (*Rsh*) to reduce the effect of the shale (Dwiyono and Winardi, 2014). The Indonesia equation can be written with the following equation:

$$\frac{1}{\sqrt{R_t}} = \frac{\Phi^{m/2}}{\sqrt{\alpha \times R_w}} + \frac{V_{sh}{}^{1-0.5V_{sh}}}{\sqrt{R_{sh}}} \times S_w{}^{\frac{n}{2}} \qquad (5)$$

Where:
S_w = Water saturation (%)
R_w = Formation water resistivity (ohm.m)
R_t = Formation true resistivity value (ohm.m)
Φ = Porosity (%)
V_{sh} = Shale Volume (%)
R_{sh} = Resitivity of shale
a = Tortuosity factor (1)
m = Cementation exponent (2)
n =Saturation exponent (2)

Permeability

Permeability is the ability of rocks to be passed by fluids. In this study, the Coates Free Fluid Index equation was used. The Coates Free Fluid Index equation can be written with the following equation:

$$K = \left(C * (\Phi)e^2 \ \frac{(1 - Swirr)}{(Swirr)}\right)^2 \qquad (6)$$

Where:
K = Permeability (mD)
$(\Phi)_e$ = Effective porosity (%)
Swirr = Irreducible water saturation (%)
C = The coates constant (70)

Cut-off Evaluation

Cut-off value is calculated to determine the reservoir zone with high prospect of hydrocarbon. This calculation is based on the crossplots on porosity-permeability, shale-porosity volume and water-porosity saturation (Worthington and Cosentino, 2005). Indriyani et al. (2020) proposed Western Culture method to determine the cut-off value for porosity, shale volume, and water saturation; whereas the cut-off value of permeability is assumed as the minimum absolute permeability value (Worthington and Cosentino, 2005).

The assumption for the cut-off value of permeability is derived from the assumption of the fluid type in the reservoir zone. If the type of fluid is gas, the minimum absolute permeability is 0.1 mD; while oil has the minimum absolute permeability of 1 mD (Worthington and Cosentino, 2005). The well report of the study area reveals that the type of its reservoir fluid is gas, thus the

minimum absolute permeability is 0.1 mD. This cut-off permeability value is used to determine the effective porosity value from the porosity-permeability crossplot and then applying the western culture method, the cut-off value of porosity is used to determine the cut-off value of shale volume wich was obtained from the shale volume versus porosity crossplot. The same porosity value is also used to determine the cut-off value of water saturation deriving from the water saturation versus porosity crossplot.

Net Reservoir and Net Pay

Net Reservoir represents the total value of the formation thickness which has the quality of reservoir rock. Net Pay shows the value of the reservoir rock interval of hydrocarbon reservoir. Net Reservoir and Net Pay can be obtained from the petrophysical parameters by determining the cut-off value.

Based on Figure 6, it shows the presence of gross rock which determines all reservoir rock intervals that being evaluated. Gross reservoir is a part of the gross rock that meets the shale volume cut-off value. Net Reservoir is a fraction of the gross reservoir that fits the cut-off of

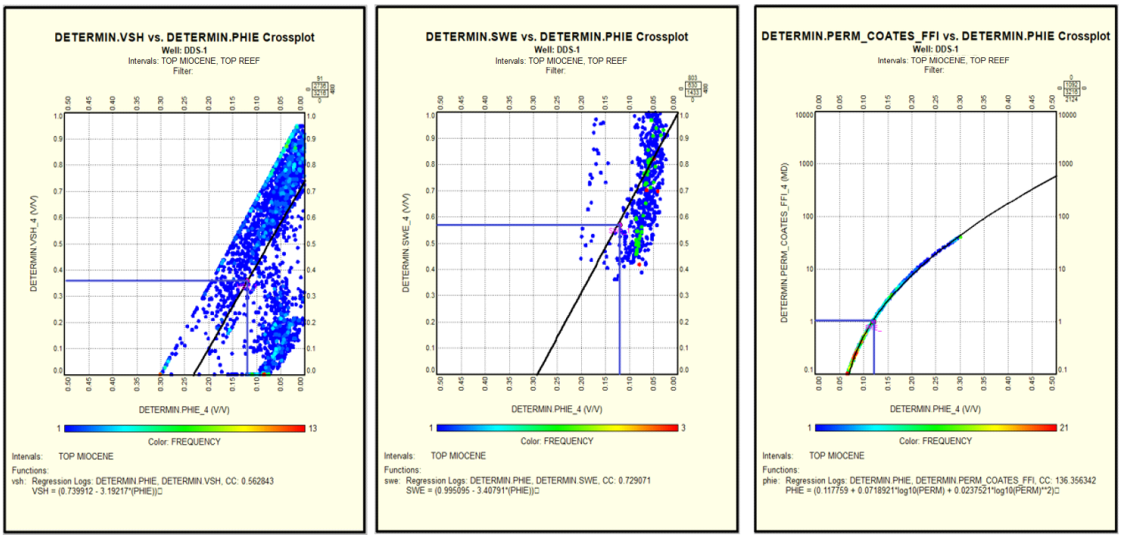

Figure 5. Crossplots of petrophysical parameters in Well DDS-1

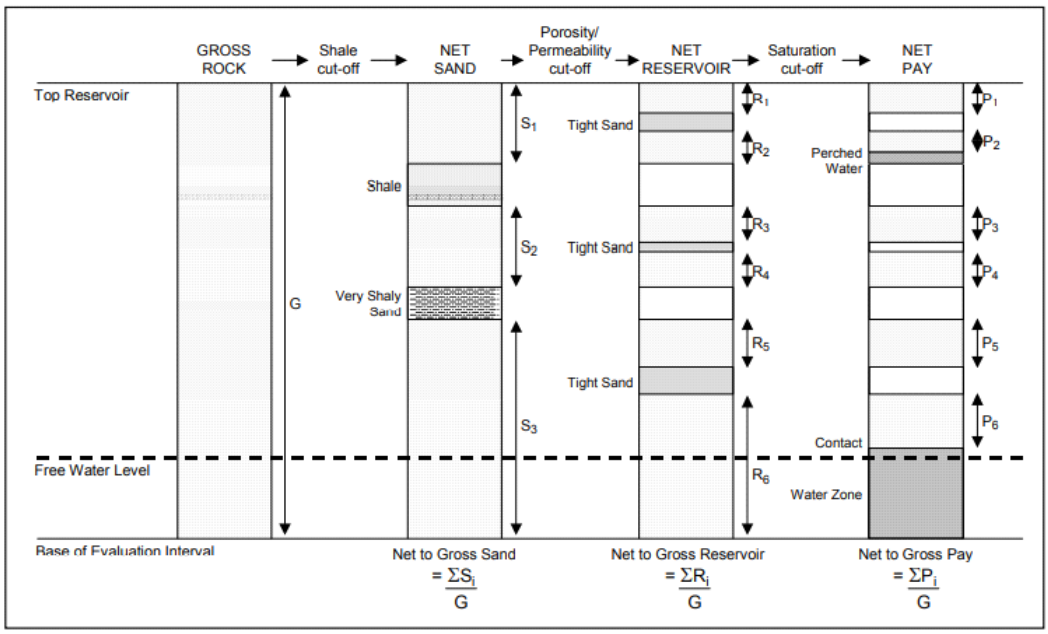

Figure 6. Schematic of net parameters (Worthington and Cosentino, 2005)

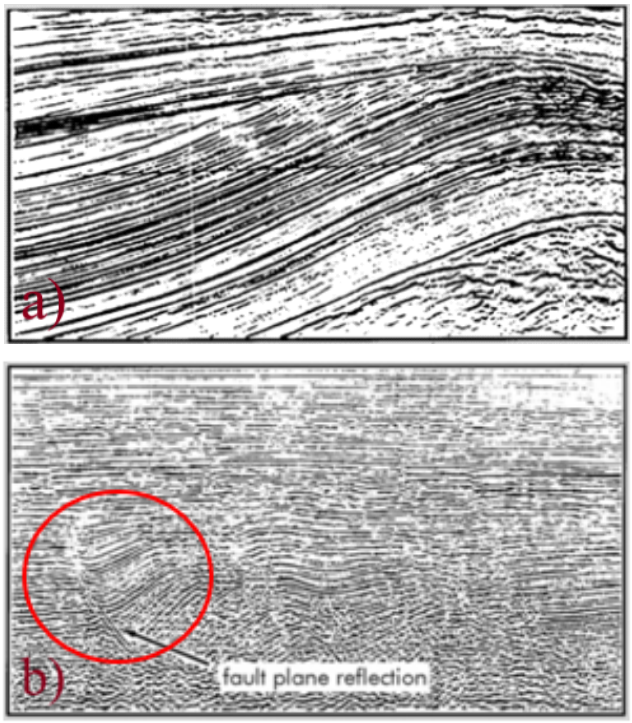

Figure 7. Sedimentary reflections (a) and non-sedimentary reflections (b) (Veeken, 2007)

porosity and permeability value. Net Pay denotes a portion of the Net Reservoir that fulfills the cut-off of water saturation value (Worthington and Cosentino, 2005).

Seismic Stratigraphy Analysis

Seismic stratigraphy analysis is conducted to determine the order of the subsurface rock types containing stratigraphic information based on the interpretation of the 2D seismic data (Veeken, 2007). One of the basic concepts of seismic stratigraphy is that sedimentary reflections can respond as a single timeline. These reflections represent time intervals of continuous sedimentation conditions. Each reflector coincides with a period of time of a similar depositional state in a geological sense (Setiady et al., 2017).

In seismic stratigraphy, there are two types of subsurface seismic reflections. The first is sedimentary reflections which represent the area of the bedding, showing conformity changes in the depositional regime (Figure 7a). The second, non-sedimentary reflections which indicate the presence of a fault plane characterized by prominent seismic reflections. It is usually observed when a high impedance acoustic contrast exists between two different lithologies on either side of the fault plane (Figure 7b). The coherence of the fault plane energy is normally attenuated in seismic processing because of its high dip. Fluid contact between porous bodies, such as fluid (oil-gas-water) contact or water presence in the hydrocarbon-bearing reservoir, also shows its reflection (Veeken, 2007).

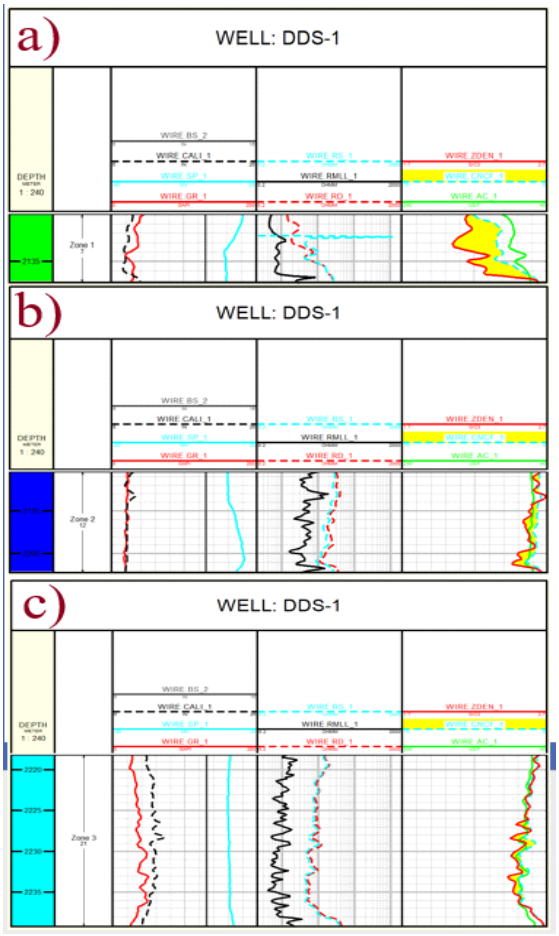

Figure 8. Reservoir zone 1 (a), zone 2 (b) and zone 3 (c) of Well DDS-1

RESULTS

Purba et al. (2020) argued that Well DDS-1 has good porosity based on the overlay of its density and neutron logs along with the acoustic value of slow-wave propagation time of its sonic log. Analyzing log curve patterns of Well DDS-1 lithology to identify the characteristic of the reservoir zone results in three reservoir zones, namely Zone 1 at the depth of 2130 - 2137 meters, Zone 2 at the depth of 2190 - 2202 meters, and Zone 3 at the depth of 2218 - 2239 meters. (Figure 8).

Shale volume calculation gives the average value of 52.25% for Zone 1, 54.66% for Zone 2 and 49.22% for Zone 3. Based on these results, all of the three zones have clay or shale content, but they can potentially become hydrocarbon reservoir rocks after correcting the calculation of the effective porosity and water saturation as proposed by Kamel and Mabrouk (2003).

The calculation of effective porosity yields the average value of 18.48% for Zone 1, 10.27% for Zone 2, and 9.33% for Zone 3. The porosity classification of Koesoemadinata (1980) shows that Zone 1 has good porosity, Zone 2 has fair porosity, and Zone 3 has poor porosity.

Calculating water saturation results in the average value of 39.84% for Zone 1, 40.9% for Zone 2 and 56.33% for Zone 3. The water saturation values in these three zones reveal that each value is considered as low (<60%), which means that the saturation value of the hydrocarbons is high, thus indicating the presence of hydrocarbon fluids.

Table 1. Petrophysic Calculation of Reservoir Zone in Well DDS-1

Well	Zone	Depth (m)	Shale Volume (%)	Effective Porosity (%)	Water Saturation (%)	Permeability (mD)
DDS-1	1	2130 - 2137	52.25	18.48	39.84	13.03
	2	2190 - 2202	54.66	10.27	40.9	1.14
	3	2218 - 2239	49.22	9.33	56.33	0.22

Table 2. Cut-off Values of Reservoir Zones in Well DDS-1

Cut-off Parameters	Cut-off Value
Permeability (mD)	≥ 0.1
Porosity (%)	≥ 12
Shale Volume (%)	≤ 36
Water Saturation (%)	≤ 57

The potential for hydrocarbon reservoirs in the three zones is confirmed by the permeability parameter as the final result of petrophysical calculations, providing the information on the ability of rocks to pass the fluid. With reference to the parameter of permeability, the average value is 13.03 mD for Zone 1, 1.4 mD for Zone 2 and 0.22 mD for Zone 3.

All the petrophysic calculation results of Well DDS-1 analysis are listed in Table 1 below.

Determining the petrophysical cut-off values derived from the cross-plot results, the permeability cut-off value is ≥ 0.1, the porosity cut-off is ≥ 12%, the shale volume cut-off is ≤ 36%, and the water saturation cut-off is ≤ 57% (Table 2). These results can be used to eliminate intervals outside the cut-off value to define the net reservoir and net pay zones.

The lumping processing on the results of the cut-off values obtains Net Reservoir and Net Pay and determines whether the reservoir zone has good reservoir characteristics or not. Applying it, table 3 shows that Zone 1 has Net Reservoir value of 2.14 meters at the intervals of 2130.93 - 2133 meters and of 2133.37 - 2153.53 meters; Zone 2 has values of 0.3048 meters at the interval of 2197.23 - 2197.46 meters and 0.92 meters at the intervals of 2200.58 - 2201.42 meters; whereas Zone 3 does not have Net Reservoir value. Consequently, reservoir zones that are good for passing fluid are Zone 1 and Zone 2.

Table 4 shows that Net Pay found in Zone 1 has values of 0.61 meters at the intervals of 2133.6 - 2134.06 meters and of 0.76 meters at the intervals of 2134.82 - 2135.53 meters; Zone 2 has values of 0.3048 meters at the intervals of 2197.3 - 2197.46 meters and 0.91 meters at the intervals of 2200.65 - 2201.42 meters. The existence of Net Pay values indicate that reservoir rocks found in Zone 1 and Zone 2 have the potential to store and release hydrocarbon fluids.

Table 3. Net Reservoir Values of Reservoir Zones of Well DDS-1

Zone	*DEPTH TOP* (METER)	*DEPTH BASE* (METER)	*GROSS* (METER)	*NET RESERVOIR* (METER)	*NET TO GROSS*
1	2130.93	2133	3.96	2.14	0.54
	2133.37	2135.53	2.44	2.14	0.88
2	2197,23	2197.46	33.38	0.3048	0.01
	2200.58	2201.42	3.96	0.92	0.23
3	2218	2239	20.88	0	0

Table 4. Net Pay Values of Reservoir Zones of Well DDS-1

Zone	*DEPTH TOP* (METER)	*DEPTH BASE* (METER)	*GROSS* (METER)	*NET PAY* (METER)	*NET TO GROSS*
1	2133.6	2134.06	359.13	0.61	0
	2134.82	2135.53	1.37	0.76	0.56
2	2197.3	2197.46	33.38	0.3048	0.01
	2200.65	2201,42	3.96	0.91	0.23
3	2218	2239	20.88	0	0

Analyzing the 2D seismic data of Line S88, some formations are adjusted referring to the marker data in the well report and the horizon picking, as well as depiction of the fracture structures seen during the fault picking (Figure 9).

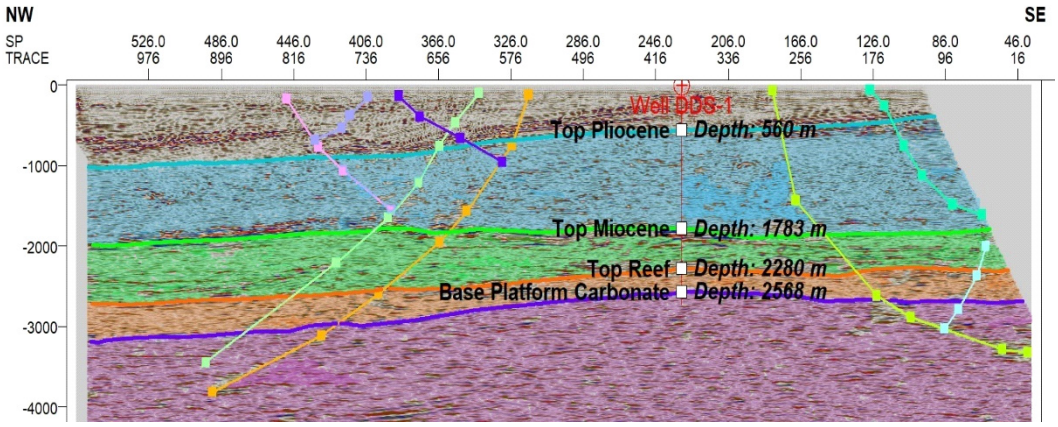

Figure 9. Results of horizon and fault picking interpreted from 2D seismic data of Line S88

DISCUSSION

The interpretation of gamma ray log of Well DDS-1 and 2D seismic section Line S88 in the Bunyu Island waters shows the presence of a petroleum system (Figure 9). The potential for source rock is between the Top Reef and Base Platform Carbonate boundaries, indicated by a high gamma-ray value. Based on the information in the well report, the source rock is in the Middle Miocene area and is comparable to the carbonate shale rock of Meliat Formation. This rock type of Meliat Formation is capable of being a place for the hydrocarbon maturation process (Setyowiyoto et al., 2019). We refer this source rock as Top Reef-Base Platform Carbonate Formation.

The hydrocarbon in the source rock moves towards the surface and migrates to the reservoir rock through reverse faults (Figure 10). The potential for reservoir rocks is between the Top Miocene and Top Reef boundaries at the depth range of 2130 to 2280 meters. As reported in the well report, the reservoir rock is in the Late to Middle Miocene area which is comparable to the carbonate claystone and limestone of Tabul Formation. According to Setyowiyoto et al. (2019), the Top Miocene-Top Reef Formation can store gaseous hydrocarbons. Based on the gamma-ray log in Figure 10, the three reservoir zones of Well DDS-1 shows low gamma-ray values. Further analysis of these reservoir zones disclose that reservoir zone 1 and reservoir zone 2 have low shale contents, hence the potential to become reservoir rocks for storing hydrocarbon (Figure 11).

Overlying the Top Miocene-Top Reef Formation is the potential caprock, indicated by high value in the gamma-ray log. The well report reveals the caprock is in the Late Miocene area which is comparable to the deltaic

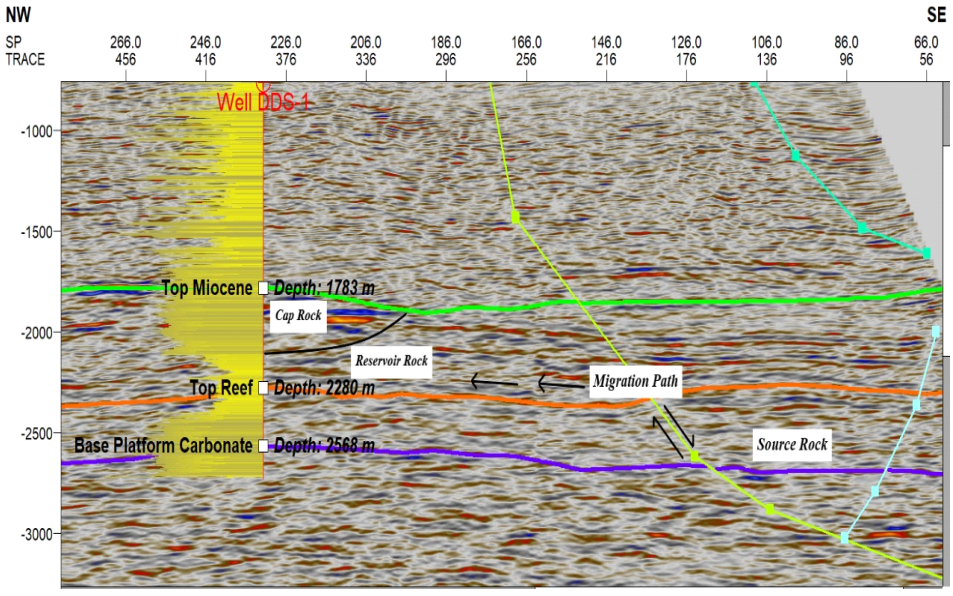

Figure 10. Seismic stratigraphy interpretation of Line S88

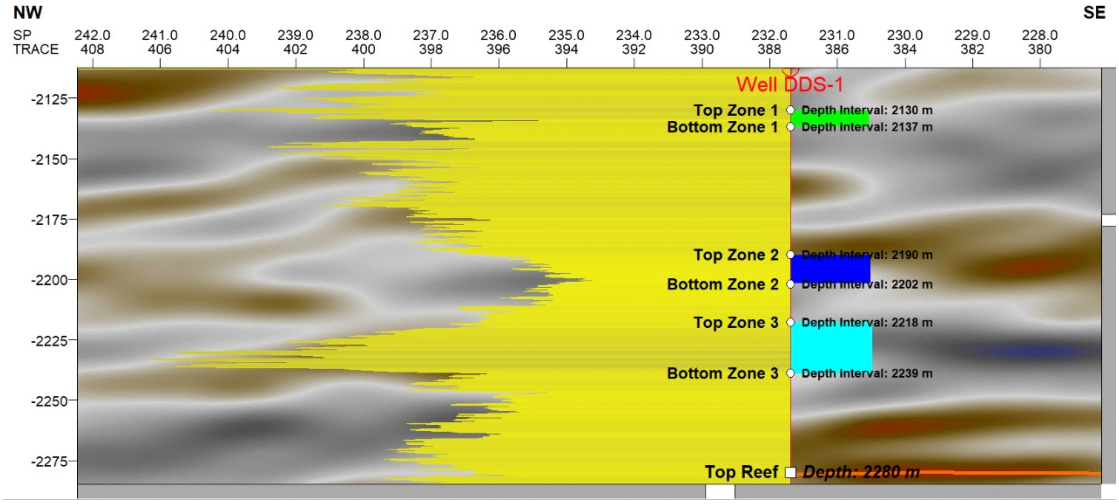

Figure 11. Reservoir zonations in Well DDS-1

claystone of Santul Formation (Setyowiyoto et al., 2019). At the upper boundary of the Top Miocene-Top Reef Formation, reflection misalignments can be seen and interpreted as a hydrocarbon trap system. Setyowiyoto et al. (2019) classified this trap type in Bunyu Islands waters as an unconformity stratigraphic trap, formed by structural processes followed by the deposition of fine sedimentary rock associated with the deltaic depositional environment.

In terms of reservoir zone determined from the Well DDS-1, the calculation of shale volume shows the highest shale content at 54.66% in Zone 2 which has the most inhibiting properties of rock in flowing fluid, compared to Zone 1 and Zone 3. Among the three zones, Zone 3 has the lowest porosity and permeability values. Therefore, Zone 3 is categorized as a bad reservoir zone.

Valuing the potential reservoirs of Zone 1 and Zone 2, their net pay parameters indicate the presence of hydrocarbon in the reservoir rock. However, based on the permeability classification of Koesoemadinata (1980), Zone 2 has a poor permeability at 1.14 mD, suggesting the zone cannot properly store fluid in the reservoir rock.

CONCLUSIONS

The petrophysical and seismic stratigraphy analysis assess the ability of reservoir rocks to store fluid based on their rock lithology. In this study, the calculation of petrophysical parameters in the Well DDS-1 shows three zones of reservoir rocks but only Zone 1 (2130 – 2137 meters) has reservoir characteristics that can store hydrocarbons, while Zone 2 (2190 – 2202 meters) and Zone 3 (2218 – 2239 meters) are not. The hydrocarbon prospects of Zone 1 indicates gas-typed hydrocarbon. Seismic stratigraphy interpretation of Line S88 determines the three reservoir zones are in the same formation, i.e., the Top Miocene-Top Reef Formation, comparable to the carbonate claystone and limestone of Tabul Formation.

ACKNOWLEDGEMENTS

Our sincere appreciation and gratitude to the honorable Head of Marine Geological Institute for his trust and supervision. Our truly appreciation to the Information Technology and Data Centre - Ministry of Energy and Mineral Resources for providing well log and seismic data.

REFERENCES

Achmad, Z. and Samuel, L., 1984. Stratigraphy and depositional cycles in the N.E. Kalimantan Basin. *Proceedings of Indonesian Petroleum Association 13th Annual Convention*, 1:109-120. http://doi.org/10.29118/ipa.2167.109.120

Darling, T., 2005. *Well logging and formation evaluation*. Elsevier Inc., 336p. http://doi.org/10.1016/B978-0-7506-7883-4.X5000-1

Indriyani, P.D., Harja, A. and Nainggolan, T.B., 2020. Petrophysical analysis to determine reservoir and source rocks in Berau Basin, West Papua Waters. *Bulletin of the Marine Geology*, 35(1):13-22. http://doi.org/10.32693/bomg.35.1.2020.659

Kamel, M.H. and Mabrouk, W.M., 2003. Estimation of shale volume using a combination of the three porosity logs. *Journal of Petroleum Science and Engineering,* 40(3-4):145-157. http://doi.org/10.1016/S0920-4105(03)00120-7.

Koesoemadinata, R.P. 1980. *Geologi minyak dan gas bumi Ed. 2*. Penerbit ITB, 296p.

Lentini, M.R. and Darman, H. 1996, Aspects of the Neogen tectonic history and hydrocarbon geology of the Tarakan Basin, *Proceedings of Indonesian*

Petroleum Association 25th Annual Convention, 1:241-251.

Nopiyanti, T., Nainggolan, T.B., Dewanto O. and Haq, D.A., 2020. Well log analysis and geochemical data to identify source rock and hydrocarbon reservoir: Northeast Java Basin study case. *AIP Conference Proceedings* 2245, 070017 (2020). http://doi.org/10.1063/5.0006978

Purba, L.R., Dewanto, O. and Mulyatno, B.S., 2020. Estimasi kandungan serpih (Vsh), porositas efektif (Øe) dan saturasi air (Sw) untuk menghitung cadangan hidrokarbon pada reservoar limestone Lapangan "PRB" di Sumatera Selatan menggunakan data log dan petrofisika. *Jurnal Geofisika Eksplorasi,* 4(3):90-102. http://doi.org/10.23960/jge.v4i3.43

Setiady, D., Astawa, I.N., Hermansyah, G.M., Lugra, I.W. and Nainggolan, T.B., 2017. Stratigrafi perairan Utara Bali dari hasil interpretasi seismik 2D. *Jurnal Geologi Kelautan*, 15(2):95-106. http://doi.org/10.32693/jgk.15.2.2017.349

Setyowiyoto, J., Fadhila, R. and Atmoko, W., 2019. Penentuan Zona Potensi Hidrokarbon pada Formasi Sembakung, Tabalar, dan Birang Cekungan Tarakan, Kalimantan Timur. *Prosiding Seminar Nasional Kebumian Ke-12, Teknik Geologi, Fakultas Teknik, Universitas Gadjah Mada*, pp. 56-87.

Syarif, A., Irwanzah, Z., Handayani, T. and Dogra, S., 2014. Successful development drilling guided by crosswell seismic imaging. *Beijing 2014 International Geophysical Conference & Exposition.* http://doi.org/10.1190/IGCBeijing2014-340

Veeken, P. C. H., 2007. *Seismic stratigraphy, basin analysis and reservoir characterisation*. Handbook of Geophysical Exploration, 37(1):528. http://doi.org/10.1017/S0016756808004329

Worthington, P.F. and Cosentino, L., 2003. The role of cut-offs in integrated reservoir studies. *SPE Reservoir Evaluation & Engineering*, 8(4):276-290. http://doi.org/10.2118/84387-PA

MARINE GEOLOGICAL INSTITUTE

RESEARCH AND DEVELOPMENT AGENCIES FOR ENERGY AND MINERAL RESOURCES
MINISTRY OF ENERGY AND MINERAL RESOURCES

Jl. Dr. Junjunan No. 236, Bandung - 40174. Indonesia
http://www.mgi.esdm.go.id, Email : ejournal.p3gl@gmail.com

ISSN 1410 - 6175